Magnocellular and parvocellular visual pathways' involvement in reading

Examination of developmental trajectories, visual cortex regions and reading circuitries

Doctoral dissertation by:

Maddi Ibarbia-Garate

Supervised by:

Dr. Pedro M. Paz-Alonso and Dr. David Soto Blanco

2022

eman ta zabal zazu

Universidad del País Vasco

Euskal Herriko Unibertsitatea

Maddi Ibarbia-Garate

BCBL Basque Center on Cognition, Brain and Language

Paseo Mikeletegi, 69,

Donostia-San Sebastian, Spain

Magnocellular and parvocellular visual pathways' involvement in reading

Doctoral dissertation by:

Maddi Ibarbia-Garate

To obtain the grade of doctor by the University of the Basque Country

Supervised by:

Dr. Pedro M. Paz-Alonso and Dr. David Soto Blanco

Donostia-San Sebastián

2022

Acknowledgements

First of all, thank you Kepa to give me the opportunity to go through this amazing journey, I have learned a lot during these five years with you professionally and personally. I don't want to continue with the acknowledgements without mentioning how understandable you have been and the support you have given me in the most complicated moments that I have had during these years. Thank you also David for all your help and support in different moments of the doctoral dissertation.

To all the BCBL community and especially to the LMC group, the administration team (Maider, Leire, Eider and Larraitz), Amaia, Brendan, Piermatteo and Eugenia. And specially to Ana, our project manager, apart of helping me with all the administration issues, you have helped me a lot dealing with the difficult personal circumstances I went through during my PhD. As you told me, since I will be working in Donosti, every month or so we have to meet to have a coffee.

All my friends that are there, in the better and the worst, my friends from Orio, Barcelona, Zerain, Donosti, Mundaka, Ondarru, Bermeo, Azpeiti… with a special mention to Gax, who has been supporting me during my thesis day by day, on the good days, and not so good. All the 'eskerrik asko' are not going to be enough to thank you for having you by my side every time I have needed it. Take for sure that I will also be there whenever and wherever you want. Zelebraziyo bat pendiente dakau biyok, mano a mano.

People that I consider as my family, Maite, Mari Carmen, Mikel, Marta, and my dear family from Elgeta: Thank you with all my heart, for everything.

To my closest family, izeba, osaba, aitona and my cousins, I hope that from now on you won't have to suffer all my worries and nerves, eskerrik asko bihotzez.

Maddi Ibarbia-Garate

Amatxo, Mikel, Ane... You are the best family I could think of, with all our virtues, defects, laughts, tears, and also sometimes debates or disagreements. Asko maite zaituet, uste dezuena baina gehiago, mila-mila esker, barren-barrenetik. Bazkai on bat zor dizuet!

Amona, what a pity you left us at this very moment, I will always have your strength and courage present, as well as all the good and amazing moments I lived with you. Maite zaitut, eta faltan botatzen zaitut.

Finally, and above all, aitatxo maitia, your values, your way of seeing life, your perseverance, your sacrifice… everything you taught me the 26 years we shared, thanks to that, I can today be writing these lines of gratitude about to finish my doctoral thesis. As you told me when I finished the first year of my degree: 'Querer es vencer', and here I am. You will always be my reference, my captain, and my favorite person in the world. I hope you are proud of your 'goxua' wherever you are. Izugarri maite zaitut, eta faltan botatzen zaitut, pila bat, nere bizitzako egun guztitan.

Contents

List of Figures

List of Tables

List of acronyms

- AF = Arcuate fasciculus
- BOLD = Blood-oxygen-level-dependent response
- CSD = Constrained spherical deconvolution
- CT = Cortical thickness
- DD = Developmental dyslexia
- deoxyHb = Deoxygenated hemoglobin
- DRC = Dual Route Cascaded model
- DTI = Diffusion tensor imaging
- DWI = Diffusion-weighted imaging
- EEG = Electroencefalografy
- ERP = Event-related EEG potentials
- FA = Fractional Anisotropy
- FDR = False Discovery Rate
- FEW = Family-wise error
- FG = Fusiform gyrus
- fMRI = Functional magnetic resonance
- GLM = General lineal model
- GM = Grey matter
- HARDI = High angular resolution diffusion imaging
- IFG = Inferior frontal gyrus
- IFOF = Inferior fronto-occipital fasciculus
- IPS = Intra-parietal sulcus
- IT = Inferior temporal cortex
- LGN = Lateral geniculate nucleus

- LOC = Lateral occipital cortex
- LSF = Low spatial frequencies
- MEG = Magnetoencephalografy
- mOTS = Medial occipital temporal sulcus
- MRI = Magnetic resonance imaging
- MTG = Middle temporal gyrus
- MT+/V5 = Motion-processing region
- OFC = Orbitofrontal cortex
- OTS = Occipital temporal sulcus
- oxyHb = Oxygenated hemoglobin
- PDP = Parallel Distributed Processing model
- PET = Positron emission tomography
- pOTS = Posterior occipito temporal slcus
- PPC = Posterior parietal cortex
- PPI= Psychophysiological interactions
- RM = Randomly moving point-light dots
- ROIs = Regions of interests
- SA= Surface area
- SFM = Structures-from-motion
- SLF = Superior longitudinal fasciculus
- STG = Superior temporal gyrus
- STS = Superior temporal sulcus
- tCSFs = Chromatic temporal contrast sensitivity functions
- TWR = Traveling-wave method
- V1 = Primary visual cortex

- V2 = Secondary visual cortex
- VEPs = Visual evoked potentials
- VWFA = Visual Word form area
- vOTC = Ventro-occipitotemporal cortex
- WLG = Wernicke-Lichteim-Geschwind model
- WM = White matter

1. Resumen en castellano

El reconocimiento visual es un primer paso imprescindible para muchas de las actividades que realizamos a diario. Identificar la pastilla que tenemos que tomar, discriminar un cara familiar en una multitud, leer una novela,… son sólo algunos ejemplos de operaciones cognitivas complejas que requieren una implicación refinada de nuestro sistema visual. Las sistemas magnocelulares y parvocelulares son las principales vías del sistema visual. Las mismas muestran importantes diferencias histológicas y fisiológicas, así como en la especialización de su repuesta ante distintos tipos de estímulos. El sistema magnocelular responde a frecuencias espaciales más bajas y frecuencias temporales más altas, y tiene respuestas transitorias. El sistema parvocelular, por el contrario, es sensible al color, tiene menor sensibilidad al contraste, responde a frecuencias espaciales más altas y frecuencias temporales más bajas, y presenta respuestas sostenidas.

La información visual se analiza mediante una jerarquía de regiones visuales situadas a lo largo de la ruta visual ventral, y la mayoría de los modelos sobre el reconocimiento de objetos la han visto comúnmente como un proceso ascendente. No obstante, hay estudios que destacan que el reconocimiento visual no puede explicarse completamente mediante procesos ascendentes y hay otras teorías que sugieren que la retroalimentación o la información descendente es importante para facilitar el reconocimiento de objetos, que debe ser activado y disponible para las áreas primarias antes de que se complete el reconocimiento visual.

Aunque la evidencia empírica en humanos sobre la implicación de estas vías visuales es limitada, varios estudios previos en neurociencia cognitiva y otros campos afines han subrayado su contribución potencial y su diferente implicación en el reconocimiento de objetos, caras e imágenes. Se sabe aún menos sobre la implicación de los dos principales sistemas de visión en la lectura. Aunque haya varios estudios que asocian el sistema

magnocelular con la lectura, además de que la investigación sobre dislexia ha apoyado en parte la teoría de que el sistema magnocelular está involucrado en esta discapacidad lectora; no pasa lo mismo con el sistema parvocelular, ya que salvo uno o dos estudios, no hay ninguna evidencia todavía de que dicho sistema esté relacionado con la lectura. Por último, y hasta la fecha, conocemos muy poco sobre las trayectorias del desarrollo de estos sistemas y sus contribuciones específicas en el reconocimiento visual de palabras y objetos o imágenes.

El objetivo de esta tesis doctoral es caracterizar las contribuciones de los dos vías principales del sistema visual, la vía magnocelular y la vía parvocelular, en el reconocimiento visual de palabras e imágenes en la corteza visual y en la red de lectura, utilizando medidas conductuales combinadas con índices funcionales y estructurales obtenidos con la técnica de la resonancia magnética. Además de eso, también se ha querido estudiar el desarrollo de estos dos sistemas desde la mediana infancia hasta la adultez, enfocado principalmente en el reconocimiento de palabras. Para ello, esta tesis doctoral se ha dividido en tres partes empíricas.

En la primera parte empírica, se examinaron las trayectorias de desarrollo de los sistemas magnocelulares y parvocelulares. A día de hoy, como se ha mencionado antes, hay pocos estudios que hayan examinado la maduración de estas dos vías del sistema visual y los resultados en este sentido son mixtos. Por tanto, el objetivo principal de esta parte empírica fue analizar si las vías magnocelular y parvocelular estaban involucradas en el proceso de lectura típica. Los resultados mostraron que el sistema parvocelular parece desarrollarse antes que el sistema magnocelular. Además, también vimos que el procesamiento de palabras con sesgo magnocelular y parvocelular estaba asocian con la edad en los niños, mientras que esta asociación no estaba presente en los adultos (tanto para los tiempos de reacción como para la exactitud).

En la segunda parte empírica, se examinaron las contribuciones magnocelulares y parvocelulares de la corteza visual a la lectura y al reconocimiento de imágenes. Aunque existen teorías bien aceptadas sobre el papel de estas principales sistemas visuales en el reconocimiento de objetos o imágenes, su participación funcional en el reconocimiento de palabras ha recibido una atención considerablemente menor. En esta parte empírica buscamos abordar esta brecha en la investigación examinando los correlatos funcionales del reconocimiento de palabras e imágenes a lo largo de estas vías dentro de la corteza visual. Los resultados mostraron un gradiente funcional en la activación de la corteza visual, donde las regiones visuales posteriores se reclutaron con más fuerza para el procesamiento de los estímulos con sesgo parvocelular, mientras que las regiones más anteriores se implicaron en mayor medida en el procesamiento de estímulos con sesgo magnocelular. También se vio que la conectividad funcional entre las regiones visuales dependía de la distancia física y parecía estar segregada, observando conectividades más fuertes dentro de las agrupaciones de estas regiones más posteriores y más anteriores. En conjunto, estos hallazgos nos proporcionaron evidencia convergente de una división funcional de trabajo en la corteza visual en función de las propiedades parvocelulares y magnocelulares de los estímulos.

Por último, en la tercera y última parte empírica, se examinó la participación de las vías magnocelulares y parvocelulares en la red de lectura. Existen varias teorías que explican el proceso de lectura y su red, pero todavía hay poca evidencia sobre la contribución de estas dos vías principales del sistema visual en este proceso cognitivo. El objetivo principal de esta parte empírica fue analizar si las vías magnocelulares y parvocelulares estaban involucradas en los procesos de lectura. En dicha parte empírica, pudimos ver que las regiones del vOTC, el mOTS y pOTS, estaban más involucradas en el procesamiento de palabras que de imágenes y que el IFG estaba implicado en el procesamiento semántico de los estímulos. Además, los resultados de conectividad funcional y estructural mostraron fuertes

asociaciones entre las habilidades de lectura de los participantes y la conectividad funcional durante el procesamiento de palabras versus objetos. En concreto, se ha podido demostrar que la vía parvocelular, que de antes se sabía que está ligada a la ruta ventral, está implicada en el procesamiento de palabras en la ruta ventral, lo que implica que se encarga de procesar la parte semántica de las palabras. Por otro lado, y en línea con la literatura previa, la vía magnocelular participa en el procesamiento de palabras en la ruta dorsal, implicándose en este caso del procesamiento fonológico de las palabras, junto con el procesamiento semántico.

En resumen, los hallazgos de la presente tesis doctoral proporcionan evidencia del rol crucial de las vías magnocelulares y parvocelulares en el reconocimiento visual al igual que en la lectura. Hasta ahora no había existido ningún estudio que hubiera afrontado esta cuestión de manera que abarcase dos cuestiones que, a nuestro juicio, son importantes; por un lado, el examen del desarrollo de las dos vías principales del sistema visual teniendo en cuenta todas sus características y su contribución en el reconocimiento visual de palabras e imágenes, y el reconocimiento visual de palabras y el rol que tienen dichas vías visuales en él.

Con esta tesis doctoral hemos podido ver que el ritmo del desarrollo de las vías magnocelulares y parvocelulares en lectura es distinto, siendo el desarrollo de la vía magnocelular más lento. Aunque hemos encontrado un gradiente en el perfil de activación de la corteza visual en función de los dos sistemas de visión, no se encontraron diferencias entre las activaciones de los dos tipos de estímulos, esto es, las palabras e imágenes. Esto sugiere que el procesamiento de la lectura y la contribución de las vías magnocelulares y parvocelulares empieza en regiones más anteriores que la corteza visual, como son el vOTC o las regiones del IFG. Es importante resaltar también que en el presente trabajo se emplea un método multimodal mediante el uso de las últimas técnicas más innovadoras de neuroimagen.

Esto permite añadir un factor novedoso e importante para lograr avances científicos, permitiendo contrastar los resultados con el uso de diferentes técnicas y análisis, lo cual muestra la convergencia y solidez de los resultados obtenidos.

2. Abstract

The magnocellular and parvocellular systems are major visual recognition pathways, with distinct histological and physiological properties. Despite their critical role, there is limited evidence on the specific contributions of these visual pathways to visual recognition and to word reading, as well as in regard to their developmental trajectories. This doctoral dissertation is aimed at examining the involvement of the magnocellular and parvocellular pathways in reading over development (Empirical Part I), in visual cortex regions during reading and visual recognition (Empirical Part II) and in the two main reading circuitries, the ventral and dorsal routes (Empirical Part III). Our results reveal i) a more protracted maturation of the magnocellular pathway compared to the parvocellular pathway from middle childhood to adulthood, ii) a functional division in the visual cortex as a function of the parvocellular and magnocellular properties of the stimuli, and iii) that both the magnocellular and parvocellular pathways are involved in reading processes, with the parvocellular pathway mainly contributing to the ventral reading network and the magnocellular pathway mainly contributing to the dorsal reading network. These results are discussed in relation to their potential implications for typical and atypical reading, as well as in regard to the further research needed to better understand the contributions of these pathways to the Neurobiology of Reading.

3. Visual pathways

We are so familiar with seeing, that it takes a leap of imagination to realize that there are problems to be solved. But consider it. We are given tiny distorted upside-down images in the eyes, and we see separate solid objects in surrounding space. From the patterns of stimulation on the retina we perceive the world of objects and this is nothing short of a miracle.

Richard L. Gregory, Eye and Brain, 1966

Vision or the sense of sight is one of the five senses that humans have to receive information from the external world. How the information received by humans through the eyes is processed in the brain? How is the brain able to distinguish colors? Or to differentiate the form of the objects that we see? And to perceive motion? The images that our eyes see passes through the cornea, the pupil and the lens to reach the retina, the sensory organ of the eye and where the light is converted into an electrical signal that are sent through the optic nerve to the brain for processing it. All these signals and information is processed through the two main parallel visual hierarchical pathways, which in turn interact with each other, known as the magnocellular and parvocellular pathways. These two visual systems have different histological and physiological properties and, subsequently, differential functional roles. These pathways account for most of the axons that leave the retina and the perceived vision, as demonstrated by loss of vision when these pathways are destroyed (Schiller et al., 1990; Silveria & Perry, 1991). There is also a third pathway, known as koniocellular, that conveys much fewer inputs compared to the magnocellular and parvocellular projections which constitute the vast majority of inputs into V1 (Callaway, 2005; Casagrande, 1994; Hendry & Reid, 2000).

At the histological level, the segregation of visual information starts from the very beginning of the visual processing, in the retina. The retina is the most inner layer at the part of the eye. It entails ten layers of neurons interconnected by synapses. The primary cells that receive information in the retina are called photoreceptor cells. There are two types of photoreceptor cells, rods and cones. Rods function usually under scopotic conditions, at lowest-level of light. On the other hand, cones work under photopic conditions; they mainly contribute to day-time vision. However, the phototransduction that takes place in all these photoreceptor cells is similar. The information is projected from the photoreceptors into three types of interneurons, bipolar, horizontal and amacrine cells. The interneurons, apart of transmitting information from the photoreceptors to the ganglion cells, the output cells of the retina, they combine signal from different photoreceptors in order to have precise spatial and temporal patterns of the light that stimulates the retina. As mentioned, the output cells of the retina are called ganglion cells. There are two types of ganglion cells, parasol-magnocellular cells (also called magnocellular cells), which are the neurons that carry information in the magnocellular pathway and midget-parvocellular cells (or parvocellular cells), the neurons responsible of transmitting information through the parvocellular pathway. The axons of the ganglion cells conform the optic nerve, which projects the information to the lateral geniculate nucleus (LGN), the nucleus of the thalamus that is responsible of visual processing. Once the information reaches the thalamus, the information is projected to the visual cortex, and later into higher-level areas in order to process a given visual image.

3.1 Anatomical properties

The magnocellular cells, as mentioned before, transmit the information from the retina to the LGN. These magnocellular ganglion cells receive inputs from multiple large diffuse bipolar cells. The parvocellular pathway, in contrast, has its origin in parvocellular retinal ganglion cells, and they usually receive inputs from a single bipolar cell. Typically each

neural cell type covers completely the retina, so that the visual properties of every specialized neural cell are represented in the whole visual field. The magnocellular ganglion cells cover the retina with approximately a coverage factor of 1 (the coverage factor refers to the number of cells of a given type at each retinal point), similar to the parvocellular ganglion cells. However, the density of magnocellular cells is smaller compared to the parvocellular ganglion cells. Although single magnocellular and parvocellular cells have similar spatial resolution (Blakemore & Vital-Durand, 1986; Crook et al., 1988), due to the high sensitivity to luminance contrast of the magnocellular cells, the parvocellular cells have a higher spatial resolution.

Although the diameter of the receptive fields increases for both magnocellular and parvocellular ganglion cells as one move away from the fovea, the diameters of the magnocellular cell receptive fields are larger than the diameter of the parvocellular cell receptive fields as the parvocellular cells receive input from a single cone (Croner & Kaplan, 1995).

The human LGN consists of 6 layers, numbered from the bottom (1) to the top (6). The layers 1, 4 and 6 receive information from the contralateral eye, while the layers 2, 3 and 5 process information from the ipsilateral eye. The magnocellular ganglion cells project to the deepest layers (1-2) of the LGN, whereas the parvocellular ganglion cells project to the superficial layers (3-6) of the LGN (Leventhal et al., 1981; Perry et al., 1984). The magnocellular information from the LGN is projected primarily into layer 4C***a*** of the primary visual cortex (V1), as well as to layer 6 (the information from this layer is projected back to the LGN). On the contrary, the parvocellular-ganglion cells send synapses to layers 4A and 4C*b* of the V1 (Callaway, 2005; Casagrande, 1994; Hendry & Reid, 2000; Perry et al**.,** 1984) (see Figure 1).

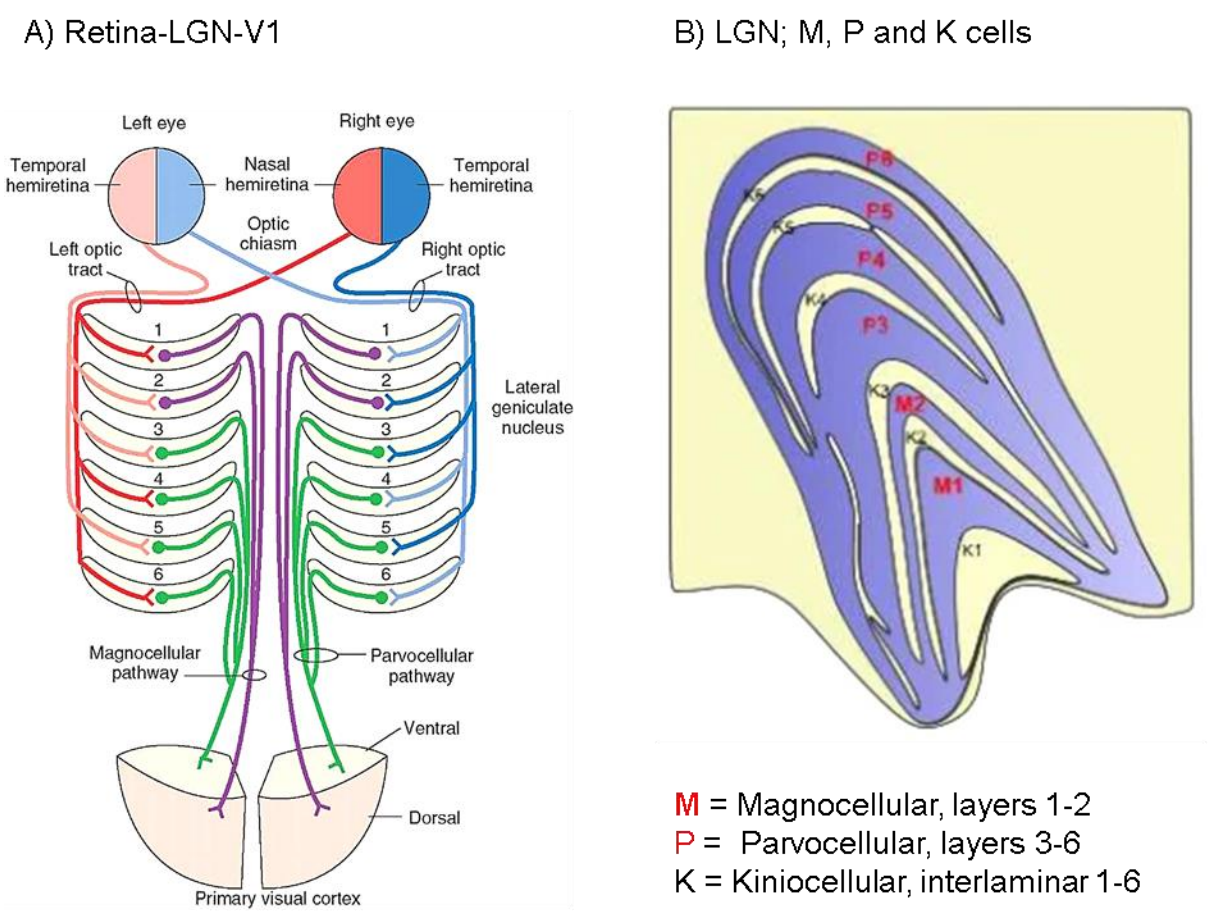

Figure 1: Main visual pathways from the retina to primary visual cortex (V1) and main layers within the LGN of the thalamus. A) Schematic representation of connections between left and right eye with the lateral geniculate nucleus (LGN) of the thalamus via anterior radiations, and between the LGN magnocellular (in purple) and parvocellular (in green) layers and the V1 via optic radiations. B) Schematic representation of LGN magnocellular (1-2) and parvocellular (3-6) layers and interlaminar kiniocellular cells (adapted from Casagrande et al., 2007).

From V1, magnocellular neurons project to the thick-stripe regions of the secondary visual cortex (V2), continuing to the motion-processing region MT+/V5, and then to the higher-order motion and attention regions in the temporal and posterior parietal cortex. The magnocellular projections comprise most of the dorsal, or "where", visual stream, which subserves spatial vision, motion detection, attention, and action planning (Goodale & Milner, 1992; Ungerleider & Mishkin, 1982). Parvocellular neurons project to V2, V4, and later to inferior temporal cortex (IT). The parvocellular pathway is part of the ventral, or "what",

visual stream (Goodale & Milner, 1992; Ungerleider & Mishkin, 1982), although it also receives some inputs of the magnocellular pathway (Merigan & Maunsell, 1993).

3.2 Physiological properties

In 1968, Gouras found that there were, on the one hand, cells responding in a tonic sustained fashion and, on the other hand, cells responding phasically to light. Later studies discovered that magnocellular ganglion cells were the ones with phasic responses and the parvocellular ganglion cells were the ones having tonic responses. The contrast gain depends on the photon flux over the receptive field (Enroth-Cugell & Shapley, 1973a, b), and magnocellular ganglion cells collect more flux compared to parvocellular ganglion cells (Croner & Kaplan, 1995; Kaplan & Shapley, 1986; Shapley, Kaplan & Soodak, 1981). However, it is yet not clear whether the contrast gain depends only in the receptive field size or there are other processes that are in charge of the high contrast gain of magnocellular cells (see Figure 2).

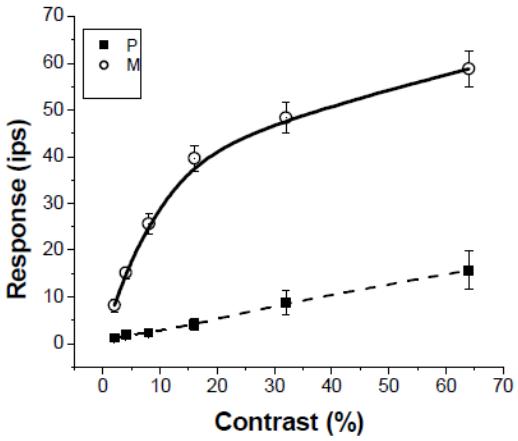

Figure 2: The luminance contrast gain of magnocellular and parvocellular cells (adapted from Kaplan, 2004).

Lee and colleagues (1989) found that when a large portion of magnocellular cells are stimulated, the surround of the receptive field of these cells produces nonlinear responses, as it happens for the parvocellular cells (Benardete et al., 1992; Benardete & Kaplan, 1997a, b,

1999). On the other hand, Shapley and Victor (1978) discovered in cat magnocellular cells *contrast gain control*, which is a type of nonlinearity, whereas in parvocellular cells this linearity was not present. This nonlinearity leads to attenuated responses to low temporal frequencies at high contrasts.

Light adaptation, as contrast gain, depends on the size of the receptive field of neural cells (Enroth-Cugell & Shapley, 1973), and it affects the dynamics of the response of these cells (De Lange, 1958; Dodge et al., 1968). Some studies showed that magnocellular cells are more transient than the parvocellular cells at a given luminance (Purpura et al. 1988, 1990). They also demonstrated that as the luminance is lower, the steady state contrast gain is lower for both cell types (i.e., magnocellular and parvocellular cells). However, and as it occurs for the contrast gain, it is not clear if there are other factors that contribute to this property (see Figure 3).

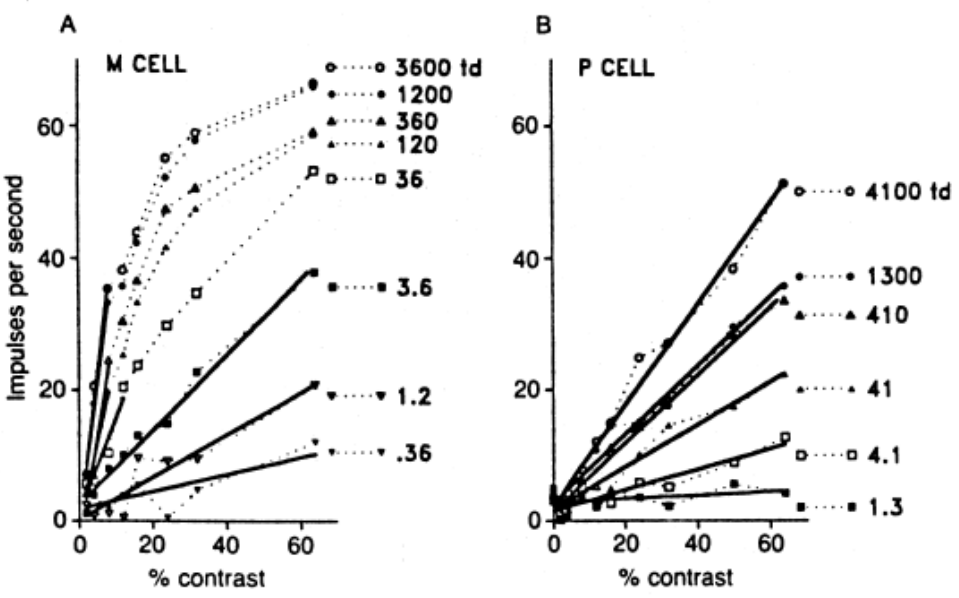

Figure 3: Light adaptation of A) magnocellular cells and B) parvocellular cells (adapted from Kaplan, 2004).

Regarding low light vision (scotopic), the gain of all retinal ganglion cells (magnocellular and parvocellular) decreases as luminance decreases (see Figure 3). At all luminance levels

the gain of magnocellular cells is higher than the gain of the parvocellular cells. Furthermore, at spontaneous activity, magnocellular cells can process visual field patterns, whereas parvocellular cells cannot process them (see Figure 4).

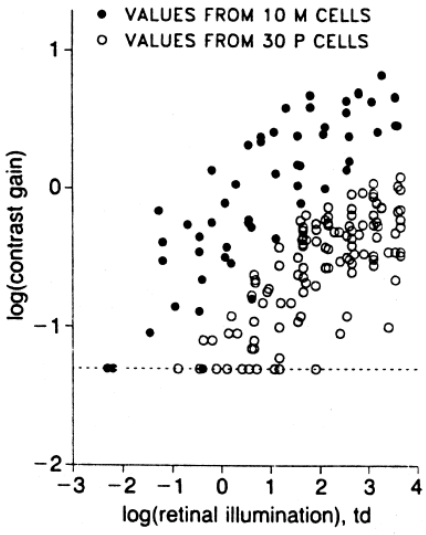

Figure 4: Light adaptation of A) magnocellular cells and B) parvocellular cells (adapted from Kaplan, 2004).

In 1966, Wiesel and Hubel stated that cells with antagonistic center-surround receptive fields had to represent space and color. In that study, investigating macaque LGN cells, they found three types of cells: cells that were chromatically and spatially opponent, cells that were chromatically but not spatially opponent, and cells that were spatially but not chromatically opponent. The magnocellular cells were mostly of the type described last or cells that were spatially but not chromatically opponent, and the parvocellular cells were mostly of the first described ones or cells that were chromatically and spatially opponent.

Table 1: Summary table of properties of magnocellular, parvocellular and kiniocellular cells.

	Type of cells		
Properties	**Magnocellular**	**Parvocellular**	**Kiniocellular**
Receptive field size	large	small	large
Luminance contrast gain	high	low	high
Response to light	tonic	phasic	phasic
Cell size	large	small	large
Response to color	insensitive to color when luminance balanced	color sensitive	sensitive to short wavelength (blue) color
Contrast sensitivity	high	low	?
Spatial frequency responses	low	high	?
Temporal frequency responses	high	low	?

3.3 Functions

The magnocellular dorsal stream is critical for detecting spatial relationships as well as rapid changes, which allows this dorsal network to be sensitive to motion (Ungerleider & Haxby, 1997). It has also been suggested that the magnocellular pathway is the dominant visual pathway for text perception (Chase et al., 2003) or reading (Conlon et al., 2004), indicating that shared neural structures within this pathway may play a role in both movement processing and visual language processing. Word recognition performance and magnocellular-related abilities have been positively correlated (Ben Shachar et al., 2007, Laycock et al., 2009, Olulade et al., 2013, Joo et al., 2017). Besides that, Levy et al. (2010) showed that coherent motion detection and word recognition present an advantage of the right visual field. Such advantage it is known to be connected with the "verbal" left hemisphere, indicating that magnocellular pathway may be involved in the language areas of the left hemisphere during visual language processing. Chouake et al. (2012) also found that

training on magnocellular-related tasks (e.g., watching motion versus stationary dots) improves visual word recognition.

In addition, research on developmental dyslexia - a neurobiological reading disorder despite normal intelligence, adequate education and lack of obvious sensory or neurological damage (American Psychiatric Association, 2013; World Health Organization, 2008), has also supported to some extent the theory that the magnocellular pathway is involved in this reading disability (Facoetti et al., 2012, Gori et al., 2015; Stein, 2001). This theory is known as the magnocellular–dorsal (M–D) theory of developmental dyslexia (Livingstone, Rosen, Drislane, & Galaburda, 1991; Stein & Walsh, 1997), which stems from the observation that a high percentage of reading disabled children have a weakened or abnormal magnocellular input to the dorsal visual pathway, causing a dysfunction of the main fronto-parietal attentional network.

The parvocellular pathway is color sensitive, has lower contrast sensitivity, is responsive to higher spatial frequencies and lower temporal frequencies, and presents sustained responses (Merigan, Katz, & Maunsell, 1991). In V1, the parvocellular pathway is responsible of processing orientation and retinotopic location (Hubel & Wiesel, 1962). In more higher-cortical regions, such as mid- and anterior inferior temporal cortex, the parvocellular pathway neurons become sensitive to more abstract, viewpoint-, location-, and illumination-invariant properties (Gallant et al., 1996; Qiu & von der Heydt, 2005; Tanaka, 1996, 1997; Vogels et al., 2001). The parvocellular pathway is also involved in recognizing objects (Bar et al., 2006a; Bar et al., 2001; Grill-Spector et al., 2001; Ishai et al., 2000; Logothetis & Sheinberg, 1996; Malach et al., 1995; Tanaka, 1996), scenes (Aguirre et al., 1998; Epstein & Kanwisher, 1998), and faces (Allison et al., 1994a; Allison et al., 1994b; Kanwisher et al., 1997; Puce et al., 1995).

In regard to reading processes, less evidence exits regarding the involvement of the parvocellular ventral pathway in this cognitive function. Although Farrag et al., (2002) found that children with dyslexia had deficits in both magnocellular and parvocellular pathways, the majority of the studies conducted did not find implications of the parvocellular pathway in reading (Chase et al., 2004; Chouake et al., 2012).

3.4 Kiniocellular pathway

The kiniocellular visual pathway is originated with the bistratified retinal ganglion cells (Hendry & Yoshioka, 1994). These ganglion cells have their end between the magnocellular and parvocellular layers in the LGN. The kiniocellular ganglion cells projects information to the layers 2 and 3 of V1. However, the number of kiniocellular cells is much fewer in LGN and V1 compared to the magnocellular and parvocellular cells (Callaway, 2005). The kiniocellular cells respond to various spatial frequencies, are sensitive to short-wavelength (blue) light, and have higher luminance contrast gain than the parvocellular cells (Hendry & Yoshioka, 1994; Hendry & Reid, 2000; Norton & Casagrande, 1982). The conduction of these cells is slow, similar to the parvocellular cells (Hendry & Yoshioka, 1994; Hendry & Reid, 2000; Livingstone & Hubel, 1988; Merigan & Maunsell, 1993). However, it is still not clear the role of these cells in visual recognition due to their diverse anatomical and functional characteristics (Kaplan, 2004).

4. Visual recognition

4.1 Visual recognition in the visual cortex

Visual information is processed in the area of the cerebral cortex called visual cortex, which is located in the occipital lobe. Human visual cortex includes the entire occipital lobe and extends significantly into the temporal and parietal lobes. The occipital lobe constitutes about 20% of cortex. The visual cortex receives the sensory input through the LGN of the thalamus, which in turn receives information from the retina.

The visual cortex extends to both hemispheres, and it is organized into visual field maps: nearby neurons have receptive fields at nearby locations in the image. By defining the unique cytoarchitectonic structures, connectivity, functional processing and visual field topography, the primate visual cortex has been parcellated into multiple visual areas (Felleman & Van Essen, 1991; Van Essen et al., 2001; Van Essen et al., 1984; Van Essen, 2003, Van Essen et al, 1990). Although the first evidence regarding visual areas comes from research with primates, with more than thirty areas being identified in macaque monkeys, nowadays there is solid evidence describing more than ten human visual areas.

In the last century, an ophthalmologist called Inouye, and 10 years later, a neurologist called Holmes, found strong associations between visual field deficits and the location of lesions within V1 (Fishman, 1997; Holmes,1918; Inouye, 1909; Teuber et al., 1960). This work helped to define the visual field map in V1. They found that the left hemisphere receives signals from the right hemifield (i.e., one half of visual space), whereas the right hemisphere receives signals from the left visual field. They also found that the central fovea is represented over a larger fraction of cortical surface than a comparable extent of the peripheral visual field. In electrophysiological studies using rabbits, cats and squirrel monkeys researchers uncovered a second map, called V2 that is adjacent and surrounding to V1 (Cowey, 1964; Talbot & Marshall, 1941; Talbot, 1940, 1942; Thompson et al., 1950;

Tusa et al., 1978). Two decades later, another two visual regions were detailed, V4, which is adjacent to the early visual regions, and the region MT+/V5, which is more distant to the early visual cortex regions (Allman & Kaas, 1971). Since then, several investigations of visual regions have been reported, and strong progress has been made since the introduction of functional magnetic resonance (fMRI) and novel data-analysis methods which allows to measure the intact human visual cortex structurally and functionally (DeYoe et al., 1996; Engel et al., 1994; Engel et al., 1997; Ogawa & Lee, 1990; Ogawa et al., 1990, 1992; Sereno et al., 1995).

The visual field map is a visual area with a complete representation of visual space, where neurons that represent adjacent locations on the retina (and visual space) are also adjacent in cortex. Visual field maps are defined with respect to the fixation point. Stimuli to the right of a central fixation are in the right visual field, stimuli to the left of a central fixation are in the left visual field; stimuli above fixation are in the upper field, and in contrast stimuli below fixation are in the lower field. Although the visual field is fixed with respect to the retina, it shifts with eye position, so they are also known as retinotopic maps (Wandell et al., 2007).

Visual field maps are usually measured using fMRI, where the stimulus location that causes the largest response at each cortical position is measured. The most common measuring technique is called the traveling-wave method (TWR) where ring and wedge stimuli are used to measure these visual field maps (DeYoe et al., 1996; Dumoulin et al., 2003; Engel et al., 1997; Sereno et al., 1995; Wandell et al., 2005; Warnking et al., 2002). In order to measure the eccentricity, a series of contrast patterns in concentric rings at different diameters are presented. To estimate the most effective angle, the responses to a series of contrast patterns comprising wedges that rotate around the fixation point are interpolated. With these two measures, it is possible to have the polar coordinates of a visual field, which is the most effective visual field position.

4.1.1 Visual regions

The regions of the visual cortex that have been studied in this thesis will be explained in detail below. The order in which they are introduced is from the more posterior regions to the more anterior regions of the visual cortex.

The posterior regions of the visual cortex, also known as early visual areas (typically V1 and V2), contain a complete eccentricity and polar angle map (De Yoe et al., 1996, Sereno et al., 1995). The V1 that is extended in the calcarine cortex receives direct inputs from the LGN. The areas V2 and V3, that encircles the area V1, occupy a side of the cortex (1-3 cm). They both contain discontinuous hemifield maps, since they are divided along the horizontal meridian. Early retinotopic areas V1, V2, and V3 show a high degree of retinotopy, with eccentricity representations run in register. The eccentricity map begins at the large foveal representation on the ventral-lateral surface near the occipital pole, and increasingly peripheral stimuli are represented at increasingly anterior positions along the medial surface. In addition to the parallel eccentricity maps, the vertical meridian representations of V1/V2 are adjacent to one another, as are the horizontal meridian representations of V2/V3. The relationship between cortical position and eccentricity is approximated by a simple exponential function (Dougherty et al., 2003; Engel et al., 1997; Qiu et al., 2006, Wandell et al., 2007). However, for V3 there are different points of view. On the one hand, Van Essen and colleagues proposed to divide V3 into a dorsal map V3 and a ventral map V3, since they found anatomical differences in the surrounds of V2 between the dorsal and ventral quarterfield representations (Burkhalter et al., 1986). On the other hand, studies in macaque revealed that the connectivity between V3 and the ventral posterior (VP) area is similar, suggesting that V3 is a single functional area (Lyon & Kaas, 2002; Wandell et al., 2005; Zeki, 2003) (see Figure 5).

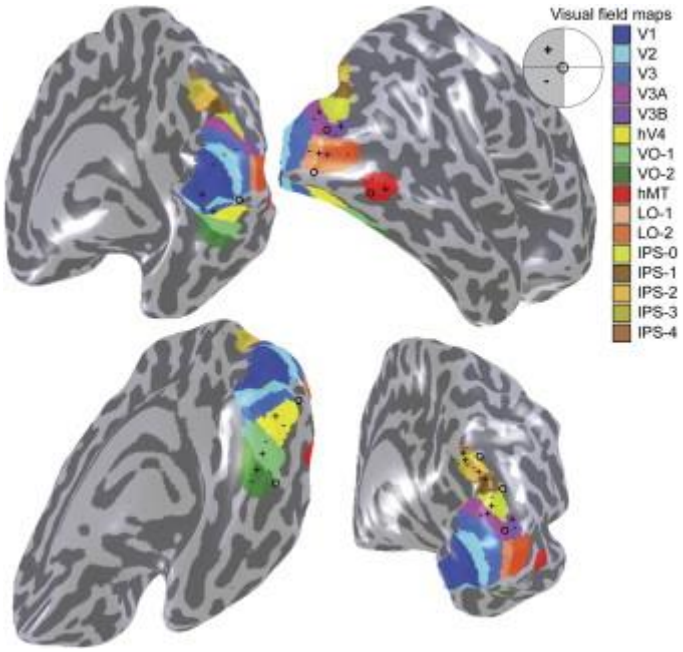

Figure 5: Position of the visual cortex areas in an inflated rendering of the cortical surface of a right hemisphere (adapted from Wandell et al., 2007.)

V1, V2, and V3 receive inputs from both the magnocellular and parvocellular pathways (Rauschecker et al., 2011). Indeed, in monkeys, it has been shown that the magnocellular pathway project mostly to the occipital areas of the dorsal stream, beginning with the visual area V1, going through V2, then to V3, and the motion-processing region MT+ (also known as V5) and to the posterior parietal cortex. The parvocellular pathway project to the occipital areas of the ventral stream, beginning with the visual area V1, going through V2, V3, and then to the color processing region hV4, and lastly to the complex form analysis regions in the inferior temporal (IT) cortex. It has been demonstrated in several studies that V1 responds to stimulus orientation (Pascual-Leone et al., 1995), is color sensitive (Wandell et al., 1998), sensitive to motion (Zeki & Shipp, 1988), to contours (Toetell et al., 1996, 1997; Repass et al., 1997) and to low contrasts (Toetell et al., 1995). The V1 visual field representation is replicated in V2 and V3. However, other studies in humans, such as the Musel et al. (2013), have observed that low spatial frequencies (LSF, associated with the magnocellular pathway) activate V1, whereas high spatial frequencies (HSF, associated with the parvocellular

pathway) activate V2 and V3. Castelo-Branco and colleagues also reported that these early visual areas are in charge of local motion processing (Castelo-Branco et al., 2002).

hV4 is a hemifield map that is adjacent to the ventral portion of V3. The reason why an 'h' is added to the V4 region is to differentiate it from the analogous region in macaques, since there are substantial differences (Brewer et al., 2002, 2005). hV4 eccentricity is parallel to the early visual regions V1, V2 and V3, although shorter than V3 (Tyler et al., 2005), and it has a lower retinotopic specificity. Studies with clinical patients found that the damage in ventral occipitotemporal cortex (vOTC) is correlated with color vision loss (achromatopsia) (Damasio 1980, Pearlman 1979, Zeki 1990), which led to suggest that there is a color center in the human brain. Later, several studies found that the region hV4 (Bartels & Zeki 2000, Lueck et al. 1989, McKeefry & Zeki 1997) was more strongly engaged to colored patterns compared to luminance-defined stimuli.

The area called lateral occipital complex (LOC), which includes subregions LO1 and LO2 is located between the dorsal part of visual area V3 and visual area MT+/V5. Each of these regions contains a topographic representation of the contralateral visual hemifield. Although it was thought that LOC is not retinotopically organized (Grill-Spector et al., 1998b; Tyler et al., 2005a), Larsson and colleagues demonstrated the opposite (Larsson et al., 2006) (see Figure 5).

It is known that the LOC is more strongly engaged to images of familiar or unfamiliar objects compared to non-object controls (Grill-Spector et al. 2001, Kanwisher et al. 1996, Malach et al. 1995) and specially that LO2 is significantly more strongly recruited to objects than LO1 (Larsson et al., 2006). Furthermore, LO1 region tends to show orientation-selective responses to simple grating stimuli, whereas LO2 does not. LOC has also been demonstrated to be involved in motion boundaries (Dupont et al., 1997; Van Oostende et al., 1997; Larsson

et al., 2006), illusory contours (Mendola et al., 1999), boundaries defined by depth structure (Tyler et al., 2006), and second-order gratings (Larsson et al., 2006).

The MT+/V5, the homolog of macaque MT also have two hemifield representations, labeled TO1 and TO2 (Amano et al., 2009). This region was identified using moving stimuli versus stationary stimuli and it has high contrast sensitivity (Tootell et al. 1995; Watson et al. 1993; Zeki et al. 1991) and it is located at the temporo-parietal occipital junction (Tootell et al. 1995b, Watson et al. 1993) (see Figure 5). It is well known that this region contains direction-selective neural populations (Huk et al., 2001, Tootell et al., 1995a). Rees and colleagues found that MT+/V5 activation increases linearly with the coherence of motion by comparing coherent versus incoherent motion of light points, where dots move independently (Rees et al., 2000).

4.2 Visual recognition models

Recognizing the objects we are looking at, discriminating familiar faces and reading are some of the activities that we perform on a daily basis where the visual system plays a crucial role. These operations are really complex, not only in regard to the cascade of neural processes that they entail and that need to be orchestrated in an organized subsequent manner, but also in its main initial step: visual recognition.

The first models of visual recognition were commonly viewed as a feedforward, bottom-up processes. These models established that visual information is processed sequentially with increasing complexities from lower- to higher-level cortical areas (Grossberg, 1982; Kosslyn, 1994). Specifically, the visual cortex regions are activated hierarchically, starting from the V1 until the information reaches high-level visual cortical areas. The visual information is then separated into a dorsal and a ventral stream. The ventral stream reaches the temporal

lobe. In regard the dorsal stream, there is still debate about which regions reaches in its final steps (Felleman & Van Essen 1991).

Due to the complexity of the visual information, there are studies highlighting that visual recognition cannot be fully explained by bottom-up processes (Bullier, 2001; Lamme & Roelfsema, 2000; Mumford, 1994). According to Bullier and colleagues, information must be exchanged between distant regions, and for that, feedback connections are essential. As stated by their model, the visual input from the magnocellular layers of the LGN is first processed in the parietal cortex. Then, the processed information is sent back to early visual cortex regions, which will be necessary for further computations in the parvocellular pathway in the inferotemporal cortex.

There are several studies that emphasize that to facilitate the bottom-up processing, top-down information must be activated and available to the low-level areas before recognition is completed. In 1980, Grossberg indicated that the efficient representation of the visual information is achieved by means of the correspondence between top-down and bottom-up information through a pattern-matching algorithm. The neural signal is amplified once the prediction patterns are matched with the sensory-based representations. In contrast, when the predicted patterns and sensory-based representations do not match, the signal is further extended and a new pattern must be generated, which is a combination of the initial prediction and the updated ones (Grossberg, 1980). In 1992, Mumford proposed a model in which multiple bottom-up and top-down circuits transfer information through adjacent levels of the hierarchy. These circuits contain information that has been already processed as well as the input that needs to be processed in lower-level regions or in the following circuits. According to this model, both types of bottom-up and top-down circuits are used for lower-level visual processes, as well as for higher-level processes (Mumford, 1992). According to

Ullman's (1995) visual theory, visual input is processed in parallel bottom-up and top-down streams. Both streams activate multiple candidate interpretations, and the overall representation is achieved once the representations are matched and the bottom-up stream and top-down stream meet (Ullman, 1995).

Although the models described above discuss some of the mechanisms involved in processing visual information, they do not specify how top-down predictions occur in different brain regions and how the information is transferred through the different cortical regions involved. In this vein, Moshe Bar proposed a theory in 2003 proposing a mechanism for fast triggering of top-down facilitation. According to this theory, a rough part of the visual input, mainly composed by LSF, is rapidly projected from early visual regions to the orbitofrontal cortex (OFC) (see also Barcelo et al., 2000). LSF images are enough to activate the initial predictions of the objects that are being recognized. Afterwards, visual representations from object processing in the ventral temporal cortex are activated by these predictions; so that the complete visual recognition is performed by biasing the bottom-up processes to concentrate on a small set of the most likely object representations (see Figure 6).

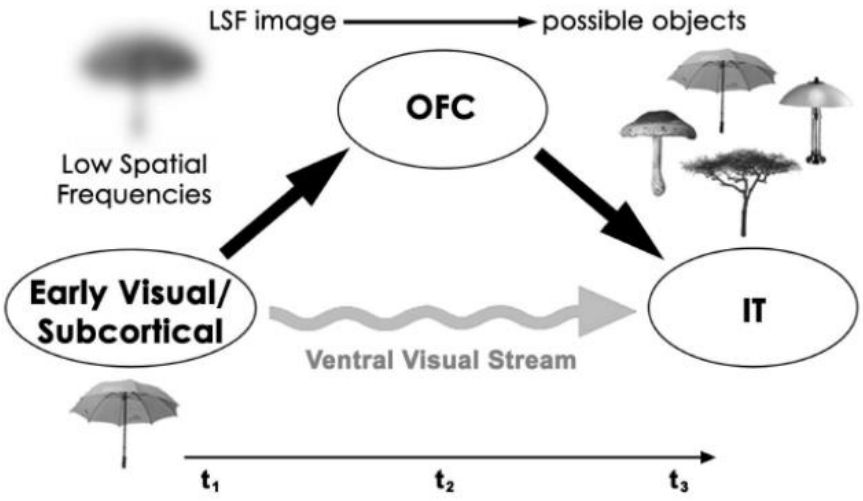

Figure 6: Bar's top-down facilitation model (adapted from Bar et. al., 2003)

Several studies have supported this theory by integrating fMRI (Kveraga et al., 2007) and magnetoencephalography (MEG; Bar et al., 2006) evidence, where they found that images with LSF information activated differentially OFC and also that this activation occurs early in the visual recognition process. For instance, to test if rapid activation of OFC was triggered by magnocellular versus parvocellular projections in the visual recognition of objects, Kveraga et al.'s (2007) fMRI study used stimuli designed to bias visual processing toward either the magnocellular or the parvocellular pathway. They found that OFC activity predicted the performance advantage for the magnocellular-biased stimuli, but not for the parvocellular-biased stimuli, whereas the opposite was true in the fusiform gyrus (FG). Also, using effective connectivity they showed that magnocellular-biased stimuli significantly activated pathways from occipital visual cortex to OFC and from OFC to FG, and that parvocellular-biased stimuli significantly activated a pathway from the occipital visual cortex to FG. These findings highlight the differential contribution of the main visual pathways to visual recognition, a critical process for object recognition, face identification, and reading.

In sum, visual recognition is a first necessary step for multiple activities we perform on daily basis. Although in the beginning it was thought that visual recognition was based on

bottom-up processes, later studies demonstrated that top-down facilitation is essential to complete the overall representation of the visual information that our brain processes.

5. Neurobiology of reading

Reading, and in more general terms, language, is one of the skills that differentiates humans from other animals. Through language, humans have the ability to communicate with each other. It is not yet clear when humans started talking, although researchers have been researching it for decades. Modern humans arrived to Europe 42.000-45.000 years ago, while Neanderthals were still there and researches believe that one of the main differences between them was speech (Donald, 1991). However, writing and consequently reading are much more modern skills than speech, and they are dated approximately 4.000-5.000 years ago. Specifically, between 4.000 and 3.000 B.C, Sumerians used pictograms and counting methods for commerce purposes. On the other hand, Egyptian hieroglyphics date from 2.000 to 1.500 BC. In addition, around 1.700 BC started the first phonetic written system, which was the first step to link speech and external symbols. Moreover, around 850 B.C the first work of the Greek literature was written, *Iliad and Odyssey*, and 100 years later (750 B.C), they revised the Phoenician alphabet to include both consonants and vowels (Robinson, 2009).

On this matter, writing systems have been evolving along the social expectations and assumptions about reading (Finkelstein & McCleery, 2013). However, more or less until the last century, writing and reading were limited to the elite or the upper social classes. Given the importance of literate abilities, it was expanded to the point that nowadays is a fundamental part of Western societies, where we are constantly receiving and reading written messages in different media (e.g., advertisements, television, etc.) or by new technologies (e.g., mobile phones, computers, tablets, etc.), becoming the most important way of communication between humans in the XXI century.

Reading involves the visual recognition of a word and to link the orthography, its letter strings, to phonology, its corresponding units of speech, which means that the reader needs to represent the connections between the components of printed words and spoken words. Furthermore, it is necessary to access to the meaning of those words (i.e., semantics). Therefore, reading is a complex human ability that requires the interaction between visual, orthographic, phonologic and semantic systems.

5.1 Language models:

One of the first and most popular neurobiological models of language was proposed in the 19th Century based on neuropsychological research with patients, which was the main source of neurobiological information. This model, known as the Wernicke-Lichteim-Geschwind (WLG) model, states that Wernicke's area is involved in speech comprehension and Broca's area in speech production, while the white-matter fiber tract termed as the arcuate fasciculus is connecting both regions. This language model was widely used until new theoretical models were proposed in the 1980's, which were more focused on computational approaches and artificial intelligence, trying to model the existing behavioral data. Based on empirical evidence, two models in regard to reading processing were proposed: the Parallel Distributed Processing (PDP) model (Harm & Seidenberg, 1999; Plaut et al., 1996; Seidenberg & McClelland, 1989; Seidenberg, 2012) and the Dual Route Cascaded (DRC) model (Coltheart et al., 2001).

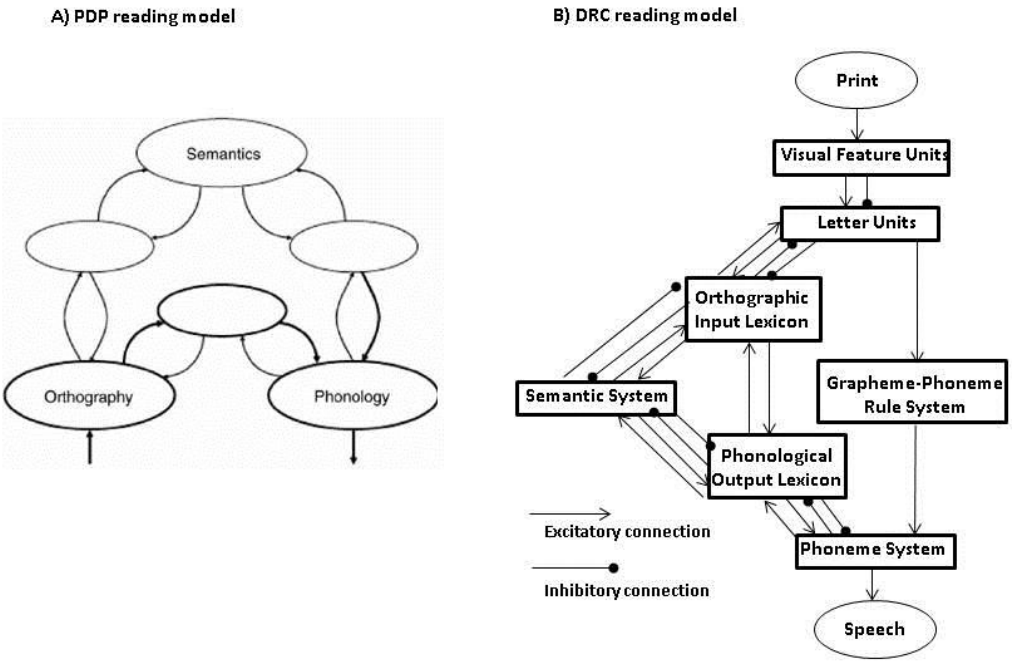

Figure 7: Theoretical models of reading from the Cognitive Sciences. A) PDP model of reading (adapted from Seidenberg & McClelland, 1989) and B) DRC model of reading (adapted from Coltheart et al., 2001).

On the one hand, the PDP account is a theory-driven approach because the model derives from a set of principles concerning neural computation and behavior. According to this model, a single parallel-distributed processing model is enough for the processing of lexical and semantic information. In the process of learning to read, the connections between the letters and the sounds needs to be modified, since when a printed word is not known, it cannot be decoded into its corresponding sound. This model proposed that the same connections, operating in parallel, are in charge of both familiar and novel words, and the changes in the letter-to-sound connections occur because of the exposure to print words (see Figure 7A).

On the other hand, the DRC model states that printed words are processed through two distinct and independent routes: the lexical and sublexical routes. The lexical route finds the

mental representation of printed words, and if it does, accesses its pronunciation. The sublexical route is used when the mental representation of a given word is not available. With the sublexical route, readers can pronounce a word using rules that relate units of spelling of sounds. Therefore, during the process of learning to read, the sublexical route is predominantly used, while when the words have already been learned, the lexical route is which readers rely on (see Figure 7B).

The PDP and DRC models were one of the first models describing the systems that were necessary to read as well as the systems to process the information. However, both of these two models make predictions at the neural level. Since the late 1980s, and thanks to new neuroimaging techniques such as magnetic resonance imaging (MRI), positron emission tomography (PET) or electroencefalografy (EEG), new models began to emerge. In this regard, Goodale and Milner (1992) proposed the dual-steam hypothesis of reading.

5.1.1 Dual-stream hypothesis

As mentioned above, Goodale and Milner presented the ventral and dorsal route model, which was originated in vision research. Based on this hypothesis, there are two routes, the ventral and the dorsal route that contribute differently to reading processes (Pugh et al., 2001; Schlaggar & McCandliss, 2007). Furthermore, based on neuroimaging results, they found that the engagement of regions along the ventral and dorsal pathways was different (Jobard et al., 2003; Saur et al., 2008). The ventral pathway, encompassing the vOTC and the *pars triangularis and orbitalis* regions in the inferior frontal gyrus (IFG), supports mapping orthographic-lexical stimuli onto semantic representations (Sandak et al., 2004). The dorsal pathway, including the posterior IFG *pars opercularis* region, posterior parietal cortex (PPC), and the superior temporal gyrus (STG), supports phonological processing. Thus, recognizing

a word that already pertains to our lexicon involves the ventral stream, while learning a new world is processed through the dorsal stream.

5.1.2 Standard reading model

Cohen, Dehaene and colleagues (2000, 2002) described the standard reading model, where they stated that regions along the vOTC are involved in the interpretation of word forms. They discovered that there was a word responsive region in the vOTC, which they called the visual word form area (VWFA). However, although there is an agreement that the VWFA is involved in the word recognition processes, there is still a debate among two theories of word recognition, that differ in whether word recognition in the vOTC is supported by rapid, automatic feedback from higher-order language areas or not.

One of these theories is the local combination detector model (Dehaene & Cohen, 2011), where the visual stimulus feeds into the lexical level hierarchically, and that the orthographic representations feed into higher-level linguistic representations in a bottom-up processing of information. In other words, the vOTC can detect the legality of words because there are neurons sensitive to brigrams, and that the VWFA can detect words even after processing the meaning. The other theory, called the interactive account model (Kronbichler et al., 2004; Price & Devlin, 2011) stated that is necessary a top-down influence from higher-level linguistic information to process the visual orthographic information. Specifically, Kronbichler and colleagues (2004) showed that the activation of the VWFA is associated with word frequency, which was further supported by later studies (Schuster et al., 2016; Yarkoni et al., 2008).

5.1.3 Reading models

In the last two decades, multiple reading models have been proposed, which, although they have a similar general structure, differ in subtle differences. Among them, there are

studies focused on speech comprehension or semantic memory. Within the studies of speech comprehension, Hickok and Poeppel (2000, 2004, and 2007) proposed a dual-stream model with a dorsal stream implicated in mapping sound onto articulatory-based representations, and a ventral stream involved in mapping sound onto meaning. On the other hand, Friederici (2002, 2011) described the auditory sentence comprehension, specifying a bilateral fronto-temporal network that underlay semantic, syntactic and prosodic processing. According to this theory, semantic information is processed in the left hemisphere, whereas prosodic information is right-lateralized. In 2011, they showed using diffusion-weighted imaging (DWI) that structural connections between temporal and frontal regions are mediated by different ventral and dorsal fiber tracts. Besides, there are other theories explaining a widely distributed network of semantics in the brain (Lau et al., 2008; Binder & Desai, 2011).

One of the main goals of this doctoral dissertation is to investigate the contributions of the magnocellular and parvocellular pathways to reading processes. To assure that the participants were actively participating in the reading tasks we utilized, and that the semantic component was involved in them, participants were asked to make semantic a specific judgment [natural (i.e., non man-made) or artificial (i.e., man-made) judgements]. Therefore, in the following subsections the two reading models highlighting semantic components will be explained, the model of semantics proposed by Lau and colleagues (2008) and Binder and Desai's (2011) model.

5.1.3.1 Cortical semantic processing model

Lau and colleagues (2008) proposed a model focused on semantic processing based on the localization of the N400 effect in the anatomical regions that are specialized for different aspects of semantic processing. The posterior temporal cortex, and specifically the left mid-posterior middle temporal gyrus (MTG) and the surrounding superior temporal sulcus (STS) and IT are involved in long-term storage of lexical representations. These regions mediate the

access to information associated with lexical representations. On the other hand, they stated that the anterior temporal cortex is implicated in sentence processing, rather than in word-list processing or sentences of pseudowords, which means that they integrate the lexical input into larger units under construction. Finally, the IFG shows different patterns of activation in the dorsal and ventral areas. Whereas the anterior ventral IFG is involved in controlling semantic retrieval, the mid-posterior IFG is in charge of selection processes more generally (see Figure 8).

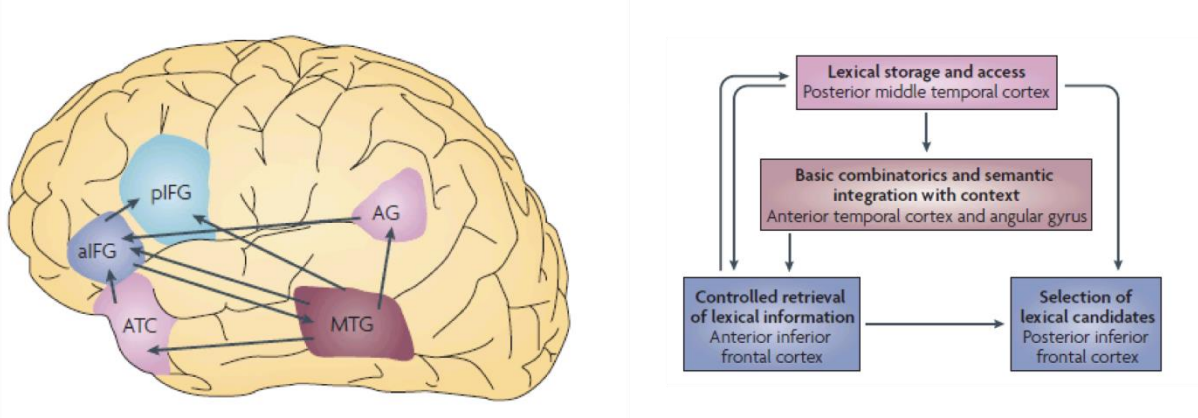

Figure 8: Cortical semantic processing model (adapted from Lau et al., 2008)

5.1.3.2 The cortical model for semantics

Binder and Desai (2011) proposed a model where semantic memory consists of both modality-specific and supramodal representations. According to this model, emotion, action and sensory systems (colored in yellow in Figure 9) sends the experiential inputs to the inferior parietal and high-level temporal regions (colored in red in Figure 9), where abstract representations of entity are stored. This stored information is selected and directed from dorsomedial and inferior prefrontal cortices (colored in blue in Figure 9). Finally the posterior cingulate gyrus and the precuneus area (green regions in Figure 9) are the interface between the semantic network and the hippocampal memory system, encoding meaningful events.

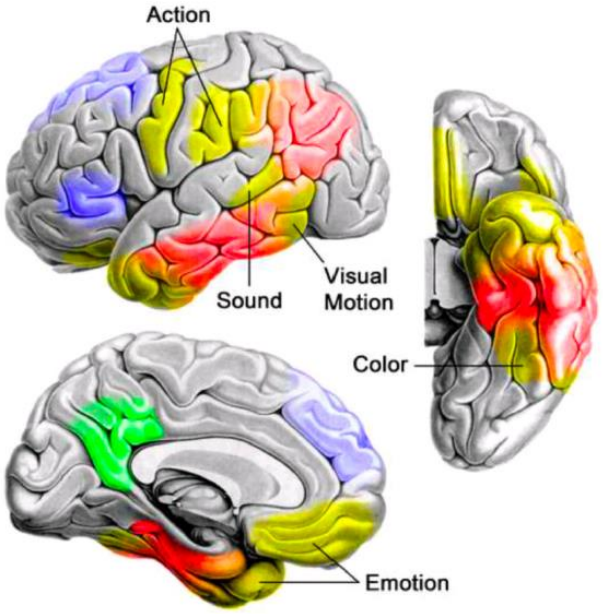

Figure 9: The cortical model for semantics (adapted from Binder and Desai, 2011)

6. Development of the main visual pathways

As it has been explained in previous chapters, the magnocellular and parvocellular pathways are the two major streams that process visual information. These two pathways have distinct physiological and histological properties, in addition to responding to different characteristics of visual stimuli. After doing an extensive search of the literature in regard the development of these two main pathways from childhood to adulthood, six studies have been found that will be reviewed in the following lines. The results of these studies are somewhat different, largely because there is great variation in terms of the experiment paradigm utilized in them, the techniques used, the age range used in the sample of the these studies or even the visual pathway in which the studies were focused on. The summary of these studies can be found in Table 2.

Table 2: Resume of developmental studies of the main visual pathways

Study	Materials	Technique	Sample	Main Results	Finding
Hammarrengen et al., (2003)	Eight vertical achromatic sine-wave gratings presented at two spatial frequencies and at four contrast levels.	Visual evoked potentials (VEPs)	Infants aged between 0 and 52 weeks	P1 component, related to the magnocellular pathway, appeared faster than the N1 component, which is related to the parvocellular pathway, continued growing until the end of the first year of life	Parvocellular delay in the first year of life
Dobkins et al., (1999)	Sinusoidal gratings projected at 5 different temporal frequencies that were either chromatically defined or luminance-defined.	Temporal contrast sensitivity functions (tCSFs)	3 to 4 month infants	tCSFs of luminance-defined stimuli are similar to the adult ones, and elevated above the chromatic tCSF in 3 months infants. In 4 months infants, chromatic tCSF starts to be more similar to the adult tCSFs, although it is still immature	Parvocellular pathway delay in the first year of life
Klaver et al., (2008)	Randomly moving point-light dots (RM), coherently moving dots that formed a 3D rotating object and static dots.	fMRI	5-6 years old children and 10 adults (20- 30 years)	In adults, RM stimuli activated more strongly the visual area V3a and middle temporal area compared to static dots. This activation was less pronounced in children, specifically in the visual area V3a	Magnocellular pathway delay in children
Parrish et al., (2005)	Participants visualized motion-defined shape stimuli, texture-defined shape stimuli, global motion stimuli, global texture stimuli, coherent motion stimuli and motion displacement direction stimuli	Behavioral	Children between 3 and 10 years old	Figure-ground segregation and shape identification based on motion, texture or luminance contrast are still maturing in school age children. Direction discrimination mechanisms continue to mature in school age children.	The visual systems are not fully developed in school age children.
Crewther et al., (1999)	Hexagons presented at 5 different temporal contrasts	Visual evoked potentials (VEPs)	Normal readers from 6 to 45 years old as well as 6 reading disabled children.	Magnocellular pathway responses showed considerable change with age. Parvocellular/Magnocellular ratio has an exponential shape that gets flat by the age of 11-12 years	Magnocellular pathway is developed by the age of 11-12 years.
Bucher et al., (2006)	Visual form discrimination task: Shapes defined by motion or luminance contrast.	ERP (event-related EEG potentials) + fMRI	Adolescents (15-17 years) and adults (20-30 years)	Similar fMRI activation patterns and ERP topographies between both groups. N1 latencies for motion-defined stimuli shorter in adults than in adolescents.	Magnocellular pathway delay

The first two studies are focused on the first year of life. Hammarrengen and colleagues (2003) investigated the developmental patterns of the magnocellular and parvocellular pathways using visual evoked potentials, focused on infants aged between 0 and 52 weeks. They found that the P1 component, related to the magnocellular pathway, emerged faster in development than the N1 component, which is related to the parvocellular pathway. Furthermore, the amplitude of P1 increased in the first months, reaching a plateau around 4-6 months of age. In contrast, as mentioned before, the N1 component appeared later and the amplitude of it continued growing until the end of the first year of life. These results suggest that the magnocellular pathway matures faster than the parvocellular pathway during the first year of life.

Another study also found a more protracted maturation associated with the parvocellular pathway in the first year of life (Dobkins et al., 1999). Specifically, their sample consisted in 58 3-month-olds and 56 4-month-olds children. They measured luminance and chromatic temporal contrast sensitivity functions (tCSFs) and compare them with data from adults. They found that the luminance functions in children were already similar in shape by 3 months of age. However, the chromatic function was not comparable to the adult pattern even at 4 months of age, suggesting once again that the parvocellular pathway has a more protracted maturation in the first year of life.

Klaver and colleagues (2008) studied the development of visual motion perception, which is a characteristic linked to the magnocellular pathway, in an fMRI experiment where they measured the response of healthy children aged 5-6 years and healthy adults aged 20-30 years to randomly moving point-light dots (RM), moving dots that formed 3D rotating structures (called structures-from-motion, SFM) and static dots used as control stimuli. They found that

during the visualization of RM stimuli, motion processing-related visual areas (visual area V3a and the middle temporal area) were more strongly recruited than during the visualization of static dots. Moreover, in children the activation of V3a was lower than the activation of V3a in adults. The left parietal shape area was more strongly recruited during 3D rotating structure stimuli visualization compared to RM stimuli visualization in adults. In contrast, in children the dorsal (V3a) and ventral brain areas of the occipital cortex (lingual gyrus) were more strongly recruited, which suggest a slower development of areas associated with the magnocellular pathway.

A study in school age children (between 3 and 10 years old) also studied properties related to the magnocellular pathway. In this study they found that the integration of local elements is already mature by the age of 3 years. However, figure-ground segregation and shape identification based on motion, texture or luminance contrast are still maturing in school age children, as well as the direction discrimination mechanisms (Parrish et al., 2005).

On the other hand, Crewther et al. (1999) studied the development of the magnocellular pathway in normal readers aged between 5 and 45 years of age. They measured parvocellular *versus* magnocellular ratios, and they concluded that the ratios related to the magnocellular pathway reach adulthood values by the age of 11 to 12 years.

Bucher and colleagues (2006) investigated the late development of the visual motion system combining fMRI and EEG techniques in a group of adolescents aged 15 – 17 years and an adult group aged 20 – 30 years. In this study, participants visualized forms being either defined by motion or luminance contrast. The fMRI results and ERP topographies did not show almost differences between adolescents and adults in both types of stimuli. However, they found that the latencies of the N1 component of adults in motion defined stimuli located in the middle temporal area were shorter than in adolescents, suggesting that

visual motion processing, related to the magnocellular pathway, keeps developing until the adulthood.

Therefore, it can be said that in these studies it has been seen that the parvocellular pathway has a slower maturation in the first year of life. Regarding the studies that focus on the magnocellular pathway, it has been seen that by the age of 5-6 years these pathways have not fully matured yet, but at the age of 11-12 years there are some aspects related to the magnocellular pathway that are comparable to the adult ones. However, it is possible that there are several properties and aspects that continue refining until adolescence or even adulthood. In addition to this, there are several studies can be found in the literature that analyze the involvement of the magnocellular pathway in dyslexia.

6.1 Implication of the magnocellular pathway in developmental dyslexia

Developmental dyslexia (DD) is a neurobiological reading disorder despite normal intelligence, adequate education and lack of obvious sensory or neurological damage (American Psychiatric Association, 2013; World Health Organization, 2008). DD has been specifically related to deficits in behaviors associated with the magnocellular stream, such as motion discrimination (e.g., Dembet al., 1998; Solan et al., 2004; Wilmer et al., 2004), contrast sensitivity for stimuli with higher temporal and lower spatial frequencies (e.g., Lovegrove et al., 1982; 1986; Mason et al., 1993), temporal processing (e.g., Eden et al., 1995; Laycock & Crewther, 2008), and visuospatial attention (e.g., Facoetti et al., 2000; Franceschini et al., 2012, 2013; Gabrieli & Norton, 2012; Ruffino et al., 2014; Vidyasagar, 2004).

Based initially on post-mortem measurements showing a reduction of 27% in the size of the magnocellular, but not parvocellular, cell bodies in the LGN of a small sample of subjects

with dyslexia (Livingstone et al., 1991), a magnocellular theory (Stein, 2014; Stein & Walsh, 1997) that suggests that malfunction of the magnocellular system in the brain is responsible for the behavioral deficits in dyslexia was put forward. This magnocellular theory has been more recently reformulated in terms of a general temporal processing deficit in dyslexia (Goswami, 2011; Lehongre et al., 2011; Vidyasagar & Pammer, 2010) suggesting that readers with dyslexia have specific deficits in processing rapid stimuli in either the visual or auditory modalities (McLean et al., 2011).

Nevertheless, evidence from neuroimaging studies showing the specific contribution of critical regions along the visual pathways, and particularly of the magnocellular stream, is scarce. Only a handful of recent structural and functional MRI studies have examined the contribution of the thalamus and the LGN to atypical reading. Preston et al.'s (2012) fMRI study found thalamic hypoactivation for late compared to early talkers on speech and reading tasks. Similarly, Diaz et al. (2012) also reported left thalamic hypoactivation for adult readers with dyslexia compared to matched controls using a phonological task, suggesting that the two main theories about the etiology of dyslexia (i.e., phonological deficit and magnocellular theories) can be complementary in determining the impaired reading output observed in readers with dyslexia. More recently, Giraldo-Chica et al. (2015) used structural MRI to examine differences in the LGN among dyslexic and control readers and showed that the left LGN of the individuals with dyslexia was significantly smaller and different in shape relative to matched control counterparts. Jednorong and colleagues (2015) also found a significant group difference in the grey matter volume in the left thalamus between dyslexic and control children in a meta-analysis they did across different country and languages.

Furthermore, other studies found that dyslexic patients have reduced structural connections in the direct pathway between the LGN and MT+/V5, visual region responsible

of motion compared to controls, whereas the structural connectivity between the LGN and V1 is similar between both groups (Müller-Axt et. al., 2017). Finally, a recent study found regional hypoactivation in readers with dyslexia specifically associated with phonological (parietal regions), orthographic (parietal regions, Broca's area, vOTC and thalamus) and semantic reading processes (angular gyrus and the hippocampus). Besides that, they also found a stronger functional connectivity in dyslexic population between the hypoactivated regions. Specifically, they found a tighter connectivity between the thalamus and vOTC while reading pseudowords and between the hippocampus and pars opercularis while reading words (Paz-Alonso et al., 2018).

7. Magnetic resonance imaging

The MRI is one of the non-invasive imaging technologies used to measure brain activation *in vivo*, along with EEG, which quantifies brain electrical activity by recording voltage differences in the scalp; MEG, which measures brain electrical activity recording magnetic fields in the scalp; or PET, which measures and reconstructs a 3D image of gamma-rays emitted by a positron-emitting tracer introduced to the subject's blood system.

Since in the present doctoral dissertation I used the MRI technique in order to test the hypotheses we had, this chapter will explain in general how MRI works and the different sequences that have been used in Empirical Part II and III.

7.1 Functional MRI

Functional MRI (fMRI) allows us to estimate brain activation by measuring changes in the local blood oxygenation level (Moseley & Glover 1995), specifically the ratio of deoxygenated (deoxyHb) and oxygenated hemoglobin (oxyHb), which is called the blood-oxygen-level-dependent (BOLD) response (Ogawa et al., 1990). While deoxyHb has paramagnetic properties and disturbs the homogeneity of the magnetic field, oxyhHb is not, and hence has not effect in the local magnetic field. As highly demanding tasks are investigated in the area of neurocognitive science, these require a large blood supply, which results in BOLD signal changes. These BOLD signal changes enables to map changes in activation associated with a cognitive task (Raichle, 2009). Precisely, this increase in neural activation starts with an initial increase in oxygen consumption, which is followed by a large increase in localized cerebral blood flow, is triggered to compensate oxygen consumption only after a delay of about 2 seconds. As a result, blood oxygenation is incremented and therefore, the level of deoxyHb is reduced. This process is thought to explain that higher signal in fMRI images correlates with neural activity. The goal of an fMRI experiment is to

examine the time series of brain voxels and to what extent a given manipulation produce BOLD signal changes in a given series of voxels in response to some specific manipulations.

7.1.1 fMRI designs

In the literature we can find two main types of experimental designs, block and event-related designs (Buckner et al., 1996; Dale & Buckner, 1997). In a block-design experiment, the different conditions are organized in independent blocks followed by rest blocks. Activation blocks for different experimental manipulations or conditions are alternated during the experiment. On the other hand, in an event-related design, each event is separated by an inter-stimulus interval ranging from few seconds to twenty seconds. These stimuli are presented in a randomized order following certain parameters that have into account the properties of the hemodynamic response function (see Figure 10).

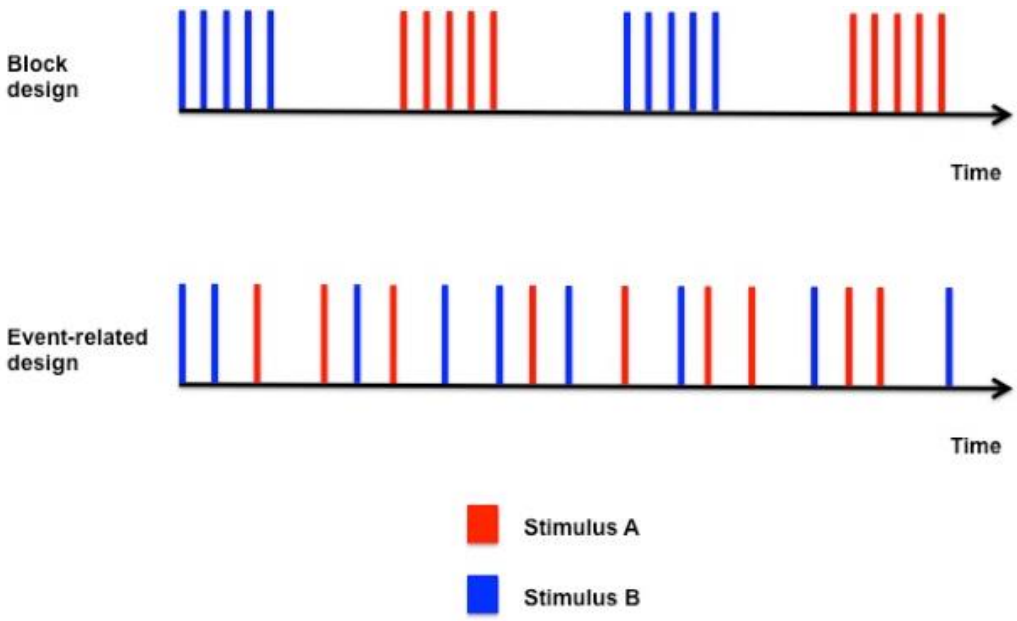

Figure 10: Schematic diagrams showing the two fMRI design types. Upper panel corresponds to a block-design. Lower panel corresponds to an event-related design.

In Empirical Part II and III we used a fMRI block design due to its robustness, since it has higher statistic power compared to event-related design paradigms. This design type is also better if the goal of the study is to detect subtle differences in BOLD signal across different

test conditions. Finally, in block-design paradigms is easier to detect non-physiological signal fluctuations (Donalson & Buckner, 2001).

7.1.2 Data preprocessing

One of the main issues while analyzing fMRI data is comparing group of images in a statistically meaningful way. The data has to be preprocessed before this statistical analysis can be performed. Data preprocessing typically includes these main steps: *slice-timing* or temporal interpolation, *realignment* or spatial interpolation, *normalization* and *smoothing*. The *slice timing* correction is used to compensate for slice acquisition delays, so that it would be equivalent to acquiring the whole-brain image at a single time point. Because subjects may move in the scanner during data acquisition and consequently the location of every voxel might vary between scans, the realignment step help to correct to some extent these motion artifacts aligning, as closely as possible, the acquired functional images. Functional images are usually coregistered with a high-resolution T1- or T2-weighted anatomical image from the same subject to increase the spatial precision of the functional images. During the *normalization* procedure subjects' brain images are warped into a standard stereotaxic space, a preprocessing step that is done in fMRI studies intended to examine group analysis. Nowadays the most commonly used templates are based on the MNI space, which is an approximation to the Tailarach and Tournoux space (Talairach & Tournoux, 1988). The main two purposes of normalization process are to reduce inter-subject anatomical variability and to be able to compare and reproduce findings across laboratories and studies. Since the BOLD response is modulated by blood flow, the rate at which the signal changes, in an activated region, is limited. Therefore, during *smoothing* voxels values are averaged with their closest neighbors in order to improve the signal-to-noise ratio. The standard procedure of spatial smoothing is employed by convolving the fMRI signal with a Gaussian function of a specific width. This so called Gaussian kernel is a kernel with the shape of a normal

distribution curve. In the figure below it can be seen a standard Gaussian with a mean of 0 and a standard deviation of 1 (see Figure 11).

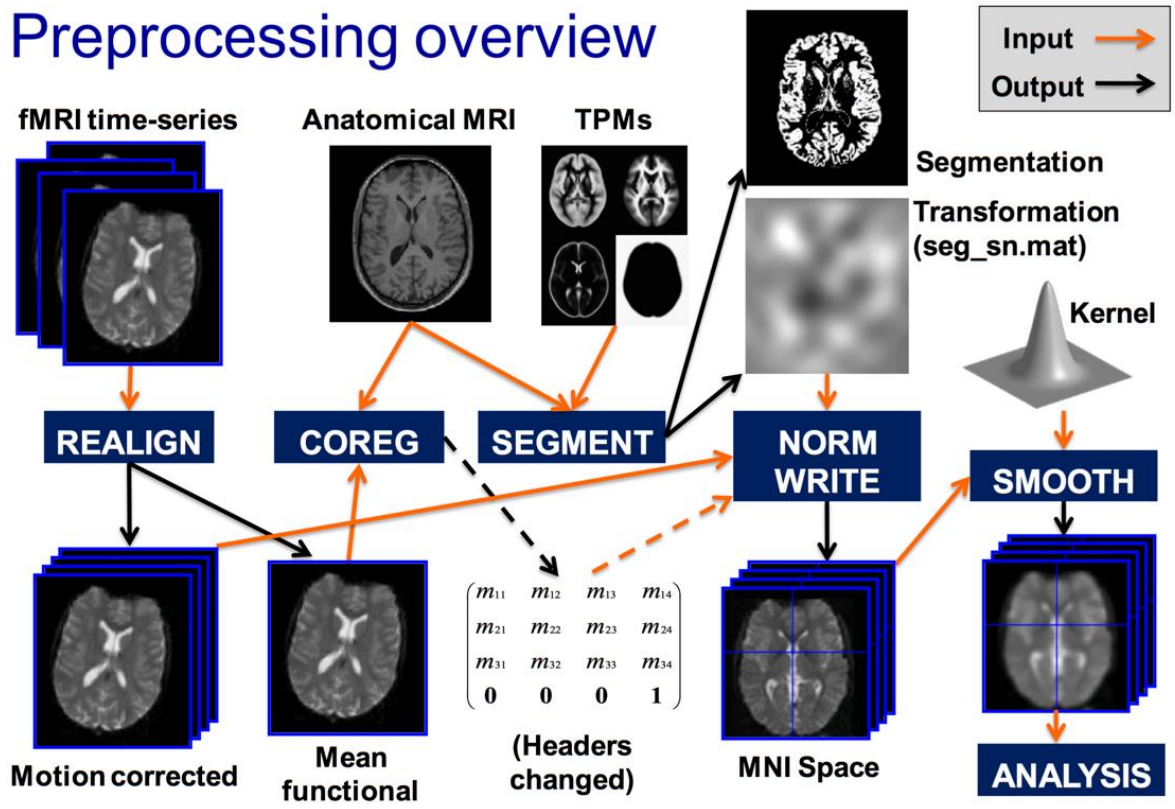

Figure 11: fMRI data preprocessing and statistical analysis (adapted from SPM12 course material) (http://www.fil.ion.ucl.ac.uk/spm/course/video/).

7.1.3 Statistical analysis

Once the functional images are preprocessed, statistical analysis can be done. The most widely used statistical technique to fit and detect variations in BOLD response is the general lineal model (GLM; Friston et al., 1995). fMRI analyses are carried out in multiple stages. For example, in a two-sample t-test, the first-level analysis involves modeling the data for each subject separately, estimating subject-specific differences upon the manipulation. The second-level analysis takes the subject-specific parameter and variance estimates from the first-level model. The within-subject variance is estimated in the first-level and the between subject variance in the second-level. Finally, the model estimates a mean for each group and the contrast of interest to compare between groups (Poldrack, 2012). For an image composed of N voxels, there are several ways to decide if there are changes in the BOLD response:

voxel-level or by testing each and every voxel in the brain, and cluster-level or by examining specific clusters of activated voxels. Importantly, when comparing multiple voxels one must avoid "multiple testing problems", such as the Type I error, which refer to the change of one or more false positives. Different methods are available to avoid this problem, such as the False Discovery Rate (FDR) or the Family-wise error (FEW) rate that can be also applied at the voxel or cluster levels. Deciding what is the most appropriate method to correct for multiple comparisons is still under discussion, especially at the cluster level (Eklund et al., 2016).

7.1.4 Task analysis

One of the common aims in fMRI analysis is to localize regions of the brain activated by a certain task or conditions, and to determine the brain networks involved in specific cognitive processes. This analysis can be carried out at the whole-brain level (i.e., voxel-wise) or focused on the activation of specific regions of interests (ROIs). Due to the statistical corrections for multiple comparisons, usually the statistical level is lower when task analyses are performed at the voxel-level. In contrast, when a study is focused on particular regions of interest in the brain based on prior evidence and the study hypotheses, the search for differences in activation can be limited to a given number of ROIs (Poldrack, 2007; Saxe et al., 2006). This approach involves the extraction of signal (i.e., parameter estimates) from specific brain regions of interest based on prior evidence suggesting the involvement of these brain regions in a specific cognitive function. There are different reasons to select this analysis. On the one hand, in complex designs, such as factorial designs with multiple levels, it can be difficult to discern the pattern of activity across conditions from an overall voxel-wise map; ROI analysis may illustrate more clearly this pattern. On the other hand, by reducing the magnitude of correction needed for a large number of voxels, one can better control for Type I errors by limiting the number of statistical tests to a few ROIs (Poldrack,

2007; Saxe et al., 2006). In the present doctoral work we performed whole-brain and ROI analyses, among several other analyses, but hypotheses testing were mainly performed at the ROI level. Specifically, in Empirical Part II we analyzed the involvement of the magnocellular and parvocellular pathways in the visual cortex using individual ROIs in the native space. On the other hand, in Empirical Part III we studied the contribution of these two pathways examining ROIs in the temporal (i.e., vOTC), parietal (i.e., intra-parietal sulcus, IPS) and prefrontal (i.e., IFG) lobes.

7.1.5 Functional connectivity

In the last years, the cognitive neuroscience community has moved to the idea that the majority of functions are supported by coordinated activation between brain regions, so that the brain works in networks (Catani et al., 2003). Consequently, there is increasing interest in implementing analysis to better understand how various brain regions interact between each other. One approach to characterize these interactions is functional connectivity. Functional connectivity refers to the influence that one neural system exerts over another. This type of analysis typically compares correlations between regions of interest (i.e., pairwise functional connectivity) or between a 'seed' region of interest and the rest of the voxels in the brain (i.e., whole-brain functional connectivity). This allows to examine patterns regarding which regions are coupled or work together in time, and to compare those patterns between networks (i.e., ventral versus dorsal networks), between groups and/or between experimental conditions.

The two most common approaches to functional connectivity are the psychophysiological interactions (PPI) and the beta-series correlation developed by J. Rissman (Rissman et al., 2004). The PPI approach looks for changes in the regression slope as a function of a condition trying to answer the question if more activation in the seed region produces more activation in the target region depending on that experimental condition. The beta-series

correlation method is a method that capitalizes on trial-to-trial variability to characterize dynamic inter-regional interactions. The premise of this method is that if two areas of the brain are functionally interacting with each other during a particular cognitive task, then the amount of activity that the two areas exhibit during that stage should be correlated across trials. The beta-series correlation method has been widely used in fMRI studies (e.g., Clapp et al., 2011; Cohen et al., 2013; Paz-Alonso et al., 2013). This specific analysis provides information about how different regions are functional connected and allows examining differences in functional connectivity at the whole-brain level (i.e., selecting a seed to examine coupling of this seed with voxels throughout the brain) and at the pairwise level (i.e., examine differences in the strength of functional connectivity between pairs of ROIs). The latest approach has been used in this doctoral dissertation to examine the coactivation of the visual cortex areas on the one hand (Empirical Part II), and the coactivation of the vOTC with the IPS and the IFG on the other hand (Empirical Part III).

7.2 Structural MRI

The neuron doctrine (Shepherd, 1991) states that the brain computations are executed by neurons using electrical potentials and synapses. Although on average there are almost 100.00 million of neurons, these compose 15% of the total amount of cells of our brains. The remaining cells are known as glia (from the Greek glue). In the recent years, glia cells have been investigated with more emphasis (Fields, 2009), and it has been seen that the glia might also be involved in coding information and cognitive processes (G. Perea et al., 2014).

Neurons are organized within the brain forming grey matter (GM) and white matter (WM). GM is mainly located in the surface of the brain, and it consists principally of neuronal cell bodies. On the other hand, WM consists of axons, which are the long strands of nerve cell extensions, and support cells (e.g., glia cells). These axons carry information from

one grey-matter region to the other, and are usually organized into bundles of axons forming the so-called fiber tracts or fascicles.

It has not been until very few years that the cognitive neuroscience field have given the importance of studying the structural properties of GM and WM, which could help to further understand brain function (Martensson et al., 2012). Structural MRI images allow examining certain morphometric features of the brain, such as volumetry, cortical thickness (CT), surface area (SA) or characteristics of the WM tracts than can be associated with cognitive functions. In the empirical parts that conform the present doctoral dissertation proposal, I used structural analyses to obtain individual ROIs in the native space for functional analysis, and DWI to study micro-structural properties of WM.

7.2.1 Diffusion weighted imaging

Water molecules diffuse in different manners along the tissues depending on its type, integrity, architecture and the presence of barriers. On the one hand, diffusion of water molecules in WM is restricted to the longitudinal axis of the axons (i.e., be anisotropic, directionally-dependent). On the other hand, in grey matter the diffusion of water molecules is less anisotropic. Finally, in CSF the water molecules can move freely in any direction (i.e., isotropic or unrestricted). Through diffusion MRI sequences one can acquire images sensitive to this preferred direction of diffusion. Depending on the level of alignment of the magnetic field gradients with the water molecule movement, the signal will increase or decrease. In order to extract and analyze the information from WM tracts, three main steps should be performed: i) acquisition of the images, ii) modeling of the data at the voxel level, and iii) creation of tracts joining voxels.

i) Acquisition of the images: Two parameters have to be taken into account when designing an acquisition sequence: the number of directions and the *b* value.

The number of directions refers to the number of different alignments used to acquire these images. The *b* value comprises a set of physical constants and experimental parameters, such as the strength or duration of the magnetic field gradients. The same directions can be acquired with different *b* values. Depending on how many *b* values are used in an acquisition, different types of acquisitions can be done, with one *b* value, the acquisition is called single-shell acquisition, while when using more than one *b* value, it is called multi-shell acquisition. The selection of parameters depends on every application; more diffusion directions and more than one *b* will result on more resolution, although it has a cost.

ii) Modeling the data: Nowadays many different ways of modeling the data at voxel level can be found. For a single-shell acquisition with a small number of directions, the data is modeled with a diffusion tensor, also called diffusion tensor imaging (DTI). However, this model cannot model fiber crossing, as it will always give the predominant direction (Tournier et al., 2011). Since around 90% of all the voxels in WM are estimated to include crossing fibers (Jeurissen et al., 2013), it is more accurate to use multi-shell acquisition combined with the acquisition of many directions, called high angular resolution diffusion imaging (HARDI). Therefore, more complex models are necessary, such as the constrained spherical deconvolution (CSD) (Jeurissen et al., 2014). These models can report and take into account multiple fiber orientations.

iii) Tractography: Combining diffusion MRI voxel information and tractography algorithms, in this last step the tracts are estimated. There are several types of

approaches, such as local or global tractography and deterministic or probabilistic tractography.

Using one of these approaches, one can calculate several indices, such as Fractional Anisotroy (FA), which provides information about WM tissue properties (Chenevert et al., 1990). FA assesses the degree of anisotropic diffusion occurring within a given tract. The FA will be high in regions heavily organized in terms of orientation (e.g., corpus callosum), intermediate in regions with some degree of organization (e.g., WM regions that have no strong predominant axon fiber axis orientation), and low in tissues where the predominant cell shapes are not specifically oriented (e.g., GM) (Pfefferbaum et al., 2000).

Within the WM higher FA values have been associated with increase variations in axon count, density of axonal packing and myelination. Myelination occurs more actively from childhood to adulthood (Ishibashi et al., 2006), which lead to increases of the space occupied by axons in a given voxel and subsequent increases in FA (Stikov et al., 2011). These developmental effects of myelination and axon density on diffusion measurements have been confirmed in animal models and also in humans (Beaulieu et al., 2005; Pierpaoli et al., 2001).

Empirical evidence suggests that the development of cognitive abilities, such as reading is correlated with increases in FA values within tracts that connect relevant regions within the reading network, such as the left arcuate fasciculus (Nagy et al., 2004; Yeatman et al., 2012a; Yeatman et al., 2012b). Thus, reading development is in part the result of WM microstructural changes, measured by FA, in tracts within the reading network (Wandell & Yeatman, 2012). Indeed, empirical evidence observed that FA values in the left temporo-parietal lobe correlated with reading performance in both poor and normal readers (Klingberg et al., 2000), which suggests that axons in this area are important for efficient connectivity between temporo-parietal and frontal regions and thus may be important for reading. Studies

such as this, demonstrate the usefulness of FA measures to investigate structural brain changes associated with specific cognitive functions. This explains why DWI has gaining increased popularity among clinicians and researchers, providing a tool for studying WM architecture in living humans.

8. Empirical Part I: Developmental trajectories of magnocellular and parvocellular pathways

There has been little research on the developmental trajectories of the main visual magnocellular and parvocellular pathways, and available findings have showed mixed results. Since the magnocellular pathway appears to be involved in text perception and reading, unveiling age-related changes in this pathway and their associations with reading and visual discrimination is critical to further understand typical and atypical reading development. Thus, the main goal of this experiment was to test the developmental trajectories of both magnocellular and parvocellular pathways and their contribution to reading. Based on previous evidence, we hypothesized that 1) the magnocellular pathway will show a more protracted maturation relative to the parvocellular pathway; 2) children's performance (i.e., accuracy and reaction times) on magnocellular-biased and parvocellular-biased word processing will show significant associations with age, which will not be the case in adults; and 3) the same pattern of age-related associations with performance in children, but not in adults, were expected in a visual discrimination task designed to determine participants ability to discriminate letters as a function of their overlap (i.e., crowding) and their visual characteristics.

8.1 Materials and Methods

8.1.1 Participants

The study sample consisted of 70 healthy children aged 8-to-14 years-old (mean age 11 ± 2 years; 35 females and 35 males) and 37 healthy adult participants (mean age 24.154 ± 4.43 years; 21 females and 16 males). The children participants were divided in two subgroups, the first one that corresponds to children aged 8-to-11 years, and a second one that corresponds to children aged 12-to-14 years.

All participants were right-handed and had normal or corrected-to-normal vision. No participant reported a history of major medical, neurological, or psychiatric disorders. The study protocol was approved by the Ethics Committee of the Basque Center on Cognition, Brain and Language (BCBL) and was carried out in accordance with the Code of Ethics of the World Medical Association (Declaration of Helsinki) for experiments involving humans. Prior to their inclusion in the study, all participants or their parents provided informed written consent. Adult participants received monetary compensation for their participation.

8.1.2 Stimuli

In this empirical part, participants were administered with two behavioral tasks, a reading task and a visual discrimination task, in order to examine age-related changes in the involvement of the magnocellular and parvocellular pathways in reading as well as in visual discrimination across early middle childhood, late middle childhood and adulthood years.

Reading task. A total of 60 words in the format of line drawings were used as stimuli. The uniform foreground of these drawings allows for precise control of luminance and chromatic properties. Half were magnocellular-biased, that is achromatic with low-luminance contrast; the remaining half were parvocellular-biased, that is, chromatically defined and isoluminant (red-green).

It is known that tuning of the magnocellular and parvocellular visual pathways differs across individuals, so we used standard procedures to adjust luminance and chromatic settings before the participants performed the reading task (Cheng et al., 2004; Kveraga et al., 2007; see also Skottun, 2013, for cautions on using isoluminant stimuli). The standard technique for establishing the luminance threshold for magnocellular-biased achromatic stimuli involves a multiple staircase procedure, during which subjects are required to answer whether or not they can identify word stimuli. Once the luminance threshold has been

established, the appropriate luminance (~3.5% Weber contrast) value is defined for the gray-scale line drawings to be used in the low-luminance-contrast, magnocellular-biased, condition. We used a common luminance value across all participants for the magnocellular-biased stimuli; we had shown that these stimuli met an 80% accuracy criterion in a normative study (N = 15) made prior to the current experiment. In that normative study, we used 40 words to determine the appropriate luminance contrast for participants to reach 80% accuracy on the achromatic magnocellular-biased stimuli. The criterion of minimum 80% of accuracy was used to guarantee enough correct responses to magnocellular-biased stimuli, since magnocellular-biased trials are, in general, more difficult to process than parvocellular-biased ones.

For the parvocellular-biased, chromatically defined stimuli, the isoluminance point was identified for each subject individually using heterochromatic flicker photometry as reported in previous studies (Kveraga et al., 2007). This procedure identifies the isoluminance point for two colors by having a stimulus rapidly alternate between them. The color values at which the stimuli appears to stop flickering indicates the narrow isoluminance interval of the steady point. Each participant was required to indicate the steady point for line drawings of words displayed in pure red and pure green before performing the reading task.

All of the word stimuli chosen in this task showed an age of acquisition under 8 years of age. These words were created in magnocellular-biased and parvocellular-biased forms. counterbalancing properly across subjects in terms of Pathway (i.e., magnocellular, parvocellular) (see Figure 12). All the selected items could be easily identified as non-manmade (i.e., *apple*) or manmade (i.e., *robot*); 50% of items were “non-manmade”, and the remaining 50% were “manmade”.

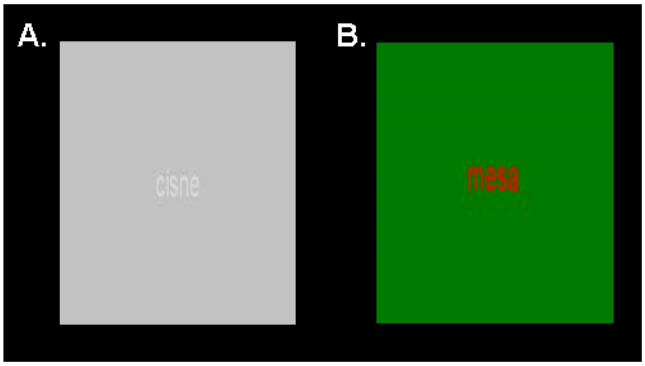

Figure 12: Experimental stimuli. We used a block design where participants made manmade (i.e., artificial) or non-manmade (i.e., natural) judgments on words that were A) magnocellular biased, with low luminance and contrast, and achromatic; or B) parvocellular biased; isoluminant (red-green) and chromatically defined. All stimuli were counterbalanced across conditions and subjects.

Visual discrimination task. Additionally, all participants performed a visual discrimination task that was used to examine visual discrimination as a function of crowding or spacing among letter stimuli, stimuli characteristics or color facilitation, and the interaction among them. The task consisted in a 3 (Spacing) X 2 (Color facilitation). The stimuli consist of triads of letters presented horizontally with: 1) three levels of spacing among letters (i.e., no overlap, partial overlap, full overlap), and 2) two levels of color facilitation (i.e., no facilitation or same color, presenting the center and the flanker letters in the same (black) color facilitation or different color, presenting the flanker distractor letters in a different colored ink). Across the 6 conditions included in the experimental design participants had to indicate whether or not the letter in the center was a "G" (see Figure 13).

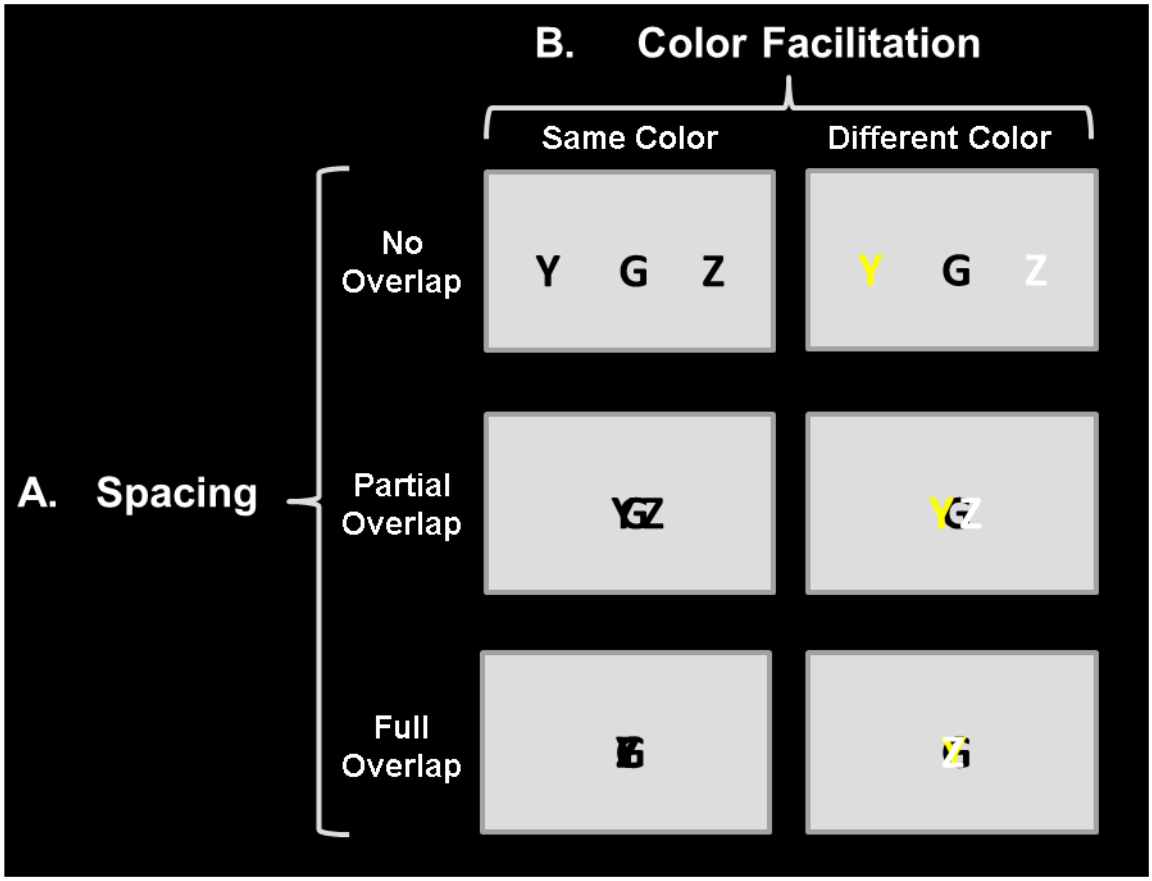

Figure 13: Visual discrimination task. Participants had to answer whether the letter in the middle of the screen was a 'G'. Stimuli were varied as a function of A) Spacing, with no overlap (upper row), partial overlap (middle row) and full overlap (bottom row); and B) Color facilitation, with characters presented in the same color (i.e., no facilitation) and different color (i.e., facilitation). Stimuli were randomly presented and counterbalanced across conditions and subjects.

8.1.3 Experimental task and procedure

Reading task. This task included two word processing conditions under the factor Pathway: magnocellular-biased and parvocellular-biased words. The task was carried out in a single run that lasted 5 min. Word stimuli were presented to participants at 100 Hz in a computer screen using MatLab Psychtoolbox (Brainard, 1997; Pelli, 1997). During the task, participants were asked to perform a semantic task, in which they indicated natural (i.e., non man-made) or artificial (i.e., man-made) judgements via key presses on the computer keyboard. A total of 60 words were presented separated in blocks of six stimuli, yielding 5 blocks for each of the 2 experimental conditions.

For this main experimental task, we conducted two separate 2 (Pathway: magnocellular, parvocellular) X 3 (Group: early middle childhood, late middle childhood, adults) repeated measures analyses of variance (ANOVA) with accuracy and reaction times as dependent measures. We used the mean ± 2.5SD criterion to remove any outliers in all measures in this study.

Visual discrimination task. The visual discrimination task conformed to a 3 (Spacing: no overlap, partial overlap, full overlap) X 2 (Color facilitation: same color, different color) design. During the task, participants were asked to answer whether the central letter was a 'G' or not via key presses on the computer keyboard. The task was divided in two runs, and it lasted approximately of 10 mins, including an initial practice run with feedback.

For the visual discrimination task, we conducted two separate 3 (Spacing: no overlap, partial overlap, full overlap) X 2 (Color facilitation: same color, different color) X 3 (Group: early middle childhood, late middle childhood, adults) ANOVAs with accuracy and reaction times as dependent measures. We used the mean ± 2.5SD criterion to remove any outliers in all measures in this study.

8.2 Results

8.2.1 Reading task

A 3 (Group) X 2 (Pathway) mixed-model ANOVA revealed a statistically significant main effect of Pathway ($F_{1,98}$= 30.72; ηp^2 =0.24, p < 0.001, BF10 = 610.94) that was qualified by a statistically significant Pathway X Group interaction ($F_{2,98}$= 10.18; ηp^2 =0.17, p < 0.001, BF10 = 152.85) for response accuracy. Simple-effect *post hoc* comparisons showed that the interaction was due to higher accuracy for parvocellular-biased words than for magnocellular-biased words in the early middle childhood and late middle childhood groups

($ts_{38} \geq 3.91$, $ps \leq 0.001$, $d' \geq 0.61$, $BF10 \geq 13.25$). This effect was not observed in adults (t_{36} 0.37, $p = 0.72$, $d' = 0.06$, $BF10 = 0.19$) (see Figure14A).

The ANOVA for reaction times to correct responses also revealed a statistically significant main effect of Pathway ($F_{1,100}= 13.58$; $\eta p^2 =0.12$, $p < 0.001$, $BF10 = 82.58$) that was due to shorter reaction times for parvocellular-biased words compared to magnocellular-biased words. The Pathway x Group interaction did not reach statistical significance ($F_{2,100}= 2.51$; $\eta p^2 =0.05$, $p = 0.07$, $BF10 = 1.74$) (see Figure 14B).

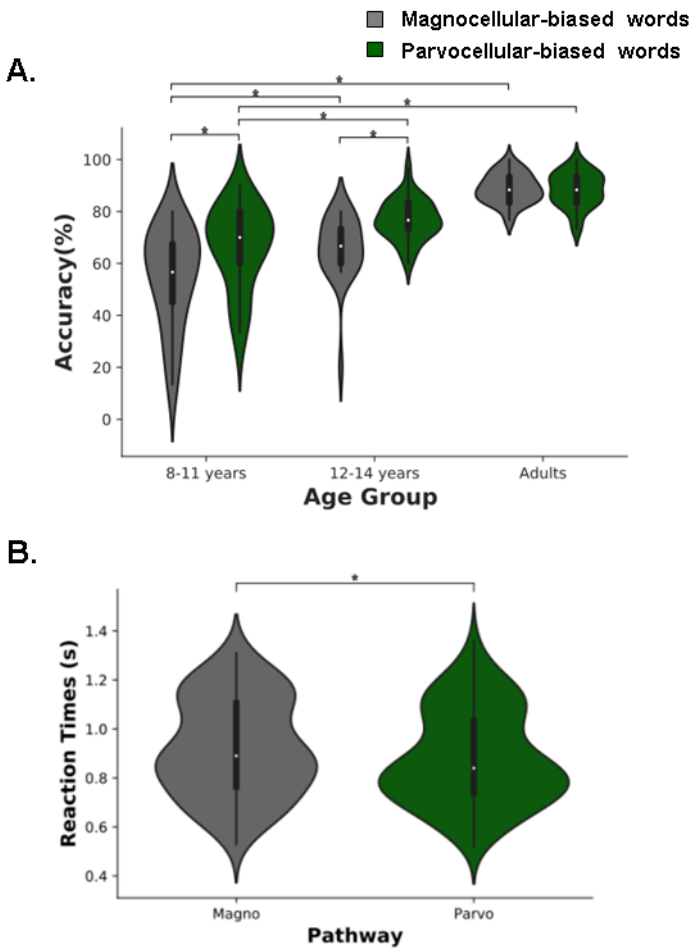

Figure 14: Behavioral results of the reading task. A) Mean percent (%) accuracy as a function of group and magnocellular and parvocellular pathways. B) Mean reaction times to correct responses as a function of magnocellular and parvocellular pathways. The white dots on the violin plots represents the median, while the black bar in the center represents the interquartile range. Thick black lines indicate statistically significant effects: *ps < .05.

Regression analyses revealed that age was associated with magnocellular-biased and parvocellular-biased word accuracy and reaction times in children, but not in adults. Specifically, age was strongly and positively associated with task accuracy across early and late middle childhood children for magnocellular-biased (r_{62} = 0.51, p < 0.001) and parvocellular-biased word processing (r_{62} = 0.53, p < 0.001; see Figure 15A). These associations between age and word processing accuracy were not observed in the adult group ($r_{35} \leq 0.19$, ps $\geq$ 0.27) (see Figure 15A). The same pattern of results emerged for reaction times; age was strongly and negatively associated with reaction times across middle childhood years for magnocellular-biased (r_{64}= -0.51, p < 0.001) and for parvocellular-biased

word processing (r_{65} = -0.68, ps < 0.001). No statistically significant associations were observed in the adult group ($r_{35} \leq$ -0.25, ps $\geq$ 0.13) (see Figure 15B).

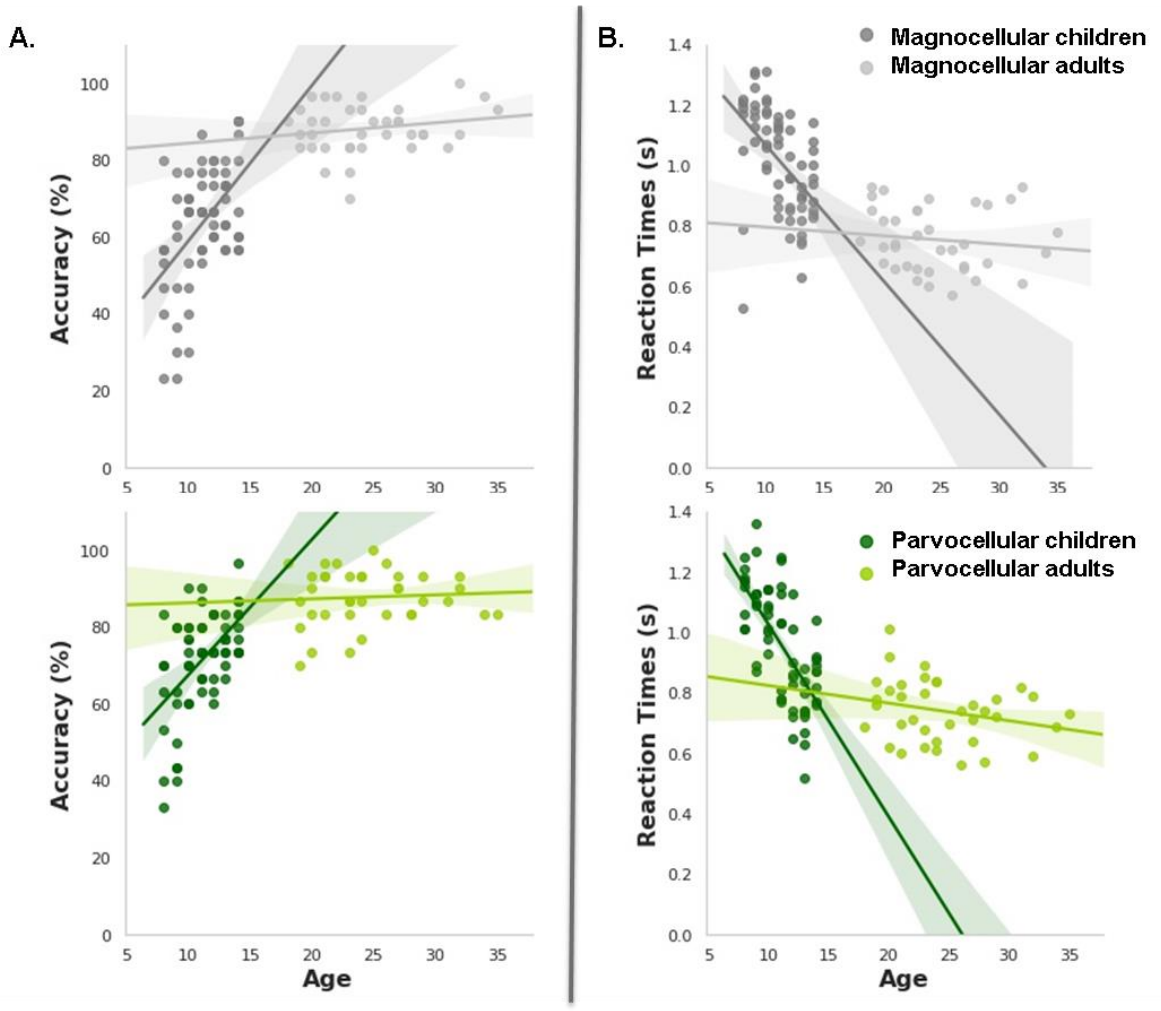

Figure 15: Associations between age and performance on the reading task for children and adults. A) Age and accuracy associations, with the upper panel showing associations for magnocellular-biased stimuli and the bottom panel showing associations corresponding to parvocellular-biased stimuli. B) Age and reaction times associations, with the upper panel showing associations for magnocellular-biased stimuli and the bottom panel showing associations corresponding to parvocellular-biased stimuli. Darker lines and dots correspond to the associations showed in children, while lighter lines and dots correspond to associations showed in adults.

8.2.2 Visual discrimination task

A 3 (Group) X 3 (Spacing) X 2 (Color facilitation) mixed-model ANOVA for response accuracy revealed that the statistically significant main effects of Spacing ($F_{2,182}$= 28.58; ηp^2 =0.24, p $\leq$ 0.001, BF10 = 4.45 e^6) and Color facilitation ($F_{1,91}$= 108.52; ηp^2 =0.54, p $\leq$ 0.001,

BF10 = 1.00 e^{16}), and interactions of Spacing X Group ($F_{4,182}$= 5.53; ηp^2 =0.11, $p \leq 0.001$, BF10 = 19.76) and Spacing X Color facilitation ($F_{2,182}$= 61.69; ηp^2 =0.40, $p \leq 0.001$, BF10 = 2.66 e^{16}), were qualified by a statistically significant Group X Spacing X Color facilitation interaction ($F_{4,182}$= 8.21; ηp^2 =0.15, $p \leq 0.001$, BF10 = 1.52 e^{21}). Since effects were only present for same color stimuli (no differences observed in response accuracy for different color stimuli), in order to further understand this triple interaction we performed a 3 (Group) X 3 (Spacing) mixed-model ANOVA for response accuracy only with same color stimuli. This ANOVA revealed a statistically significant main effect of Spacing ($F_{2,200}$= 71.33; ηp^2 =0.41, $p \leq 0.001$, BF10 = 3.75 e^{19}) that was qualified by the statistically significant Spacing X Group interaction ($F_{4,200}$= 10.85; ηp^2 =0.183, $p \leq 0.001$, BF10 = 235283.47). Simple-effect *post hoc* comparisons showed that this interaction was due to higher accuracy for the late middle childhood group than for early middle childhood for fully overlapped stimuli (t_{28} = 2.92, p = 0.02, d' = 0.54, BF10 = 6.25) and higher accuracy for adults than for early middle childhood and late middle childhood groups for partially overlapped stimuli ($t_{28} \geq 2.38$, ps $\leq$ 0.03), d' $\geq$ 0.41, BF10 $\geq$ 2.12. These effects were not present for non-overlapped stimuli (ts_{28} $\leq$ 0.53, ps $\geq$ 1.00, d' $\leq$ 0.09, BF10 $\leq$ 0.22) (see Figure 16A).

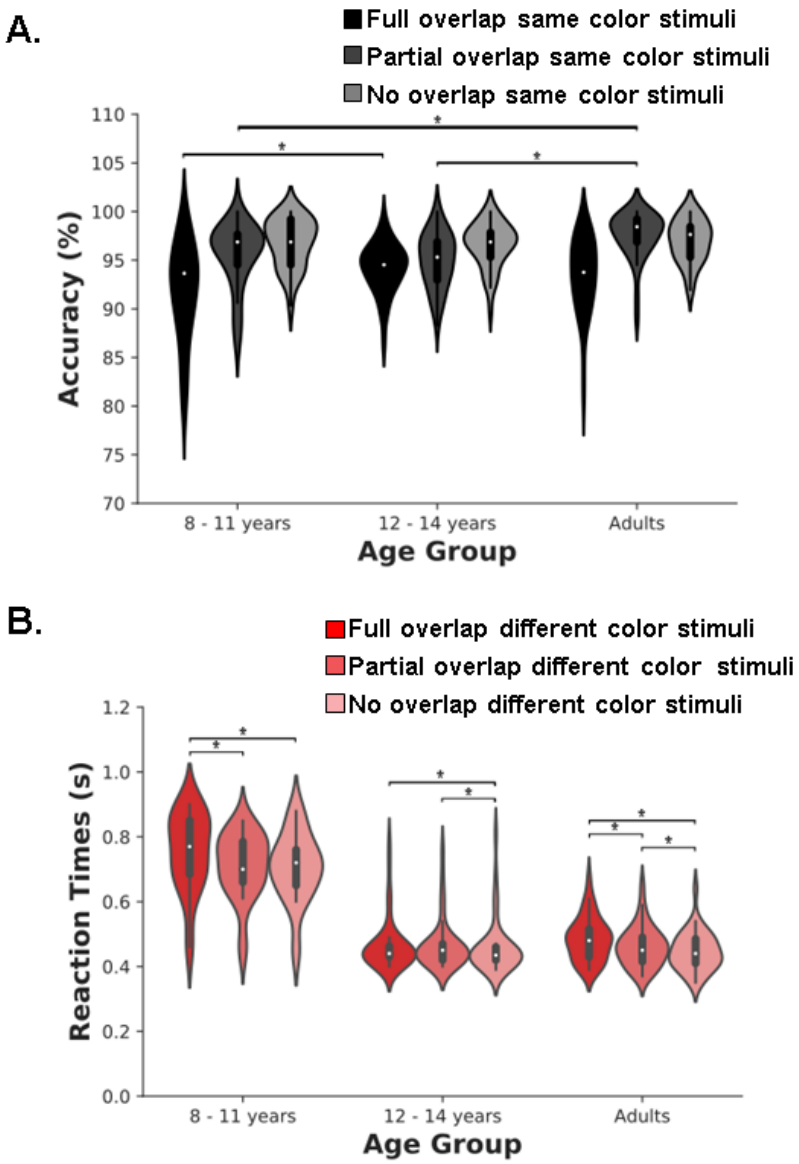

Figure 16: Behavioral results of the visual discrimination task. A) Mean percent (%) accuracy as a function of group and spacing of black stimuli. B) Mean reaction times to correct responses as a function of group and spacing of colored stimuli. The white dots on the violin plots represents the median, while the black bar in the center represents the interquartile range. Thick black lines indicate statistically significant effects: *ps < .05.

The ANOVA for reaction times to correct responses also revealed that the statistically significant main effects of Spacing ($F_{2,194}$= 202.97; ηp^2 =0.68, p ≤ 0.001, BF10 = 7.96 e^{46}), Color facilitation ($F_{1,97}$= 218.98; ηp^2 =0.69, p ≤ 0.001, BF10 = 2.17 e^{14}) and Group ($F_{2,91}$= 40.23; ηp^2 =0.45, p ≤ 0.001, BF10 = 2.35 e^{10}), significant interactions of Spacing X Group ($F_{4,194}$= 20.96; ηp^2 =0.30, p ≤ 0.001, BF10 = 5.52e^{12}), Color facilitation X Group ($F_{2,97}$=

23.25; ηp^2 =0.32, p ≤ 0.001, BF10 = 4.42 e^{12}) and Spacing X Color facilitation ($F_{2,194}$= 137.35; ηp^2 =0.59, p ≤ 0.001, BF10 = 1.14 e^{21}) were qualified by a statistically significant Group X Spacing X Color facilitation interaction ($F_{4,194}$= 10.04; ηp^2 =0.17, p ≤ 0.001, 1.26 e^{47}). Since effects were only present for different color stimuli (no differences observed in response latencies for same color stimuli), to furhter understand this triple interaction, we conducted a 3 (Group) X 3 (Spacing) mixed-model ANOVA for different color stimuli. This ANOVA revealed that the statistically significant main effect of Spacing ($F_{2,196}$= 50.29; ηp^2 =0.34, p ≤ 0.001, BF10 = 6.26 e^{14}) and Group ($F_{2,98}$= 41.676; ηp^2 =0.46, p ≤ 0.001, BF10 = 3.48 e^{10}) was qualified by a statistically significant Spacing X Group interaction ($F_{4,196}$= 7.81; ηp^2 =0.14, p ≤ 0.001, BF10 = 2227.61). Simple-effect *post hoc* comparisons showed that the interaction was due to higher reaction times for overlapped stimuli than for partially and non-overlapped stimuli (ts_{36} ≥ 4.52, ps ≤ 0.001, d' ≥ 0.74, BF10 ≥ 364.27) for the early middle childhood group. This effect was not observed between partially and non-overlapped stimuli (t_{35} = 1.74, ps = 0.09, d' = 0.29, BF10 = 0.70). For the late middle childhood group, the interaction was due to larger reaction times for overlapped and partly overlapped stimuli than for non-overlapped stimuli (ts_{29} ≥ 3.55, ps ≤ 0.001, d' ≥ 0.65, BF10 ≥ 25.63). This effect was not present between overlapped and partially overlapped stimuli (ts_{29} = -0.58, ps = 0.57, d' = 0.11, BF10 = 0.23). For adults, the three comparisons resulted statistically significant with non-overlapping showing higher reaction times compared to the other two conditions and partially overlapping showing larger reaction times relative to fully overlapped stimuli (ts_{34} ≥ 5.78, ps ≤ 0.001, d' ≥ 0.98, BF10 ≥ 10970.14) (see Figure 16B).

For the visual discrimination task, we also examined associations between age and task performance. For accuracy, the only statistically significant association with age occurred across middle childhood years for the most difficult condition: full overlap with the same color (black) stimuli (r_{67} = 0.35, p = 0.003). No other statistically significant association

between age and accuracy was found the rest of the conditions across middle childhood ($rs_{60} \leq 0.11$, $ps \geq 0.36$). In the case of adults, none of the conditions revealed age and accuracy statistically significant associations ($rs_{32} \leq 0.11$, $ps \geq 0.53$) (see Annex I, Figure 1).

For reaction times, in contrast, we found that all the conditions showed strong and negative associations between age and reactions times across middle childhood years: no overlap same color (black) stimuli ($r_{66} = -0.81$; $p < 0.001$; Figure 17A.1), partial overlap same color (black) stimuli ($r_{67} = -0.80$, $p < 0.001$; Figure 17A.2), full overlap same color (black) stimuli ($r_{65} = -0.80$; $p < 0.001$; Figure 16A.3), no overlap different color stimuli ($r_{67} = -0.79$, $p < 0.001$; Figure 17B.1), partial overlap different color stimuli ($r_{65} = -0.80$, $p < 0.001$; Figure 16B.2), and full overlap different color stimuli ($r_{65} = -0.80$, $p < 0.001$; Figure 17B.3). No associations between age and reaction times resulted statistically significant in the adult group ($rs_{33} \leq 0.13$, $ps \geq 0.47$) (see Figure 17A & 17B).

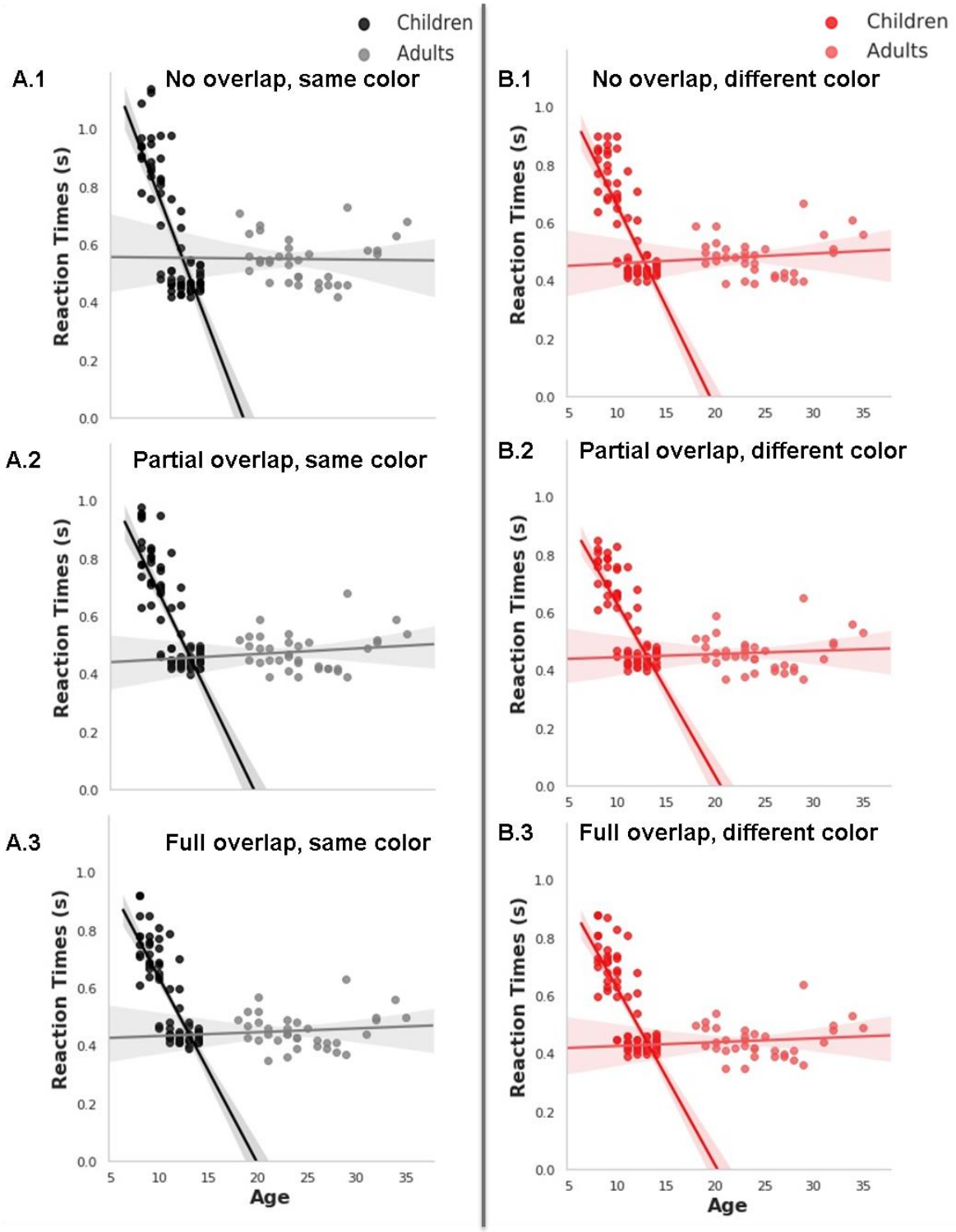

Figure 17: Associations between age and reaction times in the visual discrimination task for children and adults: A.1) No overlap, same color (black) stimuli; A.2) Partial overlap, same color (black) stimuli; A.3) Full overlap, same color (black) stimuli; B.1) No overlap, different color stimuli; B.2) Partial overlap, different color stimuli; and, B.3) Full overlap, different color stimuli. Darker lines correspond to the associations between visual discrimination stimuli reaction times and children, while the lighter lines correspond to the associations between visual discrimination stimuli reaction times and adults.

8.2.3 Associations between reading and visual discrimination tasks

Finally, in order to examine to what extent visual discrimination is differentially associated with magnocellular and parvocellular word reading processes over development we conducted regression analyses for both accuracy and reaction time among the two tasks used in this empirical part.

For the children groups together, we computed first correlations without controlling for age and then, given previous results showing age-related behavioral improvements over childhood, partial correlations controlling for the factor Age. First, for accuracy measures we did not find associations between the reading task and the visual discrimination task, either for standard bivariate correlations as well as for partial correlations controlling for age ($r_{56} \leq 0.237$, $ps \geq 0.050$). On the other hand, bivariate correlations between the latencies of the reading task and the latencies of the visual discrimination task across children groups revealed statistically significant correlations for almost all conditions. However, once these results were corrected by age, these associations disappeared ($r_{60} \leq 0.276$, $ps \geq 0.050$).

For the adult group, we computed only standard bivariate correlations since there were no associations with age for response latencies or accuracy in either of the tasks. For accuracy measures, only the accuracy in the magnocellular word processing was positively associated with full overlap stimuli for both same color ($r_{34} = 0.64$, $p \leq 0.001$) and different color stimuli accuracies ($r_{35} = 0.58$, $p \leq 0.001$). Again, the rest of the comparisons did not result statistically significant ($r_{35} \leq 0.46$, $ps \geq 0.050$). On the other hand, for reaction times, we found significant associations only between magnocellular word processing latencies and no-overlap same color stimuli response latencies ($r_{35} = 0.47$, $p = 0.048$), between the magnocellular word processing latencies and partial overlap different color stimuli response latencies ($r_{35} = 0.48$, $p = 0.048$), between the magnocellular word processing latencies and no overlap different color stimuli response latencies ($r_{35} = 0.49$, $p = 0.036$), and between the

parvocellular word processing latencies and no overlap same color stimuli response latencies ($r_{35} = 0.47$, $p = 0.048$). The rest of the comparisons did not result statistically significant ($r_{35} \leq 0.46$, $ps \geq 0.050$).

8.3 Discussion

In the current study, developmental differences in processing magnocellular-biased and parvocellular-biased words were examined. As previously indicated, there is limited evidence on the maturation of these main visual pathways, and the available empirical data in this regard is mixed. The main objective of this study was to investigate age-related changes in the magnocellular and parvocellular contributions to typical reading process. Our analytical approach included behavioral analyses of the main reading task and associations between age and performance i) on reading processes for magnocellular-biased and parvocellular-biased stimuli, as well as ii) on visual discrimination conditions that varied as a function of crowding and stimuli characteristics. Results revealed that, at least for word processing, (1) the parvocellular pathway seem to develop earlier than the magnocellular pathway; (2) magnocellular-biased and parvocellular-biased word processing performance (i.e., accuracy, reaction time) was associated with age across middle childhood years, but during adulthood; (3) age was also associated with reaction times to all stimuli in the visual discrimination task in children, but not in adults; (4) only accuracy to the most difficult visual discrimination task condition (i.e., full overlap, same color) was associated with age during middle childhood years.

The main analyses conducted for the magnocellular/parvocellular reading task revealed relevant age-related differences as a function of the visual pathway. Specifically, in both children groups, that is, in the 8-11-years-old group and the 12-14-years-old group there were differences in accuracy, with higher values for parvocellular relative to magnocellular word processing, an effect that it was not present in the group of adults. These results suggest that

the magnocellular pathway takes longer to develop compared to the parvocellular pathway. Previous research evidence examined differences among these pathways in the first year of life, showing the opposite pattern or that during the initial 12 months of life the magnocellular pathway develops faster than parvocellular pathway (Dobkins et al., 1999; Hammarrengen et al., 2003), which may be the case and that at different developmental stages these pathways show differential adaptations.

Consistent with our results, other studies have also found that the development of the magnocellular pathway is more protracted than the development of the parvocellular pathway (Bucher et al., 2006; Crewther et al., 1999; Klaver et al., 2008). However, among other things, these studies have used different developmental samples (e.g., 5-6-years-old children; 15-17-years-old teenagers; 6-to-45-years-old participants; see Table 2) and different experimental paradigms (e.g., shapes defined by motion or luminance contrast, figures varying in temporal contrasts, randomly or coherently moving point-light dots; see Table 2), so there is still not a full consensus on the specific developmental trajectories of these relevant visual pathways and further research is needed to have a more refined understanding of their development and association with reading processes. In our study we found that by late middle childhood/adolescence both the magnocellular and parvocellular pathways seem to be fully matured, with children aged 12-to-14 years showing an adult-like behavioral pattern in regard of the involvement of these pathways in reading task.

For the visual discrimination task, accuracy measures revealed that group differences were only observed for same color (black) stimuli and when there was at least a minimum of overlap between the three letters. Specifically, our data showed that when the stimuli were fully overlapped, the differences were only observed between the early and late middle childhood groups; and, when the stimuli were partially overlapped, the differences were found between the both children groups and the adult group. For reaction times, we observed

that within early middle childhood children latencies were faster for different color stimuli only if there was some separation between the stimuli (i.e., partial overlap and no overlap conditions). For the late middle childhood group, different color stimuli showed faster reaction times only for non-overlapping stimuli. And finally, the adult group pattern of results revealed a systematic reaction time reduction for color stimuli as a function of stimuli separation. These results suggest age-related differences in visual discrimination between children and adults, with overlapping stimuli (partial and full) being more difficult for both early middle childhood and late middle childhood groups relative to adults.

On the other hand, regression analyses revealed that age was consistently associated with performance on the reading task for both magnocellular and parvocellular stimuli over middle childhood years or the period during we observed developmental improvements. In contrast, by adulthood or the period when these pathways would be in principle fully developed, no association between age and performance was observed. In contrast, regressions between age and the visual discrimination task only revealed associations across stimuli for reaction times, again, only in children. For accuracy, the only association statistically significant between age and performance was observed for the most difficult condition (i.e., when letters were fully overlap and there was no color facilitation), which means that for children and adults the complexity of the task is the same, but when the participants are answering to the most difficult stimuli, the developmental differences are present.

Finally, regression analyses between the reading and visual discrimination tasks showed only associations in the adult group, and especially for processing magnocellular word stimuli. It is true that one would *a priori* expect associations between the visual discrimination task stimuli and parvocellular word stimuli, since the parvocellular pathway is in principle a more detailed system than the magnocellular system. However, during the

visual discrimination task participants were asked to respond as quickly as possible. So, one possibility is that the instructions during the visual discrimination task emphasized the magnocellular system, which, although it is a more general system, is much faster than the parvocellular system. Even so, it should be noted that the associations between the parvocellular stimuli and the stimuli of the visual discrimination task were marginal. Future studies should further examining the role of the main visual pathways in visual discrimination.

In sum, the present study constitutes one of the first attempts to examine age-related changes over middle childhood of the influence of magnocellular and parvocellular pathways in word processing or reading. Our results indicate that, compared to the parvocellular pathway, the magnocellular pathway involvement in reading has a more protracted maturation from early middle childhood to early adolescence or ages where there is a massive development of cognitive capacities. We also observed a general effect of age on reaction times for both reading and visual discrimination tasks, and in particular on accuracy for the reading task.

9. Empirical Part II: A parvocellular-magnocellular functional gradient in the human visual cortex

The magnocellular and parvocellular systems are the major visual recognition pathways, with distinct histological and physiological properties. Despite their critical role, there is limited evidence on their specific contributions to visual recognition in general and to word reading in particular. The present fMRI study was aimed at characterizing the functional contributions of the magnocellular and parvocellular visual pathways to reading, in particular, as well as to visual recognition of object images, more generally in the visual cortex. Based on previous evidence, we hypothesized that 1) peripheral or more anterior visual cortex regions would be more strongly recruited during the processing of magnocellular-biased stimuli (Maunsell et al., 1990, Tootell et al., 1995, Rees et al., 2000, Grill-Spector et al., 2004); 2) since evidence for involvement of early visual cortex regions in processing parvocellular- or magnocellular-biased stimuli is limited, and to some extent mixed, we wanted to further explore whether these regions would be differentially recruited for processing magnocellular-biased or parvocellular-biased words and images; 3) in line with hypotheses 1 and 2, we expected tighter functional connectivity within than between posterior and anterior visual cortex regions; finally, 4) we predicted laterality effects for visual recognition of letter strings in left (versus right) peripheral or anterior visual cortex regions typically associated with magnocellular operations (Ray et al., 2005) in line with left hemisphere involvement in language processing (Lau et al., 2008).

9.1 Materials and Methods

9.1.1 Participants

The study sample consisted of 34 participants (19 females and 15 males, mean age 25.37 ± 4.41 years. Three additional participants were excluded from further analyses due to

excessive head motion during scanning (see "*MRI data acquisition and analysis*" section below) or problems with their functional data. Also, one participant was excluded due to low behavioral performance on the fMRI task (less than 60% accuracy).

All participants were right-handed and had normal or corrected-to-normal vision. No participant had any history of major medical, neurological, or psychiatric disorders. The study protocol was approved by the Ethics Committee of the Basque Center on Cognition, Brain and Language (BCBL) and was carried out in accordance with the Code of Ethics of the World Medical Association (Declaration of Helsinki) for experiments involving humans. Prior to their inclusion in the study, all subjects provided informed written consent. Participants received monetary compensation for their participation.

9.1.2 Stimuli

A total of 120 line drawings of words and images were used as stimuli. The uniform foreground of these drawings allows for precise control of luminance and chromatic properties. Half were magnocellular-biased, that is achromatic with low-luminance contrast; the other half were parvocellular-biased, that is, chromatically defined and isoluminant (red-green).

It is known that tuning of the magnocellular and parvocellular visual pathways differs across individuals, so we used standard procedures to adjust luminance and chromatic settings before MRI scanning (Cheng et al., 2004; Kveraga et al., 2007; see also Skottun, 2013, for cautions on using isoluminant stimuli). The standard technique for establishing the luminance threshold for magnocellular-biased achromatic stimuli involves a multiple staircase procedure, during which subjects are required to answer whether or not they can identify image and word stimuli. Once the luminance threshold has been established, the appropriate luminance (~3.5% Weber contrast) value is defined for the gray-scale line

drawings to be used in the low-luminance-contrast, magnocellular-biased, condition. We used a common luminance value across all participants for the magnocellular-biased stimuli; we had shown that these stimuli met an 80% accuracy criterion in a normative study (N = 15) made prior to the current experiment. In that normative study, we used 40 words and 40 images (i.e., line drawings corresponding to each of these words), in a counterbalanced fashion, to determine the appropriate luminance contrast for participants to reach 80% accuracy on the achromatic magnocellular-biased stimuli. The criterion of minimum 80% of accuracy was used to guarantee enough correct responses to magnocellular-biased stimuli, since magnocellular-biased trials are, in general, more difficult to process than parvocellular-biased ones.

For the parvocellular-biased, chromatically defined stimuli, the isoluminance point was identified for each subject individually using heterochromatic flicker photometry as reported in previous studies (Kveraga et al., 2007). This procedure identifies the isoluminance point for two colors by having a stimulus rapidly alternate between them. The color values at which the stimuli appears to stop flickering indicates the narrow isoluminance interval of the steady point. Each participant was required to indicate the steady point for line drawings of images displayed in pure red and pure green before undergoing MRI scanning.

All of the images and word stimuli were designed in both a magnocellular-biased and a parvocellular-biased form and each word had a corresponding image, so that all stimuli were properly counterbalanced across subjects in terms of Pathway (i.e., magnocellular, parvocelullar) and Stimuli (i.e., words, images) (see Figure 18). All the selected items could be easily identified as non-manmade (i.e., *apple*) or manmade (i.e., *robot*); 50% of items were "non-manmade", and the remaining 50% were "manmade".

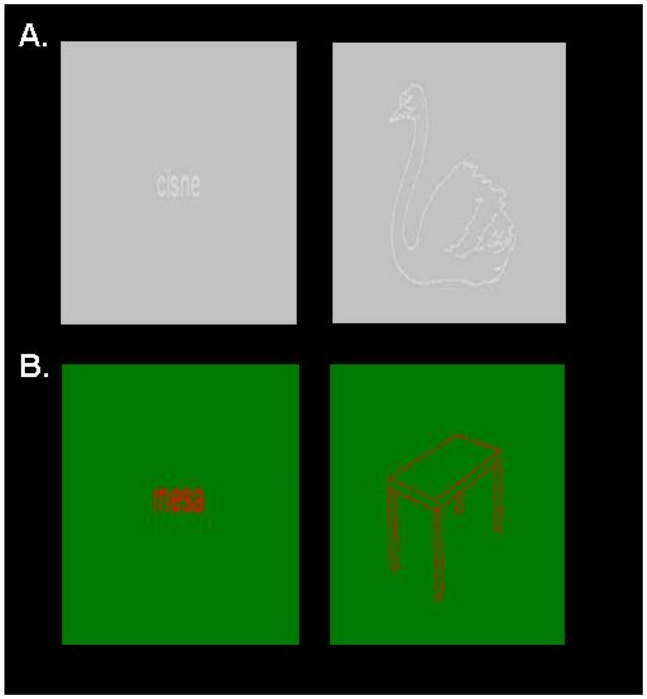

Figure 18: Experimental stimuli. We used a hybrid event/block design where participants made manmade (i.e., artificial) or non-manmade (i.e., natural) judgments to words and images that were A) magnocellular biased, having a low-luminance contrast and achromatic; and B) parvocellular biased, being isoluminant (red-green) and chromatically defined. All stimuli were counterbalanced between conditions and subjects.

9.1.3 Experimental task and procedure

Functional and structural data was collected at the BCBL MRI scanner (see *MRI data acquisition* section below). The fMRI task conformed to a 3 (Pathway: magnocellular, parvocellular) X 2 (Stimuli: words, images) visual recognition experimental design, which was carried out in a single functional run that lasted 10 min. During the task, participants were asked to perform a semantic task, in which they indicated natural (i.e., non man-made) or artificial (i.e., man-made) judgements via key presses on a two-button fiber-optic box. Six stimuli were presented in each activation block of 20.3 s duration. Activation blocks were alternated with rest-fixation periods of 16 s to allow the hemodynamic response function (HRF) to return to baseline. A total of 90 words and 90 images were presented across activation blocks, yielding 5 activation blocks for each of the 4 experimental conditions. The

stimuli were presented at 100 Hz using a Barco projector (model F35); the refresh rate was confirmed using The Black Box ToolKit v2™.

For behavioral analysis, we conducted two separate 2 (Pathway: magnocellular, parvocellular) X 2 (Stimuli: words, images) ANOVAs with accuracy and reaction times as dependent measures. Only blocks with at least 60% correct responses were included in the behavioral and fMRI analyses [total number of excluded blocks from the final sample (N = 34) = 57; mean excluded blocks per subject = 0.08). We used the mean ± 2.5SD as a criterion to remove outliers values in all measures in this study.

We applied multiple comparison corrections to all behavioral as well as functional MRI results. We also computed effect sizes and Bayes factor values ($BF10 > 3$ suggests substantial evidence for a difference between pairs; $BF10 < 0.3$ suggests substantial evidence for a null effect, see Jeffreys, 1961).

9.1.4 MRI data acquisition

Whole-brain MRI data acquisition was conducted on a 3-T Siemens PRISMA Fit whole-body MRI scanner (Siemens Medical Solutions) using a 64-channel whole-head coil. Functional images were acquired in a single gradient-echo echo-planar multiband pulse sequence with the following acquisition parameters: time-to-repetition (TR) = 1000 ms; time-to-echo (TE) = 35 ms; MB acceleration factor = 5; 65 axial slices with a 2.4 mm^3 voxel resolution; no inter-slice gap; flip angle = 56º; field of view (FoV) = 210 mm; 880 volumes. High-resolution MPRAGE T1-weighted structural images were also collected for each participant with the following parameters: TR = 2530 ms; TE = 2.36 ms; flip angle = 7°; FoV = 256 mm; voxel resolution = 1 mm^3; 176 slices.

9.1.5 MRI data analysis

For ***structural analysis*** of the T1-weighted images, we used the Freesurfer 6.0 pipeline (Fischl et al., 2004) to perform volumetric gray- and white matter segmentation, providing several automated cortical parcellations for use in subsequent analyses. After obtaining the gray-matter segmentation with Freesurfer, we ran Benson's Neuropythy visual cortex segmentation tool (Benson et al., 2014) to obtain visual cortex regions at the individual-subject level.

For ***functional data preprocessing and analysis***, we used SPM12 (Wellcome Center for Human Imaging, London) preprocessing routines and analysis methods. Images were corrected for differences in slice acquisition timing across every functional scan and then realigned for motion correction. Afterwards, each subject's functional volumes were smoothed using a 2-mm full-width half-maximum (FWHM) Gaussian kernel. Motion parameters were extracted from the realignment step to inform a volume repair procedure (ArtRepair; Stanford Psychiatric Neuroimaging Laboratory) that identified bad volumes on the basis of scan-to-scan movement (>0.5 mm) and signal fluctuations in global intensity (>1.3%) and corrected bad volumes via interpolation from the nearest non-repaired scans. One participant with more than 20% to-be-corrected outlier volumes was excluded. For the final sample of participants, the average percentage of repaired volumes was 2% (SD = 3%). After volume repair, high-resolution anatomical T1 images and functional volumes were coregistered and resliced from the original 2.4 x 2.4 x 2.4 mm functional voxel dimensions to 1 x 1 x 1 mm voxels in anatomical T1 space. Finally, time series were temporally filtered to eliminate contamination from slow frequency drift (high-pass filter: 128 s). Once all functional images were in the same space as the individual anatomical images, we ran Benson's Neuropythy tool (Benson et al., 2014) to segment visual cortex regions of interest at the individual-subject level.

Statistical analyses were performed on individual-subject data using the general linear model (GLM). A series of impulses convolved with a canonical hemodynamic response function (HRF) were used to model the fMRI time series data. The four main experimental conditions in our design (i.e., magnocellular-biased words, magnocellular-biased images, parvocellular-biased words, and parvocellular-biased images) were modeled from the onset of the presentation of the first stimulus within each block until the end of the presentation of the last experimental stimulus within the block, resulting in 20.3 s epochs. These functions were used as covariates in the GLM. The motion parameters for translation (i.e., x, y, z) and rotation (i.e., yaw, pitch, roll) were used as covariates of non-interest in the GLM. SPM12 FAST was used for temporal autocorrelation modeling in this GLM due to its optimal performance in terms of removing residual autocorrelated noise in first-level analyses (Olszowy et al., 2019), especially relevant for the present study since data was processed in individual-subject space. The least-squares parameter estimates of the height of the best-fitting canonical HRF for each condition were used in pairwise contrasts. Importantly, blocks with less than 60% correct responses were modeled separately and not considered in the main analyses [the total number of excluded blocks across the final sample (N = 34) = 57; mean excluded blocks per subject = 0.08. As previously indicated, an additional participant with more than 10 blocks with less than 60% correct responses was excluded from the final sample.

9.1.6 ROI definition

Given that the main interest of the study was to examine the involvement of visual cortex in visual recognition of letter strings, a total of six left-lateralized visual regions of interest were examined. These regions, extracted were V1, V2, V3, hV4, lateral occipital (LO1), and temporal occipital (TO1). The corresponding right-lateralized regions were also extracted to

examine whether they would follow the same functional patterns as the left hemisphere ones (see Annex II).

9.1.7 Data analysis

Individual ROI analysis. ROI analysis was performed with the MARSBAR toolbox for use with SPM12. Then, in line with our main experimental design, and in order to avoid problems associated with greater signal in more posterior compared to more anterior areas, we extracted parameter estimates (i.e., scaled % signal change values; Mazaika, 2009) and signal t-values for specific contrasts related to the factor Pathway (i.e., Magnocellular > Parvocellular Words; Magnocellular > Parvocellular Images; Parvocellular > Magnocellular Words; Parvocellular > Magnocellular Images) for each single region at the individual-subject level. Finally, 6 (ROI: V1, V2, V3, hV4, LO1, and TO1) X 2 (Stimuli: words, images) repeated measures ANOVAs were performed. Results were corrected using the false discovery rate (FDR) correction for multiple comparisons.

Probabilistic maps. Four surface-based probabilistic maps were calculated using Analysis of Functional Images (AFNI) software (Cox et al., 1996, Cox et al., 1997, Saad et al., 2004) to examine the differential contribution of voxels within visual cortex ROIs (i.e., V1, V2, V3, hv4, LO1, TO1). First, the activations inside the six visual cortex ROIs were binarized for the two contrasts by using a threshold common to all the subjects (i.e., for every subject, all voxels that had a positive t-values were scored 1 and used for the magnocellular-biased maps with the rest zeroed, whereas all voxels that had a negative t-values were scored 1 and used for the parvocellular-biased maps with the rest zeroed). Thus, the binarization step initially yielded four different binarized maps: Magnocellular > Parvocellular Words; Magnocellular > Parvocellular Images; Parvocellular > Magnocellular Words; and, Parvocellular > Magnocellular Images. Due to the lack of significant interactions involving

the factor Stimuli in ROI analyses, we also obtained probabilistic maps for Magnocellular > Parvocellular and Parvocellular > Magnocellular contrasts across stimuli conditions. As all ROI and related functional data was in individual-subject space, the binarized maps and the ROIs were normalized to MNI space using the Advanced Normalization Toolbox (ANTs) to obtain these probabilistic maps. After normalization to standard space, corresponding ROIs from every subject were superimposed on the four maps. For each ROI, a probability map was generated by dividing, at each particular voxel, the number of times that that voxel belonged to that ROI by the number of subjects included for that ROI. A voxel would have a 100% value if all subjects had this voxel activated for the indicated contrast. A voxel would have a 0% value if none of the subjects had this voxel activated for the indicated contrast.

Functional connectivity analysis. Functional connectivity analyses were conducted via the beta-series correlation method (Rissman et al., 2004), implemented in SPM12 with custom Matlab scripts. The canonical HRF in SPM was fit to each trial from each experimental condition and the resulting parameter estimates (i.e., beta values) were sorted according to the study conditions to produce a condition-specific beta series for each voxel. Pairwise functional connectivity analysis between each pair of visual cortex ROIs (i.e., V1, V2, V3, hV4, LO1, TO1) were conducted at the individual-subject level. This was done by applying an arc hyperbolic tangent transform (Fisher, 1921) at the subject level to the beta-series correlation values (r values) of each pair of ROIs and each experimental condition. Since the correlation coefficient is inherently restricted to range from −1 to +1, this transformation ensured the null hypothesis sampling distribution approached that of the normal distribution. First, we created correlation matrices with the mean correlation values of all subjects for each experimental condition, where significant correlations, $r \geq 0.57$ were colored red. In this case, Pearson's r values were corrected using Bonferroni correction (Pair of ROIs x Conditions x Hemisphere), which is more conservative than FDR, since we were

testing coactivation between adjacent regions. Afterwards, we examined the association between functional connectivity strength and physical distance (i.e., the Euclidean distance between the center of mass of two ROIs) of the given ROI pair per subject. The Euclidean distance between the center of mass of two ROIs was computed by averaging the left and right hemisphere Euclidean distance values. Finally, to test for significant differences in the coupling strength of the pairwise connectivity, Fisher's Z normally distributed values for each pair of ROIs for each participant and condition were submitted to 6 separated 5 (ROI Pair) x 2 (Pathway) x 2 (Stimuli) repeated measure ANOVAs. Results were corrected using the Bonferroni correction for multiple comparisons.

Laterality analyses. Lateralization indexes of the signal t-values for the four conditions of interest, i.e., magnocellular-biased words, magnocellular-biased images, parvocellular-biased words and parvocellular-biased images were calculated. For this purpose, the standard lateralization index (LI) was computed:

$$LI = \frac{tVal_{LH} - tVal_{RH}}{tVal_{LH} + tVal_{RH}}$$

This index produces values between -1 and 1 and relates the left-right signal t-value difference to the mean of the left-right signal t-values. Positive values correspond to stronger left than right t-values; conversely, negative values correspond to stronger right than left t-values.

Since LI values must be between 0 and 1, the t-values were first normalized to values from 0 and 1 using a linear scaling procedure. Once signal t-values were normalized, the laterality of words and images was computed for the magnocellular and parvocellular pathways within the visual regions. Then, paired t-tests between words and images LIs were performed for each of the pathways and ROIs. Results were corrected using the false

discovery rate (FDR) correction for multiple comparisons. The laterality of two pathways was not compared since the ROI analysis, probabilistic maps, and functional connectivity analysis did not reveal relevant significant effects of hemisphere as a function of pathway.

9.2 Results

9.2.1 In-scanner behavioral results

A 2 (Pathway) X 2 (Stimuli) ANOVA revealed a statistically significant main effect of Pathway ($F_{1,31}$= 12.84; ηp^2 =0.29, p < 0.001, BF10 = 9.91), (see Figure 19*A*), showing that accuracy was higher for parvocellular-biased than magnocellular-biased stimuli.

The ANOVA for reaction times to correct responses also revealed significant main effects of Pathway ($F_{1,33}$=48.489; p ≤ 0.001, η_p^2 =0.595, BF10 = 94896.73) and Stimuli ($F_{1,33}$=33.30; p ≤ 0.001, η_p^2 =0.50, BF10 = 106557.38). Simple-effect *post-hoc* analyses revealed the main effect of pathway was due to longer response latencies for magnocellular-biased than parvocellular-biased stimuli (see Figure 19*B*). The main effect of Stimuli was driven by longer response times for words (M = 1.00 s; SD = 0.16 s) than images (M = 0.92 s; SD = 0.15 s). The Pathway X Stimuli interaction was not significant ($F_{1,33}$=2.18; p = 0.149, η_p^2 =0.06, BF10 = 0.39).

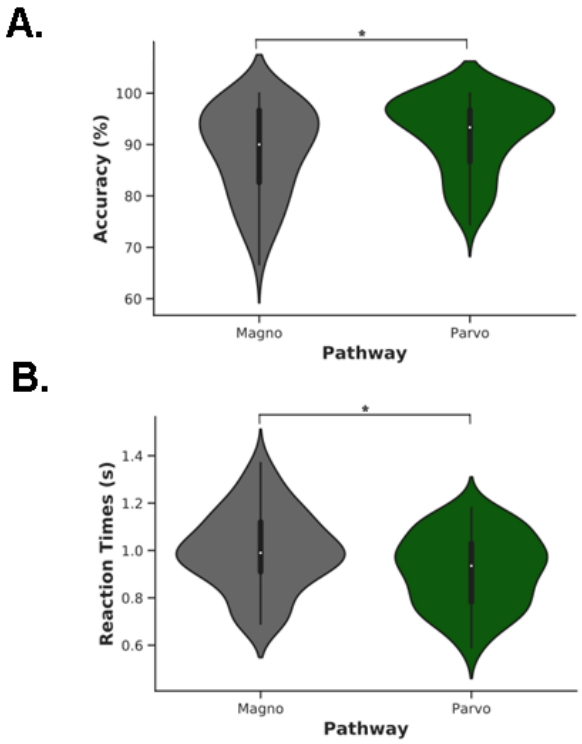

Figure 19: In-scanner behavioral results. A) Percent (%) mean accuracy of manmade and non-manmade judgments as a function of visual magnocellular and parvocellular pathways. B) Correct-response reaction times as a function of magnocellular and parvocellular pathways. The white dots on the violin plots represents the median, while the black bar in the center represents the interquartile range. Thick black lines indicate statistically significant effects: *ps < .05.

9.2.2 fMRI analytical approach and results

We used four analytic approaches to examine visual recognition of words and images in the visual cortex and the degree of involvement of the two main magnocellular and parvocellular visual pathways. All analyses were conducted in individual-subject space. First, given that the activation signal tends to be stronger in the more posterior relative to the more anterior visual areas, we used specific contrasts in ROI-related analyses, including both percent signal change and signal t-value dependent measures, to examine the recruitment of visual cortex regions in line with our experimental design. Second, to further investigate differential contributions of visual regions to the two main visual pathways for reading and image recognition, we created probabilistic maps using the same contrasts utilized in the ROI analyses. In our third analytical approach, we used functional connectivity methods to

examine differential coactivation among visual regions during task processing. We computed the relationship between the pairwise-connectivity correlation values and the Euclidean distance between the physical distances of the center of mass of each of the ROI pairs, along with analyses comparing the strength of coactivations between pairs of regions. Finally, we investigated lateralization effects associated with word and image processing specifically for each visual pathway given the lack of differences between hemispheres for the pathway factor in our previous analyses.

All these analytical steps, except the laterality analysis, were conducted for left-lateralized visual regions because our focus was on language-related processes. Nevertheless, we also present the corresponding right-hemisphere analyses in the Annex II.

9.2.2.1 Individual ROI analyses

ROI analyses were conducted at the individual-subject level to characterize the activation profile of regions within the left visual cortex. To avoid potential biases in the observed effects due to stronger signal strength in more posterior relative to more anterior regions, parameter estimates (i.e., scaled % signal change and signal t-values) for the specific contrasts (Magnocellular > Parvocellular Words and Magnocellular > Parvocellular Images) were extracted and submitted to a 6 (ROI: V1, V2, V3, hV4, LO1, TO1) X 2 (Stimuli: words, images) repeated measures ANOVA. This analysis revealed main effects of ROI ($F_{5,150}$ = 50.01; $p \leq 0.001$, $\eta_p^2 = 0.62$, BF10 = 2.38 e^{31}) and Stimuli ($F_{1,30}$ = 1.21; p = 0.006, $\eta_p^2 = 0.25$, BF10 = 547.25). Simple-effect analyses for the ROI main effect revealed an anterior to posterior functional gradient with stronger engagement of the more anterior relative to the most posterior visual cortical regions (see Figure 20*A*, upper panel). All comparisons were statistically significant (qs ≤ 0.001, d' ≥ 852, BF10 ≥ 120170.861; V2-hV4 and LO1-TO1 qs ≤ 0.014, d' ≥ 0.33, BF10 ≥ 2.79), with the exception of hV4-V3, the only comparison that did not show a statistical difference (q = 0.493, d' = 0.09, BF10 = 0.18). In regard to the main

effect of Stimuli, these regions in visual cortex were in general more strongly engaged for processing words (M = -0.11; SD = 0.32) than images (M = -0.20; SD = 0.33).

Second, the same analysis was carried out with t-values instead of % signal change values. The same general pattern of results emerged (ROI main effect, $F_{5,130} = 49.68$; $p \leq 0.001$, $\eta_p^2 = 0.66$, BF10 =2.01 e^{34}), except that main effect of Stimuli did not reach significance ($F_{1,26} = 3.04$; $p = 0.093$, $\eta_p^2 = 0.11$, BF10 = 2.47). Simple-effect analysis for the ROI main effect also confirmed an anterior-posterior functional gradient for the scaled % signal change values. All comparisons were statistically significant ($qs \leq 0.001$, $d' \geq 0.79$, BF10 $\geq$ 184534.83; LO1-TO1, $q = 0.003$, $d' = 0.39$, BF10 = 9.34), except the hV4-V3 comparison, which revealed no statistical difference ($q = 0.052$, $d' = 0.26$, BF10 =0.89). Figure 20 shows the ROI analysis for Magnocellular > Parvocellular contrasts across stimuli conditions, given that the interaction ROI x Stimuli was not significant (Figure 20*A*: the upper panel corresponds to % signal change values; the bottom panel corresponds to signal t-values).

Third, the same 6 X 2 repeated measures ANOVAs using % signal change and t-values as dependent measures was conducted for the specific contrasts Parvocellular > Magnocellular Words and Parvocellular > Magnocellular Images for each left visual cortex ROIs. Again, the same pattern of results emerged in the ANOVAs and post-hoc analyses. % signal change (Figure 20*B*, upper panel) showed main effects of ROI ($F_{5,130} = 48.09$; $p \leq 0.001$, $\eta_p^2 = 0.65$, BF10 = 2.37 e^{31}) and Stimuli ($F_{1,26} = 9.00$; $p = 0.006$, $\eta_p^2 = 0.26$), while t-values (Figure 20*B*, bottom panel) showed a main effect of ROI ($F_{5,135} = 49.75$; $p \leq 0.001$, $\eta_p^2 = 0.65$, BF10 = 2.03 e^{34}).

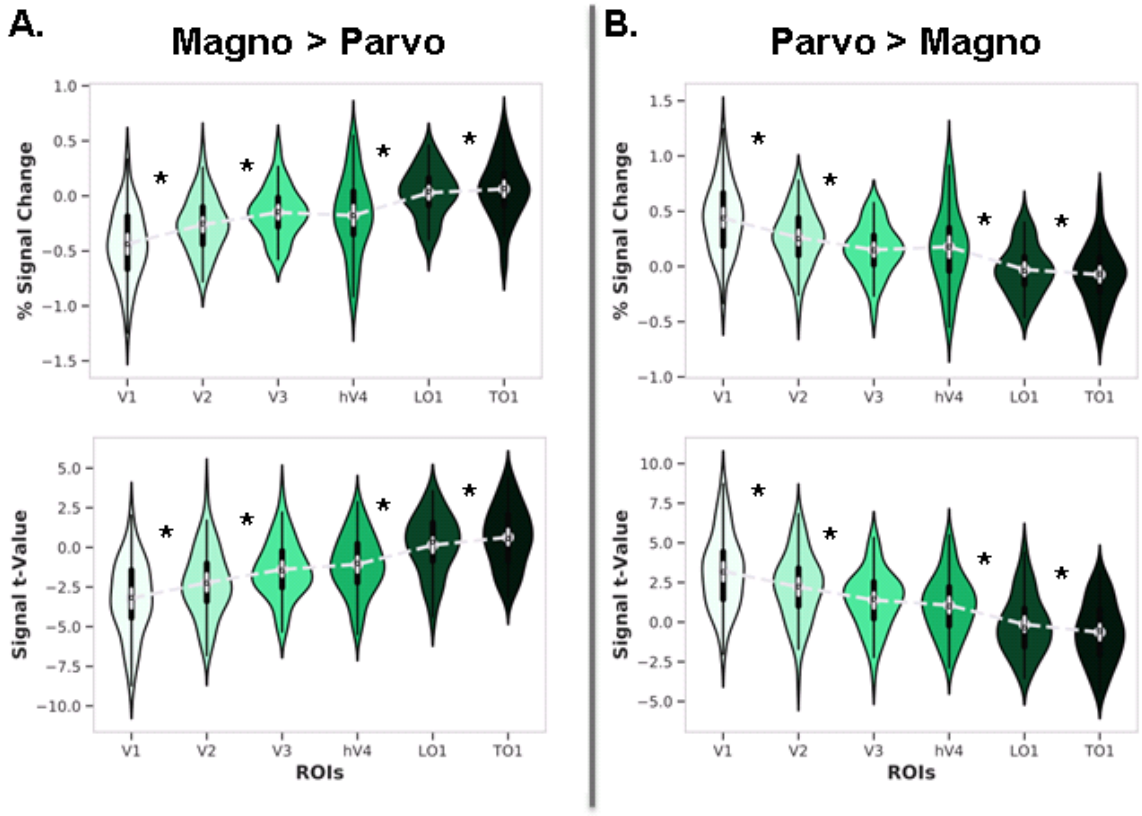

Figure 20: ROI analyses. A) Percent signal change (top panel) and regional t-values (bottom panel) of left hemisphere visual cortex ROIs for the Magnocellular > Parvocellular contrast. B) Percent signal change (top panel) and regional t-values (bottom panel) of left hemisphere visual cortex ROIs for the Parvocellular > Magnocellular contrast. The black bar in the center of the violins represents the interquartile range, while the gray dash lines reflect the median. * asterisks denote statistically significant effects (FDR corrected). Magno = magnocellular; Parvo = parvocellular.

Finally, identical analyses were carried out for the right visual cortex (see Annex II). Findings were similar to those observed for left visual cortex in terms of the anterior-posterior functional gradient (i.e., ROI main effect; Figure 1Annex II). However, in contrast to the left hemisphere where we observed a main effect of Stimuli for % signal change values (but not signal t-values), the right hemisphere analysis did not show a main effect of Stimuli in either the % signal change or signal t-values dependent measures. This suggests that the left hemisphere might be more sensitive in differentiating the two types of stimuli (words and images), but only when parameter estimates are used as the dependent measure.

9.2.2.2 Probabilistic maps

To further examining the robustness of the functional gradient observed for the Pathway factor in terms of % signal change and signal t-values, we conducted an additional fMRI analysis using left visual cortex surface-based probabilistic maps. This allowed us to examine the probability that a given voxel was significantly engaged in a functional contrast of interest. Since we did not observe any significant interactions with the factor Stimuli in the ROI Analysis, we performed probabilistic maps for Magnocellular > Parvocellular and Parvocellular > Magnocellular contrasts across stimuli conditions (see Figure 2 Annex II for probabilistic maps for words and images). These maps revealed that in the Magnocellular > Parvocellular contrast, higher probabilities were located in more anterior regions within the visual cortex (i.e., LO1, TO1; see Figure 21*A*). In contrast, the probabilistic map for Parvocellular > Magnocellular showed higher probabilities in more posterior regions, including primary visual cortex (V1, V2, V3 and hV4; Figure 21*B*). Color-coding denotes the likelihood of each voxel being assigned to one or the other pathway in the probabilistic map. Maps are not fully complementary since probability is assigned based on each specific contrast.

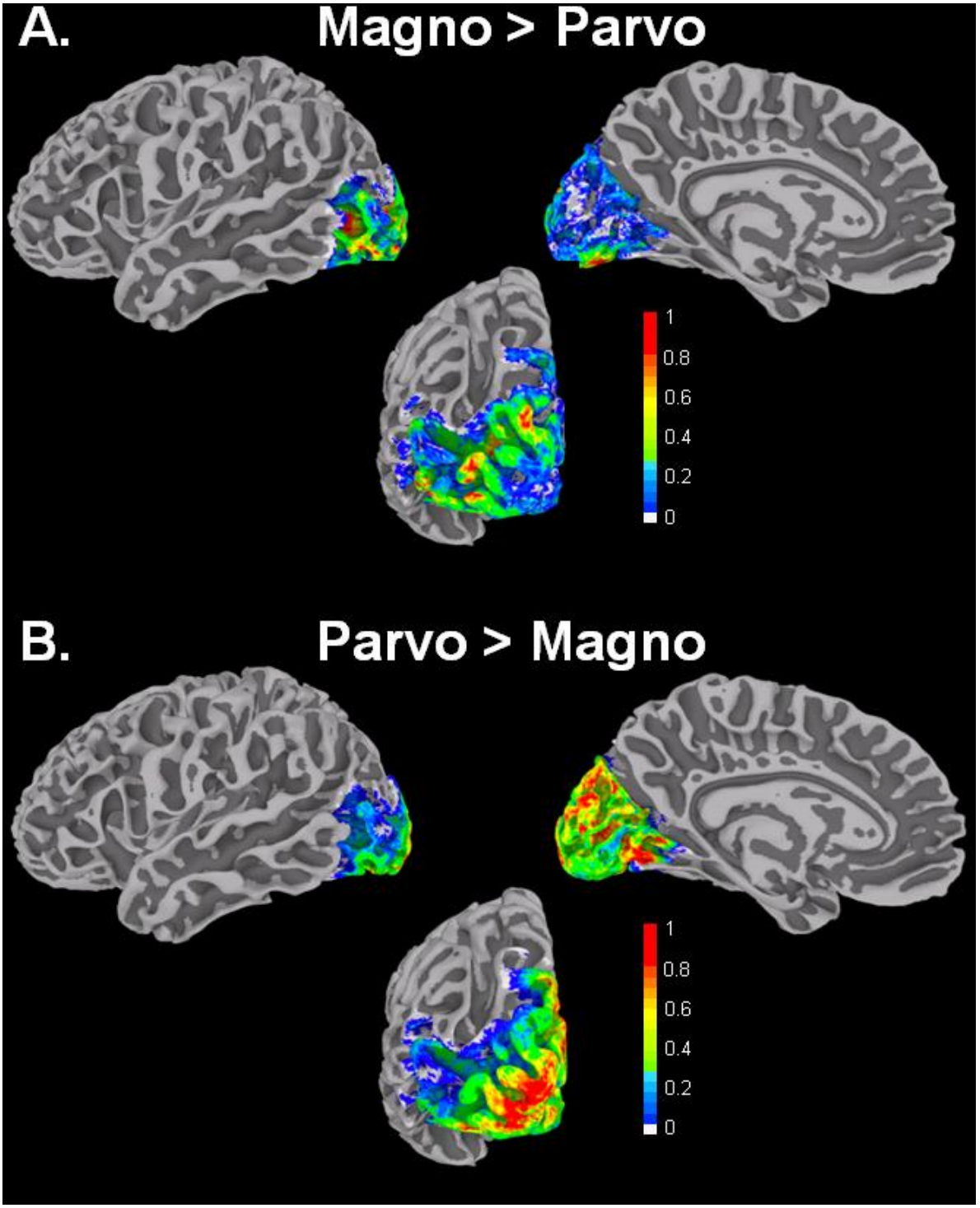

Figure 21: Probabilistic maps showing the percentage of involvement of left visual cortex voxels on surface renderings for the contrasts A) Magno > Parvo and B) Parvo > Magno. The two probabilistic maps are not fully complementary: although they represent opposite contrasts, they were generated by separate analyses. Magno = magnocellular; Parvo = parvocellular.

Probabilistic maps for the right visual cortex showed a similar pattern to those for the left hemisphere, with stronger probabilities for the involvement of anterior regions in the

Magnocellular > Parvocellular contrast and for posterior regions in the Parvocellular > Magnocellular contrast (see Figure 3 Annex II; and also Figure 4 Annex II for right hemisphere probabilistic maps for words and images).

9.2.2.3 Pairwise functional connectivity analysis

To examine patterns of functional connectivity between left visual cortex regions, we first characterized overall coupling strength across study conditions. Figure 22*A* shows the correlation matrix for Pearson's r values between pairs of ROIs (red colored circles indicate statistically significant FC values, $r \geq 0.57$, Bonferroni corrected) and a representation of Euclidean distance against Pearson's r values between each pair of nodes (shadowed areas indicate significant FC). Figure 22*B* shows a surface rendering with statistically significant functional connectivity between visual cortex regions displayed as edges. Overall, stronger coactivations were found among posterior visual regions (i.e., V1, V2, V3) and anterior visual regions (i.e., hV4, TO1, TO1). In contrast, more distant anterior-posterior regions did not show statistically significant FC.

Second, to more closely examine FC in the left visual cortex, in line with our experimental questions, Fisher's *Z* transformed FC values were submitted to a series of 5 (ROI Pairs) X 2 (Pathway) X 2 (Stimuli) separate repeated measures ANOVAs, one for each of the examined visual cortex regions. All of the analyses revealed a main effect only for ROI Pair ($F_{4,64} \geq 5.84$; $ps \leq 0.001$, $\eta_p^2 \geq 0.24$, $BF10 \geq 210.15$) (Figure 22*C*). From more posterior to more anterior, simple-effect analyses revealed that *V1* was functionally more strongly tied to V2 than to V3, hV4, LO1 and TO1 ($ps \leq 0.04$, $d' \geq 0.26$, $BF10 \geq 6.39$); but no differences in FC emerged between V1-LO1 or V1-TO1 or between V1-hV4 or V1-TO1 ($ps \geq 0.12$, $d' \leq 0.23$, $BF10 \leq 2.20$; see Figure 22*C*). Second, there was stronger FC between *V2* and V3 than between V2 and all the other visual regions (i.e., V1, V3, hV4, LO1 and TO1; $ps \leq 0.04$, $d' \geq 0.27$, $BF10 \geq 6.62$); again, with no significant differences emerging in FC between V2-LO1

and V2-TO1 ($p > 0.05$, $d' = 0.02$, $BF10 = 0.10$). Third, a similar pattern of results emerged for *V3*: stronger FC for the V3-V2 contrast than for contrasts between V3 and the rest of the visual regions (i.e., V1, hV4, LO1 and TO1; $ps \leq 0.02$, $d' \geq 0.28$, $BF10 \geq 9.84$; no FC differences between V3-LO1 and V3-TO1, V3-V1 and V3-hV4, V3-V1 and V3-LO1, or V3-V1 and V3-TO1 [$ps \geq 0.76$, $d' \leq 0.16$, $BF10 \leq 0.47$]).

On the other hand, more anterior visual cortex regions hV4, LO1 and TO1 presented a similar FC pattern. hV4 showed stronger connectivity with V3 relative to either V2 or V1 ($ps \leq 0.01$, $d' \geq 0.31$, $BF10 \geq 31.71$), but there were no differences in coactivation between hV4-V1 and hV4-LO1, hV4-V3 and hV4-LO1, hV4-V2 and hV4-LO1, hV4-V2 and hV4-TO1, hV4-V3 and hV4-TO1, or hV4-LO1 and hV4-TO1 ($ps \geq 0.05$, $d' \leq 0.10$, $BF10 \leq 0.19$; see Figure 22*C*). FC of the *LO1* was similar to visual regions V3, hV4, and TO1; and stronger to all of these regions than to visual cortex regions V1 and V2 ($ps \leq 0.001$, $d' \geq 0.38$, $BF10 \geq 265.74$); but there were no differences in coactivation, between LO1-V3 and LO1-hV4, LO1-V3 and LO1-TO1, or between LO1-hV4 and LO1-TO1 ($ps \geq 0.05$, $d' \leq 0.06$, $BF10 \leq 0.12$). Finally, FC of the *TO1* was similar to that for visual regions TO1 and hV4; exhibiting stronger connections to these two regions compared to visual cortex regions V1, V2, and V3 ($ps \leq 0.01$, $d' \geq 0.29$, $BF10 \geq 265.74$). There were no differences in the coactivation between TO1-V3 and TO1-hV4, TO1-V3, or TO1-LO1 or between TO1-hV4 and TO1-LO1 ($ps \geq 0.12$, $d' \leq 0.22$, $BF10 \geq 0.12$).

In sum, V1, V2, and V3 were tightly coupled to each other as a function of their proximity, showing statistically significant lower FC with the more anterior visual cortex regions (LO1, TO1) (Figure 22C). Anterior regions hV4, LO1, and TO1 were also strongly coupled to each other but showed statistically lower FC with posterior regions V1 and V2. FC

results for the right hemisphere are reported in the Annex II (see Figure 5 Annex II). They followed a similar pattern as those described for the left hemisphere.

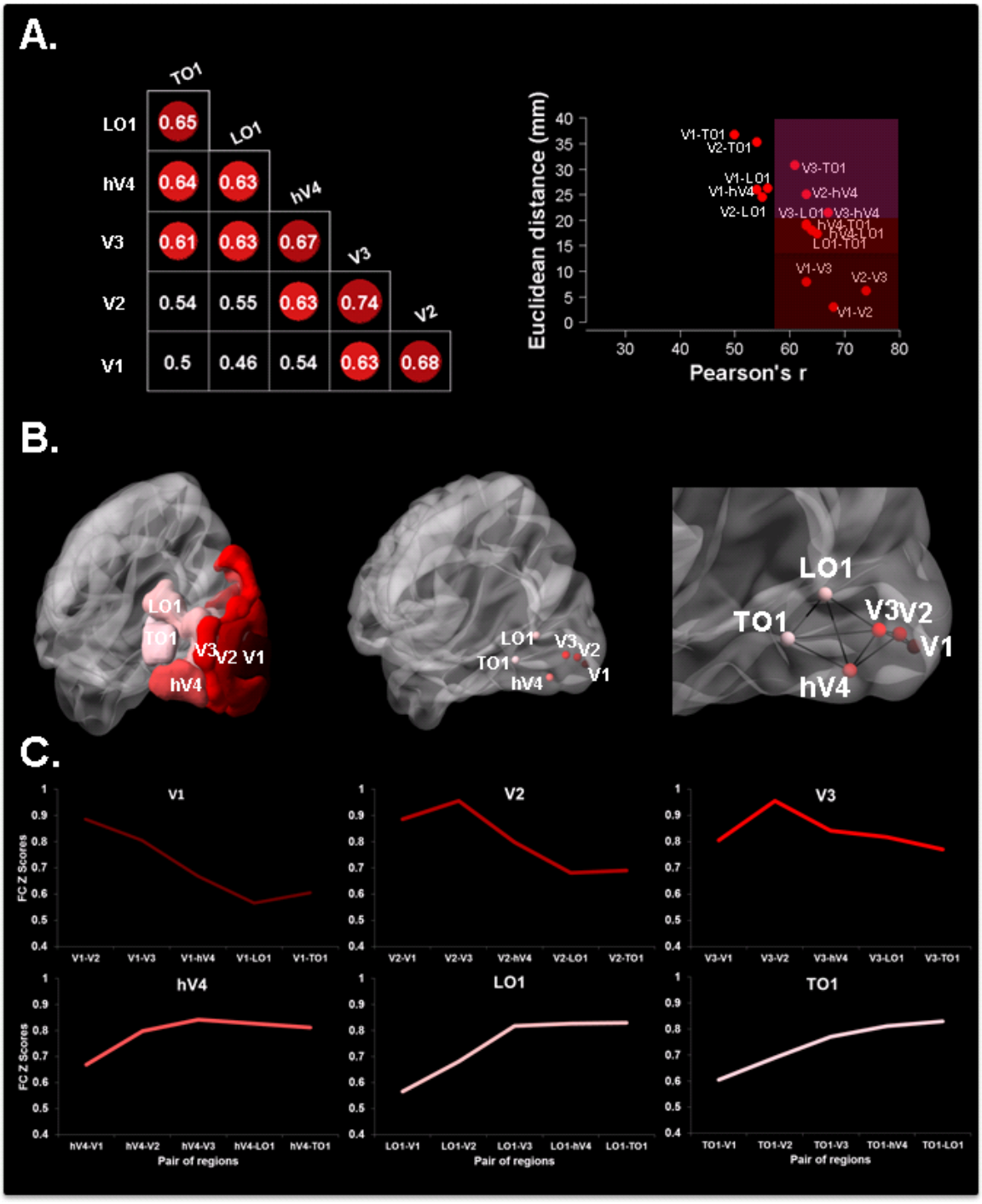

Figure 22: Task-related pairwise functional connectivity between left visual cortex ROIs across experimental conditions (i.e., magnocellular-biased words, parvocellular-biased words, magnocellular-biased images, parvocellular-biased images). A) Left panel shows the correlation matrix with significant Pearson's r correlations (r ≥. 57) colored in red tones. Right panel shows Euclidean distances from posterior (V1, 0-value) to anterior (TO1) left visual cortex regions plotted against Pearson's r values for each ROI pair; shaded areas

indicate pairs with significant coupling. B) Left panel shows the sagittal rendering of the left visual cortex ROIs. Central panel shows the sagittal rendering of left visual cortex nodes centered at the ROIs center of mass. Right panel shows statistically significant pairwise correlations (i.e., edges) between left visual cortex nodes in a posterior sagittal rendering section. C) Task-related pairwise functional connectivity (Z scores) between left visual cortex ROI pairs across experimental conditions. The upper left panel shows Z scores between V1 and the rest of the ROIs, upper middle panel shows Z scores between V2 and the rest of the ROIs, and upper right panel shows Z scores between V3 and the rest of the ROIs. The lower left panel shows Z scores between hV4 and the rest of the ROIs, lower middle panel shows Z scores between LO1 and the rest of the ROIs, and lower right panel shows Z scores between TO1 and the rest of the ROIs.

9.2.2.4 Laterality analysis

To study hemispheric specialization, paired t-tests were conducted on laterality indexes of words and images for each ROI within each pathway. Laterality analyses comparing the two pathways were not performed since ROI analysis, probability maps, and FC analysis did not reveal relevant significant hemispheric effects as a function of pathway. Comparisons between magnocellular-biased words and images revealed that the LO1 region was more left lateralized for words (LI = 0.09) than images (LI = -0.16) ($q = 0.003$, $d' = 0.68$, BF10 = 63.83). For the parvocellular pathway, results showed that the V1 region was also more left lateralized for images (LI = 0.02) than words (LI = -0.10) ($q = 0.022$, $d' = 0.52$, BF10 = 7.12). All the other comparisons did not reveal any statistically significant effects ($ps \geq 0.05$, $d' \leq 0.44$, $BF10 \leq 2.92$).

9.3 Discussion

In the current study, visual cortex magnocellular and parvocellular contributions to reading and object recognition were examined. Although there are well-accepted theories regarding the roles of these main visual pathways in object recognition, their functional involvement of the in word recognition has received considerably less attention. The present study sought to address this gap in the research by examining the functional correlates of word and image recognition along these pathways within the visual cortex. Our analytical approach included behavioral analyses and both regional and connectivity functional MRI

measures in individual-subject space. Results showed (1) an advantage for parvocellular-biased over magnocellular-biased stimuli in terms of accuracy and reaction times; (2) differential recruitment of posterior versus anterior visual cortex regions as a function of the parvocellular versus magnocellular pathway manipulation in our experimental design; (3) functional coupling as a function of the distance between regions, with more clustering within than between posterior and anterior regions (4) more left lateralization of words in more peripheral regions of the visual cortex, but more left lateralization of images in more posterior regions of the visual cortex. The relevance of these findings for reading are discussed next.

Magnocellular-biased stimuli are less bright and more difficult to recognize than parvocellular-biased stimuli. This led to lower accuracy and longer reaction times for these stimuli than either the parvocellular-biased or neutral non-biased stimuli in the behavioral results – even though we had conducted a pilot study to ensure high accuracy (i.e., 80%) and a sufficient number of correct answers for the magnocellular-biased stimuli.

Regional activation profiles and probabilistic maps revealed different functional patterns of activation within the visual cortex, along a gradient across the regions of the visual cortex, with parvocellular-biased stimuli recruiting posterior visual cortex regions more strongly than magnocellular-biased stimuli, and magnocellular-biased stimuli engaging anterior visual cortex regions more strongly than parvocellular-biased stimuli. Previous evidence from monkeys has revealed that posterior visual cortex regions (V1, V2, and V3) respond to both magnocellular-biased and parvocellular-biased stimuli. Other studies in humans, such as Musel et al. (2013), have observed that low spatial frequencies (associated with the magnocellular pathway) activate V1, whereas high spatial frequencies (associated with the parvocellular pathway) activate V2, V3. Here we found that areas V1, V2, V3 all showed a

preference for parvocellular- over magnocellular-biased stimuli. However, unlike Musel et al. (2013), our stimuli were designed to take all the properties associated with the magnocellular and parvocellular bias into account, not only spatial frequency. This may have led to the different patterns of activation observed in the two studies.

Following the gradient of the visual cortex and in line with previous findings, the hV4 region was also more strongly recruited by parvocellular- than magnocellular-biased stimuli. This result is highly consistent with previous neuroimaging studies with both healthy and clinical patients, which demonstrated that the hV4 region is in charge of color processing (Bartels & Zeki, 2000; Lueck et al. 1989; McKeefry & Zeki 1997; Pearlman et al., 1979; Zeki et al., 1990). Similarly, previous visual recognition studies have suggested that hV4 forms part of the ventral visual stream, which is mainly associated with object, feature, and form processing (Arcaro et al., 2009; Bartels & Zeki, 2000; Brewer et al., 2005).

In contrast, anterior visual cortex areas LO1 and TO1 showed stronger activation for magnocellular- than parvocellular-biased stimuli (Sayres et al., 2008; Skottun et al., 2015, Stigliani et al., 2017). MT+/V5 region, part of TO1, is a region with high contrast sensitivity that processes motion, and is therefore activated more by moving than stationary stimuli. Tootell et al. (1995) showed that MT+ contains direction-selective neural populations; while as Huk et al. (2002) demonstrated that this region contains pattern-motion cells. Although the LO complex has always been seen as an object processing region, Larsson et al., (2006) found that LO1 responds to stimuli designed to test orientation selectivity, a property that is associated with magnocellular pathway processes.

Our results represent solid and converging evidence for a posterior to anterior functional gradient within the visual cortex for processing parvocellular- and magnocellular-biased stimuli. Further, we have shown that this effect holds regardless of the nature of the stimuli

(words or images), and is largely similar across the left and right hemispheres. These findings hold considerable promise for further research aimed at unraveling the contributions of the visual cortex to reading processes. Future studies should examine to what extent the contributions of the magnocellular and parvocellular systems to reading and visual recognition change over development, especially after reading acquisition, and examine potential differences in these functional gradients in typical and atypical readers (Müller-Axt et al., 2017).

Pairwise functional connectivity analyses revealed differential functional coupling as a function of physical distance between pairs of ROIs, regardless of the visual pathway or stimuli type. We observed significant functional connections between regions within the posterior or early visual cortex (i.e., V1, V2, V3) and between regions in the more anterior and peripheral regions (LO1 and TO1). Region hV4 was an exception, exhibiting an intermediate pattern of activation, with tight coupling to both more posterior and more anterior regions.

Furthermore, we demonstrated that pairwise functional connectivity between regions in the visual cortex is closely related to their physical distance, with decreasing functional connectivity coefficients for greater physical distances. This was established by our analysis of correlations between the functional connectivity and physical distance between pairs of regions as well as by ANOVA analyses of Z-scores for functional connectivity (ROI Pair x Pathway x Stimuli). Studies using resting-state functional connectivity have previously reported that physical distance and connectivity measures are strongly related (Dawson et al., 2016; Genç et al., 2015).

Turning to the question of hemispheric lateralization, in line with our hypothesis, we found that word stimuli were left-lateralized in more anterior regions, specifically LO1, for

magnocellular-biased stimuli, while image stimuli were left-lateralized in V1 for parvocellular-biased stimuli. Recent neuroimaging studies have suggested that there is a left lateralized region involved in word recognition, which they have called the Occipital Word Form Area (OWFA) (Strother et al.; 2015; Strother et al., 2017; Yu et al., 2015). For instance, Strother et al. (2017) reported that the OWFA is located intermediate to hV4, and within the lateral occipital gyrus (LO). Furthermore, in line with our results, Brederoo et al.'s (2017) study found left lateralization for global linguistic and non-linguistic stimuli (global processing can be associated with the magnocellular pathway). Nevertheless, contrary to our results, the same study found a right hemisphere preference for non-linguistic stimuli, whereas we found left-hemisphere preference for images in the primary visual cortex. This may be due to differences in the stimuli and tasks used in the two studies. While we used line drawings as images that were chromatically defined and isoluminant, Brederoo et al. (2017) used compound stimuli with targets made up of black diamonds or plus signs and distractors made up of rectangles or crosses, all displayed against white backgrounds, following classical Navon (1977) task procedures.

In sum, in our study we found a functional gradient in the activation of the visual cortex, where posterior visual regions were more strongly recruited for parvocellular-biased stimuli, whereas more anterior regions were more engaged by magnocellular-biased stimuli. Functional connectivity between visual regions depended on physical distance and appeared to be segregated, with the strongest FC observed as clusters within these more posterior and anterior regions. Finally, we saw that left-lateralization for words occurred in more anterior regions for magnocellular-biased stimuli but in more posterior regions for images. Altogether, these findings provide converging evidence for functional division of labor in the visual cortex as a function of the parvocellular and magnocellular properties of the stimuli.

10. Empirical Part III: Involvement of the magnocellular and parvocellular pathways in reading

In the previous empirical part we showed converging evidence revealing a functional gradient in the human visual cortex with early regions being more recruited for processing parvocellular-biased stimuli and peripheral and the more anterior visual cortex regions being more involved in processing magnocellular-biased stimuli. In this experiment, we wanted to examine the contribution of the magnocellular and parvocellular pathways to reading processes; specifically we sought to investigate the involvement of regions along the ventral and dorsal reading networks (i.e., vOTC, IPS and IFG) in processing magnocellular- and parvocellular-biased stimuli. Although the reading circuit has been extensively investigated, to date little is still known about the role that the magnocellular and parvocellular pathways play in it. Furthermore, the dorsal and ventral reading networks are structurally connected, as it was already showed in the 19s century, finding that some WM fiber bundles are essential for speech perception and speech perception (Wernicke, 1874). Later neuroimaging studies also found that reading development is associated with increases in FA values within tracts that connect relevant reading regions, such as the arcuate fasciculus (AF) (Yeatman et al., 2012a). Specifically, numerous studies relate the inferior fronto-occipital fasciculus (IFOF) to the ventral pathway (Friederici et al., 2015; Sarubbo et al., 2013; Saur et al., 2008; Saur et al., 2010), while the AF and the superior longitudinal fasciculus (SLF) with its three branches (i.e., SLF I-II-III) are related to the dorsal pathway (Frey et al., 2008; Makris et al., 2005; Thiebault de Schotten et al., 2012; Yagmurlu et al., 2016). However, there are some studies that have demonstrated that the AF contains a dorsal and a ventral subdivision (Fernandez-Miranda et al., 2014; Glasser and Rilling, 2008; Yagmurlu et al., 2016). Thus, the AF might contribute to both the dorsal and ventral pathways of language processing, although anatomically it has been typically consider a dorsal WM tract.

The main objective of this study is to examine the involvement of ventral and dorsal reading networks in processing magnocellular- and parvocellular-biased stimuli and to what extent processing parvocellular stimuli relies on the ventral reading network and processing magnocellular stimuli relies on the dorsal reading network. Based on previous evidence, we hypothesized that 1) the vOTC will be more strongly engaged for word stimuli compared to images, however, and in the absence of previous evidence, we wanted to explore how different regions within the occipital temporal sulcus (OTS; see Lerma-Usabiaga et al., 2018), in particular the medial OTS (mOTS) and the posterior OTS (pOTS), behave in relation to the two main magnocellular and parvocellular visual pathways; 2) the three IFG regions are expected to be more strongly recruited for word stimuli versus image stimuli since these regions are typically involved in semantic processing, and we sought to explore to whether or not these IFG regions respond differently to parvocellular and magnocellular stimuli; 3) based on previous evidence, we expect to find associations between reading abilities and the functional connectivity of parvocellular-biased words between regions of the ventral reading route: mOTS (i.e., the vOTC region that integrates information with other regions along the reading network), *pars orbitalis* and *pars triangularis*, and associations between reading abilities and the functional connectivity of magnocellular-biased words between regions of the dorsal reading route: IPS and *pars opercularis*; and 4) it is expected that FA values of white-matter tracts of interest will contribute significantly to reading abilities, specifically the IFOF to the ventral route and the SLF tract and its three branches to the dorsal route. In the case of AF, given previous mixed findings and evidence that this WM tract has endings in mOTS and different IFG regions, we will explore its involvement in the ventral route.

10.1 Materials and Methods

10.1.1 Participants

The study sample was the same as for the Empirical Part II. The only difference is that for DWI data, the sample consisted of 26 participants (14 females and 12 males, mean age 24.65 ± 3.88 years).

10.1.2 Stimuli

A total of 180 line drawings of words and images were used as stimuli. The uniform foreground of these drawings allows for precise control of luminance and chromatic properties. 60 were magnocellular-biased, that is achromatic with low-luminance contrast; other 60 were parvocellular-biased, that is, chromatically defined and isoluminant (red-green), and the remaining 60 were neutral non-biased. Unlike in the Empirical Parts I and II, this empirical part includes a new neutral non-biased condition, where words and images are neither magnocellular- nor parvocellular-biased, for the reason of having a relevant additional baseline condition (see Figure 23).

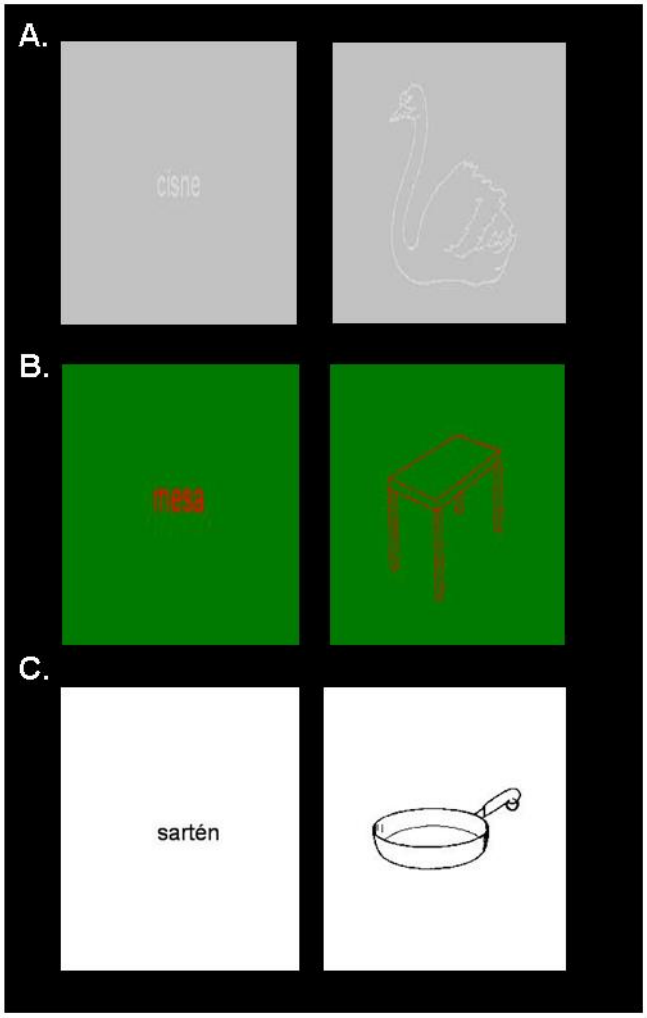

Figure 23: Experimental stimuli. We used a hybrid event/block design where participants made manmade (i.e., artificial) or non-manmade (i.e., natural) judgments to words and images that were A) magnocellular biased, having a low-luminance contrast and being achromatic; B) parvocellular biased, being isoluminant (red-green) and chromatically defined; and C) neutral non-biased. All stimuli were counterbalanced between conditions and subjects.

The procedures to adjust luminance and chromatic settings before MRI scanning for the magnocellular-biased and parvocellular-biased stimuli were identical to the ones described in Empirical Part I and Empirical Part II (please see those parts for further details).

All of the images and word stimuli were designed in magnocellular-biased, parvocellular-biased and neutral non-biased forms and each word had a corresponding image, so that all stimuli were properly counterbalanced across subjects in terms of Pathway (i.e., magnocellular, parvocellular, neutral non-biased) and Stimuli (i.e., words, images) (see

Figure 23). All the selected items could be easily identified as non-manmade (i.e., *apple*) or manmade (i.e., *robot*), with half of presented items being "non-manmade", and the remaining half being "manmade".

10.1.3 Experimental task and procedure

Functional and structural data was collected in the MRI scanner (see *MRI data acquisition* section below). The functional MRI task conformed to a 3 (Pathway: magnocellular, parvocellular, neutral non-biased) X 2 (Stimuli: words, images) visual recognition experimental block design, which was carried out in a single functional run that lasted 15 min. During the task, participants were asked to perform a semantic task, in which they indicated natural (i.e., non man-made) or artificial (i.e., man-made) judgements via key presses on a two-button fiber-optic box. Six stimuli were presented in each activation block of 20.3 s duration. Activation blocks were alternated with rest-fixation periods of 16 s to allow the hemodynamic response function (HRF) to return to baseline. A total of 90 words and 90 images were presented across activation blocks, yielding 5 activation blocks for each of the 6 experimental conditions. The stimuli were presented at 100 Hz using a Barco projector (model F35); the refresh rate was confirmed using The Black Box ToolKit v2™.

Additionally, to identify at the individual-subject level the mOTS and pOTS regions within vOTC, an independent functional localizer with a block design was used adapted from Lerma-Usabiaga et al. (Lerma-Usabiaga et al., 2018). We selected four experimental conditions: real words (RW), consonant strings (CS), pseudowords (PS) and checkedboards (CB). Similar to the original paradigm we used the same as task, which consists on pushing a button every time a stimulus appeared inside of a black frame. After MRI data acquisition, participants performed a lexical decision task in a behavioral room, which was used as a proxy to individual reading abilities. This lexical decision task did not include any word or

string character previously presented to the participants in the main fMRI or in the independent fMRI localizer.

10.1.4 MRI data acquisition

Whole-brain MRI data acquisition of structural T1 and functional images was identical to Empirical Part II (see section 8.1.4 for further details). For this Empirical Part III, we additionally acquired diffusion-weighted images (DWIs) in a single sequence. The sequence had 50 diffusion-encoding gradient directions with a b value of 1000 s/mm^2, and 50 with a b-value of 2000 s/mm^2, six interleaved b0-s and A >> P phase encoding direction. The parameters of the sequence were the following: TR = 3600 ms, TE = 73 ms, FA = 78°, isotropic 2 mm3 voxel size, 72 slices with 0% gap—and were acquired with a multiband acceleration factor of 3.

10.1.5 MRI data analysis

The ***structural analysis*** of the T1-weighted images and functional data preprocessing was identical to Empirical Part II (see 8.1.5 section for further details).

For ***functional data preprocessing and analysis***, there were some differences compared to Empirical Part II. Concretely, instead of modeling four experimental conditions (i.e., magnocellular-biased words, magnocellular-biased images, parvocellular-biased words, and parvocellular-biased images), in this empirical part we modeled six experimental conditions, which are the same four of the Empirical Part II adding the neutral non-biased words and neutral non-biased images conditions.

For the functional localizer task, the four main experimental conditions of the design (i.e., RW, PS, CS and CB) were modeled from the onset of the presentation of the first stimulus within each block until the end of the presentation of the last experimental stimulus within

the block, resulting in 12 s epochs. The rest of the protocol followed the same steps as the main functional fMRI task.

Diffusion-weighted-imaging preprocessing and analysis. We quantified the fractional anisotropy (FA) profiles of 15 pairs of well-known white matter tracts using the Reproducible Tract Profiles tool (RTP; Lerma-Usabiaga et al., 2020). Briefly, the reproducible, containerized and automatized diffusion pipeline consists of three steps: anatomical processing, diffusion preprocessing and tractography pipeline.

In the first step the anatomical T1w image is processed and several individual subject space ROIs are calculated. These ROIs are used in the third step: tractography and tractometry. We re-ran Freesurfer (version 7.1.1) and Neuropythy to segment the T1w image and to obtain the visual cortex volumetric ROIs. Next, to obtain volumetric ROIs of the lateral geniculate nucleus we ran a probabilistic thalamic nuclei segmentation tool (Iglesias et al. 2018). In the last step, we converted several MNI space ROIs to the individual-subject space. These MNI ROIs, used to segment a set of 10 pairs of well-known white matter tracts, originated from Mori's atlas (Setsu et al., 2007; Kaoru et al., 2021). The SLF is one of those tracts. We used Anemiya et al.'s (2021) study ROIs to further segment the SLF in 3 segments. For the MNI to individual-subject space conversion, we registered the high-resolution MNI152 template where the ROIs were drawn to the anatomical T1w image of the subject using ANTs (Avants et al., 2008). With the resulting registration file, we converted the MNI space ROIs to the individual-subject space.

In the second step diffusion data were preprocessed using a combination of tools from MRtrix (Tournier et al., 2019), ANTs (Tustison et al., 2010) and FSL (Jenkinson et al., 2012). We denoised the data using (i) principal component analysis (Veraart et al., 2016), (ii) Rician based (Gudbjartsson et al., 1995), and (iii) Gibbs ringing corrections (Kellner et al., 2016).

We corrected for motion, eddy currents, and geometric distortions using FSL's topup tool (Andersson et al., 2016). We performed bias correction with ANTs (Tustison et al., 2010) and registered the diffusion data to the high-resolution T1w image using a different ANTs tools (Avants et al., 2008).

In the third step, the RTP pipeline performed constrained spherical deconvolution modeling on the preprocessed diffusion data using both b=1000 and 2500 s/mm^2 shells (Tournier et al., 2019), followed by whole-brain white matter streamlines estimation using ensemble tractography (Takemura et al., 2016) and SIFT correction (Smith et al., 2013). We edited the tracts that were of interest of this study from this whole-brain tractograms using ROIs as waypoint. The tracts that were extracted were the AF, the IFOF, the SLF and the subsegmentations of the main SLF using additional ROIs (SLF-I-II-III). FA metrics were obtained and sampled along the length of the white matter tracts for the b=1000 s/mm^2.

10.1.6 ROI definition

ROI analyses were performed with the MARSBAR toolbox for use with SPM12. A total of six left-lateralized ROIs in individual-subject space were examined. Three of them were extracted individually from Freesurfer's automated aparc parcellation, including left *pars orbitalis*, left *pars triangularis* and left *pars opercularis*. The medial and posterior vOTC regions, mOTS and pOTS respectively, were extracted using an adaptation of Lerma-Usabiaga et al. (2018) functional localizer. mOTS was obtained based on the maximum activation of the lexical contrast (real words vs. consonant strings & pseudowords) within the VOTC. pOTS was obtained based on the maximum activation of the perceptual contrast (real words vs. checkerboards) within the vOTC. Finally, we extracted the inferior parietal sulcus region (IPS0) using Wang's atlas (Wang et al., 2015).

10.1.7 Data analysis

Individual ROI analysis. ROI analysis was performed with the MARSBAR toolbox for use with SPM12, as in Empirical Part II. In line with our main experimental design, we extracted parameter estimates (i.e., scaled % signal change values; Mazaika, 2009) for each single region and subject individually and used them as dependent variables in 3 (Pathway: magnocellular-biased, parvocellular-biased, neutral non-biased) X 2 (Stimuli: words, images) repeated measures ANOVAs. Results were corrected using the false discovery rate (FDR) correction for multiple comparisons.

Functional connectivity analysis. Functional connectivity analyses were conducted via the beta-series correlation method (Rissman et al., 2004), see *Functional connectivity analysis* of section 9.1.7 for more details (Empirical Part II). Fisher's Z normally distributed values for each pair of ROIs for each participant and condition were submitted to correlations with reading scores. The reading scores were obtained from the lexical decision task that participants complete behaviorally after the scanning session. From this task, we created two measures, one of them corresponding to the subtraction of the average response time to real words and the average response time to consonant strings, which we called magnocellular score; and, the other one corresponding to the subtraction of the average response time to real words and the average response time to pseudowords, which we called parvocellular score.

Structural connectivity analysis. Finally, we performed a hierarchical regression analysis to test whether white matter FA values explained the reading scores significantly on top of the variance explained by the functional connectivity. We only tested some white-matter tracts, based on previous evidence and our hypotheses (i.e., SLF, AF, IFOF). To the magnocellular-biased functional connectivity values we added the SLF tract values (both the whole SLF and its corresponding I-II-III branches) and checked if the adjusted R square of

the regression improved or not. To the parvocellular-biased functional connectivity values, we added the AF and IFOF tract metrics to the regression.

10.2 Results

10.2.1 In-scanner behavioral results

For accuracy measures, the results of the ANOVA revealed the main effect of Pathway ($F_{2,60}$= 5.61; ηp2 =0.16, p < 0.05, BF10 = 7.51). Simple-effect post-hoc analysis revealed that this main effect was due to a higher accuracy for parvocellular-biased and neutral non-biased stimuli relative to magnocellular-biased stimuli (ts_{66}≥2.77, ps ≤ 0.011, d' ≥ 0.34, BF10 ≥ 4.37; see Figure 24A).

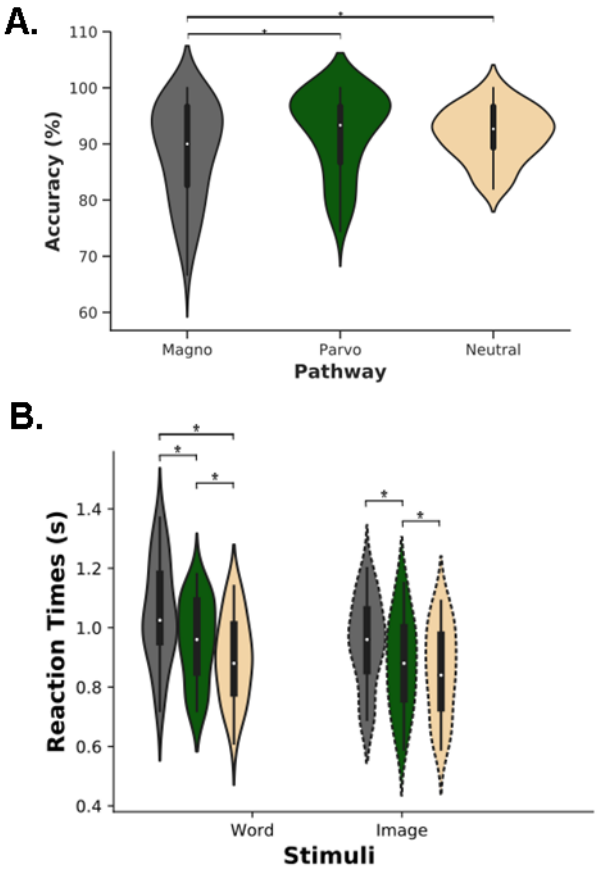

Figure 24: In-scanner behavioral results. A) Percent (%) mean accuracy of manmade and non-manmade judgments as a function of visual magnocellular, parvocellular and neutral non-biased pathways. B) Correct responses reaction times as a function of magnocellular, parvocellular and non-biased pathways and word and image stimuli. The white dots on the

violin plots represents the median, while the black bar in the center represents the interquartile range. Thick black lines indicate statistically significant effects: *ps < .05.

The ANOVA for the reaction times showed that the main effects of Pathway ($F_{2,66}$=57.17; η_p^2 =0.63, p < 0.001, BF10 = 3.50 e^{12} and Stimuli ($F_{1,22}$=30.13; η_p^2 =0.48, p < 0.001, BF10 = 188636.62) were subsumed by a significant Pathway X Stimuli interaction ($F_{2,66}$=3.31; η_p^2 =0.09, p < 0.05, BF10 = 0.72); see Figure 24B). Post-hoc analyses revealed that this interaction was due to longer response latencies for parvocellular-biased versus neutral non-biased for word stimuli (t_{35} = 4.12, p ≤ 0.001, d' = 0.69, BF10 = 121.78). This significant difference in reaction times was not present for image stimuli (t 35 = 1.46, p = 0.15, d' = 0.24, BF10 = 0.47, see Figure 24B).

10.2.2 MRI analytical approach and results

We used three analytic approaches to examine visual recognition of words and images in the reading circuitry and the role of the two main magnocellular and parvocellular visual pathways in reading processes. All analyses were conducted in individual-subject space. First, we used ROI analyses to examine the recruitment of the six ROIs that we selected from the reading circuitry (i.e., mOTS, pOTS, IPS0 and the three regions of the left IFG), in line with our experimental design. Second, to further investigate the differential contributions of the main visual pathways to reading, we examined associations between the FC among ventral and dorsal ROI pairs and reading scores that were obtained from a behavioral lexical decision task. Finally, we conducted hierarchical regression analysis to examine whether white matter FA values of ventral and dorsal bundles of interest can add to the explanation of reading performance.

10.2.2.1 Individual ROI results

ROI analyses were conducted at the individual-subject level to characterize the activation profile of regions of *a priori* interest for the main experimental conditions. Given the

importance for the present study of the ventral and dorsal reading networks, the two subregions of the vOTC were extracted using an independent functional localizer. We also extracted the IPS 0 region from the parietal cortex based on Wang's atlas, as well as the three subdivisions of the left IFG using FreeSurfer (i.e., left *pars orbitalis*, left *pars triangularis* and left *pars opercularis*). Thus, fMRI parameter estimates from these ROIs were extracted and submitted to 3 (Pathway: magnocellular-biased, parvocellular-biased, neutral non-biased) X 2 (Stimuli: words, images) repeated measures ANOVAs. Next, we describe the effects observed in these ROIs.

The ANOVA for pOTS revealed that the main effects of Pathway ($F_{2,58}$ = 15.99; p ≤ 0.001, η_p^2 = 0.36, BF10 = 44.15) and Stimuli ($F_{1,29}$ = 5.58; p = 0.025, η_p^2 = 0.16, BF10 = 56.32) were subsumed by a statistically significant Pathway X Stimuli interaction ($F_{2,58}$ = 5.65; p = 0.006, η_p^2 = 0.16, BF10 = 1.58). Post-hoc comparisons showed stronger activation for magnocellular-biased than for parvocellular-biased stimuli when processing words (t_{29} = 2.78; p = 0.023, d' = 0.50, BF10 = 4.49), for magnocellular-biased than for neutral non-biased stimuli when processing words (t_{29} = 5.01; p ≤ 0.001, d' = 0.91, BF10 = 922.18) and for parvocellular-biased than for neutral non-biased stimuli when processing words (t_{29} = 3.46; p = 0.009, d' = 0.64, BF10 =21.62). These significant effects were not observed for image stimuli (ts_{30} ≤ 1.63, ps ≥0.17, d' ≤ 0.30, BF10 ≤ 0.66, see figure 25A, middle panel). Furthermore, pOTS exhibited a stronger engagement when processing neutral non-biased images compared to neutral non-biased words (t_{29} = 3.30; p = 0.009, see Figure 25A, second row panel).

The ANOVA for mOTS revealed that the main effect of Pathway ($F_{2,60}$ = 4.02; p = 0.023, η_p^2 = 0.12, BF10 = 1.62) was qualified by a statistically significant Pathway X Stimuli interaction ($F_{2,60}$ = 6.13; p = 0.004, η_p^2 = 0.17, BF10 = 0.53). Post-hoc comparisons showed

stronger activation for magnocellular-biased and parvocellular-biased stimuli than for neutral non-biased stimuli when processing words (t_{30} = 3.57, p = 0.009, d' = 0.64, BF10 = 26.22; t_{30} = 2.85; p = 0.036, d' = 0.51, BF10 = 5.59). This significant effect was not observed for image stimuli ($ts_{30} \leq 1.26$, $ps \geq 0.391$, d' ≤ 0.23, BF10 ≤ 0.40, see Figure 25A, third row panel).

The ANOVA for IPS0 revealed the main effect of Stimuli ($F_{1,29}$ = 47.77; p $\leq$ 0.001, η_p^2 = 0.62, BF10 = 6.47 e^{11}), an effect that was due to the fact that IPS0 was more engaged in general for image processing than for word processing (see Figure 25A, lower panel). The interaction Pathway X Stimuli was not statistically significant ($F_{2,58}$ = 1.18; p = 0.32, η_p^2 = 0.04, BF10 = 0.16). It is also important to note that this region showed deactivated percent signal change values across all the conditions consistently with the pattern typically observed in some parietal regions such as precuneus and angular gyrus.

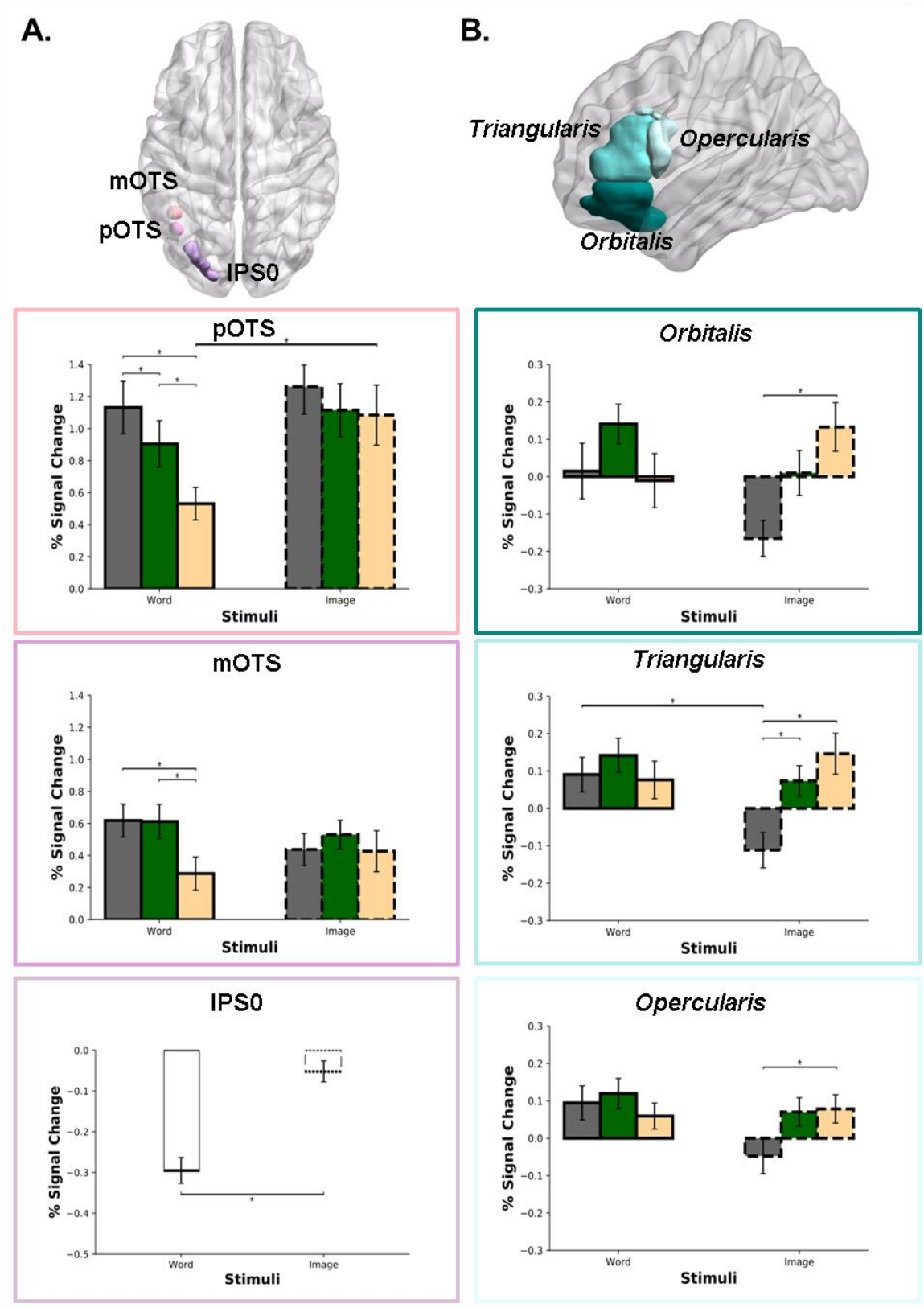

Figure 25: ROI analysis as a function of Stimuli and visual Pathway. A) Mean parameter estimates (% Signal Change) of ventral occipito-temporal cortex regions (mOTS, pOTS) and IPS0. The upper row corresponds to a render in axial view of the posterior ROIs used in the present study; second row corresponds to posterior occipitotemporal sulcus (pOTS) ROI

analysis; third row corresponds to medial occipitotemporal sulcus (mOTS) ROI analysis; and bottom row corresponds to inferior parietal sulcus (IPS0) ROI analysis. B) Mean parameter estimates (% Signal Change) of left IFG regions. Upper row shows a rendering with the three IFG regions here examined; second row corresponds to the *pars orbitalis* ROI analysis; third row corresponds to *pars triangularis* ROI analysis; and lower panel corresponds to *pars opercularis* ROI analysis. Error bars represent the error of the mean (SEM). * asterisks denote statistically significant effects.

ROI analysis for left *pars orbitalis* revealed that the main effect of Pathway ($F_{2,54}$ = 4.60; p = 0.01, η_p^2 = 0.15, BF10 = 1.53) that was qualified by a significant Pathway X Stimuli interaction ($F_{2,54}$ = 5.20; p = 0.009, η_p^2 = 0.16, BF10 = 5.21). Post-hoc analyses revealed that this interaction was due to stronger engagement for neutral non-biased images than for processing magnocellular-biased images (t_{29} = 4.64, p ≤ 0.001, d' = 0.85, BF10 = 363.25). No differences emerged between neutral non-biased images and parvocellular-biased images and parvocellular-biased images and magnocellular-biased images (ts_{28} ≤ 2.48, ps ≥ 0.083, d' ≤ 0.46, BF10 ≤ 2.60) (see Figure 25B, second row panel).

The ANOVA for the left *pars triangularis* revealed that the main effect of Pathway ($F_{2,54}$ = 4.63; p = 0.014, η_p^2 = 0.14, BF10 = 3.72) was qualified by a statically significant Pathway X Stimuli interaction ($F_{2,56}$ = 5.17; p = 0.009, η_p^2 = 0.16, BF10 = 4.20). Post-hoc comparisons showed that the interaction was due to a stronger recruitment of this region for images in parvocellular-biased and neutral non-biased stimuli than in magnocellular-biased stimuli (ts_{28} ≥ 3.35, ps ≤ 0.009, d' ≥ 0.59, BF10 ≥ 16.73). This effect was not present for words (ts_{31} ≤ 1.41, ps ≥ 0.24, d' ≤ 0.80, BF10 ≤ 0.46). Also, magnocellular-biased word stimuli showed greater activation than magnocellular-biased image stimuli (t_{29}=3.18, p = 0.009, d' = 0.58, BF10 = 11.10). No differences between word and image stimuli were observed for parvocellular-biased and neutral non-biased stimuli (ts_{31} ≤ 1.42, ps ≥ 0.24, d' ≤ 0.17, BF10 ≤ 0.54, see Figure 25B, third row panel).

Finally, the analysis for left *pars opercularis* revealed a significant Pathway X Stimuli interaction ($F_{2,62} = 3.57$; $p = 0.034$, $\eta p^2 = 0.10$, BF10 = 1.18). Simple-effect post-hoc analyses showed that this interaction was due to a stronger recruitment of this region for processing image stimuli that were neutral non-biased versus magnocellular-biased ($t_{32} = 3.52$, $p = 0.009$, $d' = 0.61$, BF10 = 25.04). This effect was not present for processing image stimuli that were neutral non-biased versus parvocellular-biased and magnocellular-biased versus parvocellular-biased ($ts_{32} \leq 2.40$, $ps \geq 0.060$, $d' \leq 0.42$, BF10 ≤ 2.23) (see Figure 25B, lower panel).

10.2.2.2 Functional pairwise connectivity and reading associations

Although previous studies and theoretical models have suggested potential ways in which left hemisphere regions interact during naming and reading tasks (e.g., Lau et al., 2008) there is less evidence of how the main two visual pathways contribute in this interactions during reading. To this end, we examined association between functional connectivity of magnocellular and parvocellular-biased words (using the images as a control reference) with reading abilities.

For this purpose, and based on our hypotheses, we performed correlations between the magnocellular lexical decision reading score and functional coupling strength during magnocellular stimuli processing between the IPS0 and IFG; here we expected that the primary dorsal route region of the IFG, the *pars opercularis*, will be the main IFG region showing the predicted associations, but we also run the correlations with the other IFG regions that are typically associated with the ventral reading network. On the other hand, we also computed correlations between the parvocellular lexical decision reading score and functional coupling strength during parvocellular stimuli processing between the pOTS/mOTS and IFG; here we expected that mainly the mOTS and the primary ventral regions of the IFG, the *pars orbitalis* and *triangularis*, will be the main IFG regions with the

mOTS showing the predicted associations, but we also run the correlations with the other IFG region (i.e., *pars opercularis*) that is typically associated with the dorsal reading network

For magnocellular-biased stimuli, results showed that the correlation between IPS0 - *pars opercularis* functional connectivity for words and the magnocellular reading score was statistically significant (r_{26} = -0.41, q = 0.024), whereas the correlation between IPS0 - *pars opercularis* functional connectivity for images and the magnocellular reading score did not result statistically significant (r_{30} = -0.08, q = 0.65). The slope difference between both correlations did not result statistically significant (p = 0.58) (see Figure 26A, right upper panel). The correlations between IPS0 – *pars triangularis* and between IPS0 – *pars orbitalis* functional connectivity and reading score were not significant neither for mangocellular-biased word nor magnocellular-biased images ($rs_{26} \leq 0.33$, $ps \geq 0.07$).

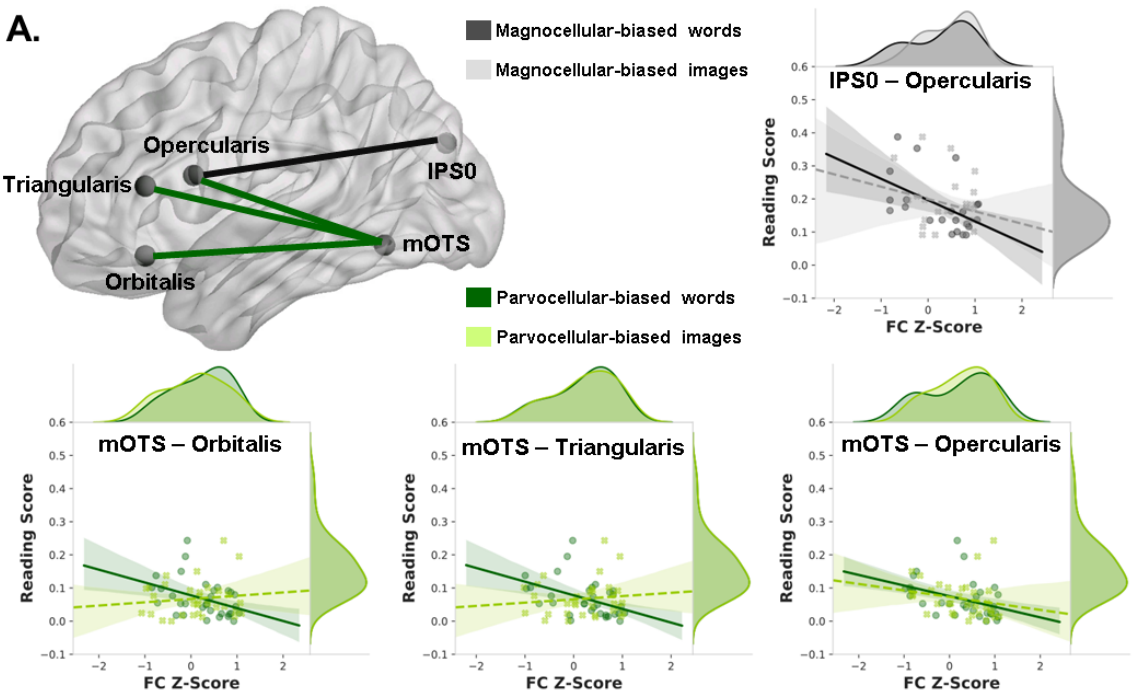

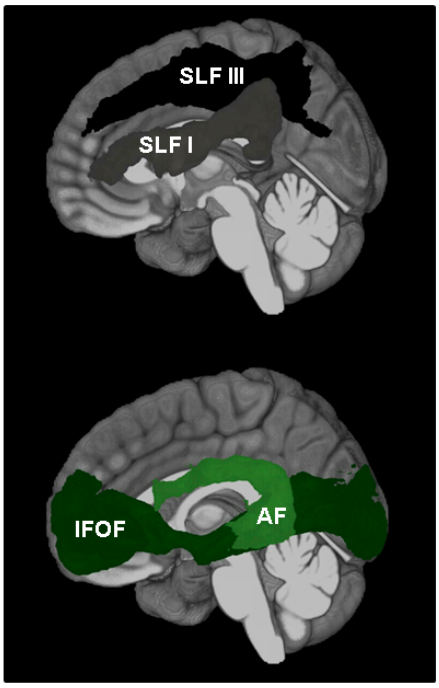

C.

Pairs of Regions	R^2 FC – Reading	R^2_{adj} FC – FA – Reading	q-values
IPS0 - Opercularis	0.27	0.35	0.02
IPS0 - Opercularis	0.27	0.29	0.02

Pairs of Regions	R^2 FC – Reading	R^2_{adj} FC – FA – Reading	q-values
mOTS - Opercularis	0.36	0.38	0.005
mOTS – Opercularis	0.36	0.39	0.005
mOTS - Triangularis	0.34	0.52	0.002
mOTS - Triangularis	0.34	0.46	0.002
mOTS - Orbitalis	0.33	0.50	0.002
mOTS - Orbitalis	0.33	0.47	0.002

Figure 26: Functional, structural connectivity and associations with reading abilities. A) Functional connectivity and reading associations. Left upper row shows a sagittal rendering with the left-hemisphere ROIs examined in the present study and significant functional connection pairs associated with reading abilities. Right upper row shows a scatterplot with associations between IPS 0 – p*ars opercularis* FC Z-score during processing of magnocellular words (darker line and points) and images (lighter line and points) and the reading score. Bottom row shows scatterplots with associations between mOTS – IFG regions (*orbitalis*, *triangularis*, *opercularis*) FC Z-Score during processing of parvocellular words (darker lines and points) and images (lighter lines and points) and the reading score. B)

Sagittal renderings showing white matter bundles of interest which the addition of their FA values to hierarchical regression models significantly improve the explanation of the reading score variance in regard to magnocellular stimuli (grey bundles: SLF-I and SLF-III) and to parvocellular stimuli (green bundles: IFOF, AF). C) Table showing R^2 values for FC for each pair of regions and reading score (firs column), adjusted R^2 FC for each pair of regions adding the structural connectivity (FA values) and reading score analyses (second column), and q-values reflecting the statistical improvement of adding structural connectivity values to the regression models. Grey rows show results for the magnocellular pathway analyses, with the addition of SLF-III FA values (darker grey) and of SLF-I FA values (lighter grey) to the models. Green rows show results for the parvocellular pathway analyses, with the addition of AF FA values (lighter green) and of IFOF FA values (darker green) to the models.

For parvocellular-biased stimuli, we found that the correlation between mOTS - *pars orbitalis* functional connectivity for words and the parvocellular reading score was statistically significant (r_{29} = -0.45, q = 0.024), whereas the correlation between mOTS - *pars orbitalis* functional connectivity for images and the parvocellular reading score did not result statistically significant (r_{29} = 0.11, q = 0.65). The slope difference between these two correlations was significant (p = 0.05) (see Figure 26A, left lower panel). Furthermore, the correlation between mOTS - *pars triangularis* functional connectivity for words and the parvocellular reading score was statistically significant (r_{29} = -0.41, q = 0.024), whereas the correlation between mOTS - *pars triangularis* functional connectivity for images and the parvocellular reading score was not statistically significant (r_{29} = 0.11, q = 0.65). The slope difference between these two correlations was significant (p = 0.03) (see figure 26A, middle lower panel). Finally, the correlation between mOTS - *pars opercularis* functional connectivity for words and the parvocellular reading score was statistically significant (r_{31} = -0.42, q = 0.024), whereas the correlation between mOTS - *pars opercularis* functional connectivity for images and the parvocellular reading score did not result statistically significant (r_{29} = -0.20, q = 0.65). The slope difference did not turn significant either (p = 0.25) (see figure 26A, right lower panel).

Since we had a few subjects less (i.e., 8 subjects) with diffusion data (N = 26), we examined these same correlations with this subset of subjects. These analyses revealed the

same statistically significant effects reported with the 8 fewer subjects with whom we carried out DWI analyses.

10.2.2.3 Functional pairwise connectivity, structural connectivity and reading associations

Finally, we create a regression model adding the structural connectivity values, specifically FA values, to test whether this addition to our simple regression models statistically improves the reading variance in line with our hypotheses. Specifically, for the magnocellular pathway, we tested the addition of the left SLF, which is the white matter tract structurally connecting the IPS0 region with the IFG. We found that for the simple regression model between IPS0 – *pars opercularis* functional connectivity during word processing and the reading score (R^2 = 0.27), adding the FA values to the model significantly improved the model prediction (R^2_{adj} = 0.32; q = 0.002). The same analysis was also conducted specifically for each of the three subdivisions of the SLF tract (i.e., SLF-I, SLF-II and SFL-III). In this case we found that the addition of the SLF-I branch (R^2_{adj} = 0.35; q = 0.02), as well as the SLF-III branch (R^2_{adj} = 0.29; q = 0.02) significantly improved the reading variance explained. However, adding the FA values of SLF-II did not improved the model prediction (R^2_{adj} = 0.26; q = 0.05) (see Figure 26 B/C).

For the parvocellular pathway, we conducted similar analyses, but in this case, we specifically test if the addition of the two tracts structurally connecting the mOTS region and the IFG would add to the reading variance already explained by functional connectivity. For the regression model between the mOTS – *pars opercularis* functional connectivity during word processing and the reading score (R^2 = 0.36), we found that the addition of both AF tract FA values (R^2_{adj} = 0.38; q = 0.005) and the IFOF tract FA values to the regression model significantly improved the reading variance explained (R^2_{adj} = 0.39; q = 0.005). for the regression model between mOTS – *pars triangularis* functional connectivity during word

processing and the reading score (R^2_{adj} = 0.34), we also found that the model was improved significantly introducing the FA values of both the AF tract (R^2_{adj} = 0.52; p = 0.002) and the IFOF tract (R^2_{adj} = 0.46; p = 0.002). Finally, for the regression model between the mOTS – *pars orbitalis* functional connectivity during word processing and the reading score (R^2 = 0.33), the model was improved significantly introducing the FA values of both the AF tract (R^2_{adj} = 0.50; p = 0.002) and the IFOF tract (R^2_{adj} = 0.47; p = 0.002) (see Figure 26 B/C).

10.3 Discussion

In the current study, we examined the magnocellular and parvocellular pathways involvement along the reading circuitry. Although several theories have been put forward to explain the reading process and its circuitry, there is still little evidence about the contribution of these two main visual pathways in this cognitive process. The main goal of this study was to investigate whether the magnocellular and parvocellular pathways are involved in typical reading processes and to what extent their functional and structural correlates can specifically contribute to explain reading performance. Our analytical approach included behavioral analyses, both regional and connectivity functional MRI measures in individual-subject space as well as structural connectivity analysis also in individual-subject space. Results revealed (1) an advantage for parvocellular-biased and neutral non-biased over magnocellular-biased stimuli in terms of accuracy and reaction times; (2) vOTC regions were more engaged for word than image stimuli processing, as the IFG was involved in semantic-related word processing; (3) strong associations between participants' reading abilities and functional connectivity during word versus image processing and in line with the dual-route model subdivision with dorsal regions being biased towards magnocellular stimuli and ventral regions towards parvocellular stimuli; and (4) structural connectivity further add to the reading variance explained by functional connectivity, with dorsal tracts (i.e., SLF)

contributing to magnocellular-related reading, and ventral tracts (i.e., IFOF) and the AF adding to the parvocellular-related reading. These results are discussed next.

First, in regard to our behavioral results, parvocellular-biased and neutral non-biased stimuli have a higher brightness and perceived recognizability compared to magnocellular-biased stimuli which makes the recognition of the magnocellular-biased stimuli harder compared to parvocellular-biased and neutral non-biased stimuli. This difficulty consistently led magnocellular-biased stimuli to lower accuracies and larger reaction times relative to the other conditions in the behavioral results of the present work. Although we tried to ensure through a pilot study a high accuracy (i.e., 80%) for the magnocellular-biased stimuli in order to have sufficient correct answers for fMRI analyses, the accuracy for parvocellular-biased and neutral non-biased stimuli was still higher relative to the magnocellular-biased stimuli.

Second, Cohen, Dahaene and colleagues in their standard reading model (2005; 2011) stated that vOTC regions participate in interpreting word forms. They called these word-responsive regions within the vOTC as the visual word form area (VWFA). Moreover, Lerma et al., (2018) found two word responsive segregated areas within the vOTC, a posterior area (pOTS) involved in visual feature extraction and structurally connected to the intraparietal sulcus via the vertical occipital fasciculus; and a more anterior area (mOTS) involved in integrating information with other regions of the language network and structurally connected to the angular gyrus via the posterior AF. In line with these results, our regional activation profiles revealed that vOTC was more strongly recruited for word stimuli compared to image stimuli. Also, our vOTC regions also showed a differential engagement as a function of pathway for the pOTS and mOTS, with the former being more strongly recruited during processing of magnocellular- than parvocellular-biased words, and the latter being similarly recruited for both parvocellular- and magnocellular-biased words. This pattern of engagement

of vOTC regions for word processing stimuli is consistent with results from Empirical Part II where we observed that more peripheral visual cortex regions (which lay contiguous to the pOTS), are preferentially engaged for magnocellular stimuli. Similarly, the fact that the mOTS supports integrating information with other regions of the language network goes along with the idea of not finding differences for word processing as a function of word stimuli being biased towards the parvocellular or the magnocellular pathway.

Regarding the engagement of more anterior regions (i.e., IFG), although we only find significant effects in the left *pars triangularis* region between word and image stimuli (and specifically for magnocellular-biased ones), we see that it is a region that is more involved in word processing rather than image processing, which is something that have been reported in the literature (Lau et al., 2006). The difficulty of the semantic retrieval is easier for neutral non-biased stimuli than for magnocellular-biased stimuli, which have a lower recognazibility and brightness. That's why we observed for the three regions of IFG that neutral non-biased images recruited more strongly than magnocellular-biased images. In left *pars triangularis* this effect was also present between magnocellular-biased images and parvocellular-biased images, because of the same reason.

Third, regarding the associations between functional connectivity and reading scores, we found substantial differences between the two main visual pathways. According to our hypotheses, for the magnocellular pathway we expected to find associations between the functional connectivity of magnocellular-biased words and reading scores in regions along the dorsal route. Our results confirmed this hypothesis, since we found significant associations between the magnocellular reading score and the IPS0 – *pars opercularis* functional connectivity during magnocellular-biased word processing. Furthermore, it is known that the dorsal route is in charge of the phonological processing (Hickok et al., 2011;

Rauschecker and Scott, 2009). As mentioned in the results section, our magnocellular reading score corresponds to the comparison between the real words and consonant strings, which means that the coupling among these regions along the dorsal magnocellular pathway is associated to phonological words processing, although also semantic words processing.

On the other hand, for the parvocellular pathway we expected to find associations between the functional connectivity of parvocellular-biased words and reading scores in regions along the ventral route. Our results confirmed this hypothesis, since we found significant associations between the parvocellular reading score and mOTS – IFG regions for the two regions typically considered as part of the ventral route: *pars orbitalis* and *pars triangularis*, but also for *pars opercularis*. Besides that, our parvocellular reading score was calculated subtracting reaction times of real words from pseudowords reaction times, which means that the coupling among these regions is associated with exclusively the semantic part of reading abilities. According to previous literature, the ventral route supports mapping orthographic-lexical stimuli onto semantic representations (Hickok & Poeppel, 2004; Hickok & Poeppel 2007; Sandak et al., 2004), as well as there are functional imaging studies suggesting the contribution of the anterior portion of the IFG (i.e., *pars orbitalis* and *pars triangularis*) in the semantic aspects of language (Rizzolatti & Matteli, 2003). Our results support this evidence, in addition to reveal that the parvocellular pathway is involved in the semantic processing of words along the ventral reading network.

Fourth, we tested whether white matter FA values of tracts from the dorsal and ventral networks helped explained reading variance on top of task-related functional connectivity. In the dorsal route, the IPS0 region and *pars opercularis* are structurally connected through the SLF (Barbeau et al., 2020), which is part of the dorsal route. Introducing SLF FA values to the simple regression between IPS0 – *pars opercularis* functional connectivity during

magnocellular word processing and reading abilities, improved significantly the explained reading variance. Supporting our results, in the literature there are several studies using DWI that have found correlations between white matter properties and reading skills in adults and children (Beaulieu et al., 2005; Deutsch et al., 2005; Niogi et al., 2006). Furthermore, it is known that the SLF supports phonological and articulatory processes (Catani et al. 2003; Duffau et al. 2008; Maldonado et al. 2011; Saur et al. 2008). For the ventral reading route, the regression model was improved by introducing IFOF FA values to the simple regressions between mOTS - IFG functional connectivity during parvocellular word processing and reading abilities. In principle, one could *a priori* expect these associations to be only present for the two main ventral regions of the IFG: *pars orbitalis* and *pars triangularis*; however, we also found significant results for the *pars opercularis*. In this vein, there is evidence that the IFOF has cortical endings reaching *pars opercularis* (Sarubbo et al., 2013). Also, the *pars opercularis* is part of the IFG and is adjacent to *pars triangularis*, so it could be that *pars opercularis* acts as an intermediate region in terms of semantic and phonological processing. These reasons may determine the fact that the functional connectivity with pars opercularis from nodes both from the ventral (i.e., mOTS) and the dorsal networks (i.e., IPS0) was associated with reading abilities.

Finally, we also found that adding FA values from the AF tract to the models examining FC during parvocellular words and reading scores between mOTS and the three IFG regions signiticantly improved the explained reading variance. Although AF is typically considered a dorsal WM tract, previous studies have demonstrated that the mOTS and IFG are structurally connected through the AF (Lerma-Usabiaga et al., 2018). Furthermore, the AF and IFOF have fibers in common, which can explain that AF is contributing to reading abilities in the ventral pathway. In fact, our results suggest that structural connectivity strongly contributes to reading abilities.

In sum, in our study we found that regions that are classically reported in the reading literature were more strongly recruited for processing words than for processing images. We found strong associations between reading abilities and the functional connectivity of the main two pathways, where the parvocellular pathway contributes to reading processes of the ventral route, whereas the magnocellular pathway contributes to the reading processes of the dorsal route. Finally, we observed that structural connectivity improved significantly these associations in order to explain reading variance. Our findings further extent previous evidence from visual recognition to typical reading processes underscoring the interplay among vOTC, IPS0 and IFG regions.

11. General discussion

The present doctoral dissertation examined the contribution of the magnocellular and parvocellular pathways to visual recognition in general and, more specifically, how these visual pathways contribute to reading processes, as well as to object recognition. Moreover, different from previous work, we studied the involvement of the main two pathways taking into account all the properties of the magnocellular and parvocellular pathways (see also Kveraga et al., 2007) and not only spatial or temporal frequencies as other previous studies did (Bartels & Zeki, 2000; Larsson et al., 2006; Musel et al., 2013; Tootell et al., 2005). It is also important to highlight that the influence of these two main visual pathways in reading from middle childhood to adulthood has not been studied yet.

In the Empirical Part I of this doctoral dissertation, we examined behaviorally age-related changes in the contribution of the magnocellular and parvocellular pathways to reading processes from early middle childhood to adulthood. We found that the magnocellular pathway seems to have a more protracted maturation compared to the parvocellular pathway in word recognition. This main result is consistent with previous empirical evidence. Specifically, Klaver and colleagues (2008) found in their fMRI study that areas of the occipital cortex associated with the magnocellular pathway were more strongly engaged in adults relative to children, suggesting that they did not reach yet the adult-like pattern of activation and that they are still under development. Moreover, Parrish et al., (2005) and Bucher et al., (2006) found that processing of motion stimuli – i.e. a main property directly linked to the magnocellular pathway, is still maturing in 5-to-6-years-old children and during adolescence. Previous research has shown that the visual cortex V5/MT+ region, also called TO complex, is involved in motion processing. In the Empirical Part II of this doctoral dissertation, which is focused on the visual cortex and the involvement of the magnocellular and parvocellular pathways in word and object recognition, we also found that this region

(TO1), as well as LO1, are more engaged for processing magnocellular-biased stimuli compared to processing parvocellular-biased stimuli. Taking together the results from both Empirical Part I and II, and in line with previous empirical findings, one possible explanation would be that the regions more involved in processing magnocellular stimuli, TO1 and LO1, mature more slowly than the regions more involved in processing parvocellular stimuli, which are the V1, V2, V3 and hV4.

To further test these possibilities it is important that future research will examine the functional and structural correlates of visual recognition processes associated with the magnocellular and parvocellular pathways with developmental samples and, if possible, using longitudinal designs. Developmental MRI results can further allow us to elucidate if differential activation or structural properties of visual cortex regions are associated with age and reading performance. This will help understanding the development of the main visual pathways and their involvement in reading processes, and will pave the way for future studies, including readers with dyslexia, to test the involvement of these visual pathways in atypical reading processes and, potentially, for interventions such as training studies on reading.

In the Empirical Part II of this doctoral dissertation, we focused on the involvement of visual cortex regions in processing magnocellular and parvocellular stimuli. In this study we found converging evidence revealing a functional gradient in the visual cortex with early regions being more recruited for processing parvocellular-biased stimuli, and peripheral or more anterior visual cortex regions being more involved in processing magnocellular-biased stimuli, regardless of the stimuli type (i.e., words and images). It is important to highlight that these results were observed following a functional MRI multimodal analytical approach using regional, probabilistic and functional connectivity analyses, all conducted in individual-

subject space and at the individual-subject level. This work is the first one demonstrating this relevant division of labor for magnocellular and parvocellular stimuli processing in the human visual cortex.

All the theories mentioned and described about reading, such as the theory of cortical semantic processing (Lau et al., 2008) or the cortical model for semantics (Binder and Desai, 2011) are focused on left-lateralized regions. In addition, Cohen, Dahaene and colleagues (2000, 2002) described the standard reading model, in which they found that the VWFA, an area that is part of the left vOTC is involved in the interpretation of word forms. Consistent with this previous evidence, one would expect that the visual regions of the left hemisphere were going to be more engaged for word stimuli than for images, or at least that we would see a left lateralization pattern in the visual cortex. However, our results did not show any of these effects, suggesting that the reading processes equally engaged bilateral visual cortex regions of the brain.

There is research evidence demonstrating that the visual cortex is retinotopically organized (Arcaro et al., 2009; Engel et al., 1997; Wandell et al., 2007). It would be ideal if future studies can further collect retinotopic data and conduct analyses in line with the functional gradient observed in the present study. Another important future research line will be to examine the other six regions of the visual cortex included in Benson's atlas. Two of them, TO2 and LO2 had similar activation profiles to their analogous regions (TO1 and LO1). The other four, which are V3a, V3b, VO1 and VO2, were not included in our study because our results would be too penalized for multiple comparison corrections, and we decided to exclude these ones because they are also the most peripheral ones.

In the third and final Empirical Part III, we analyzed the processing of magnocellular and parvocellular stimuli along the reading circuitry and the involvement of these two visual

pathways in the dorsal and ventral reading networks. We found that the vOTC, as it has already been shown in previous studies (Lerma-Usabiaga et al., 2018), is more involved in word processing than in image processing. Moreover, the more posterior vOTC region, the pOTS, was differentially engaged for magnocellular versus parvocellular stimuli, whereas the more anterior region, the mOTS, was similarly engaged for processing both magnocellular and parvocellular stimuli. Regarding the more anterior regions, the three areas of IFG were more strongly recruited for word processing, although we did not observe any differences as a function of pathway. Taking into account these results together with the results of Empirical Part II, we see that the most posterior regions do discriminate between magnocellular-biased and parvocellular-biased stimuli (i.e., pOTS), but not between word and images (i.e., mOTS). However, in the more anterior regions, the pattern is the reverse, that is, they are more engaged for word stimuli than for image stimuli, but similarly engaged for both pathways.

Along with these findings, our third study links visual recognition and reading theories. It is known that the magnocellular pathway projects to the dorsal pathway, and is in charge of processing the 'how' aspect of visual information, while the parvocellular pathway processes the 'what' aspect of visual information in the ventral pathway (Goodale & Milner, 1992; Ungerleider & Mishkin, 1982). On the other hand, according to reading theories (Jobard et al., 2003; Pugh et al., 2001; Saur et al., 2008; Schlaggar & McCandliss, 2007), the dorsal route is in charge of orthography-to-phonology mapping, while the ventral route it is mainly responsible for the semantic processing of the words (Sandak et al., 2004). Therefore, one would expect that the magnocellular pathway is in charge of phonological processing of words in the dorsal route, while the parvocellular pathway would be in charge of the semantic processing of words in the ventral route. The analysis of associations between FC and reading scores confirmed these hypotheses, where we found on the one hand, associations between magnocellular word FC between IPS and left pars opercularis and reading in the dorsal route;

and on the other hand, associations between parvocellular word FC between mOTS and the three areas of IFG and reading. Furthermore, and in line with previous findings, we found that the regression models were improved adding FA values to them (SLF FA values to the dorsal route, and IFOF and AF values to the ventral one) (Beaulieu et al., 2005; Deutsch et al., 2005; Niogi et al., 2006).

As future research lines related to the Empirical Part III, it would be desirable that further studies examine the functional and structural connectivity between vOTC and IPS, as well as associations between age-related changes and activation profiles of the regions involved in reading processes. Finally, specific neuroimaging research is needed examining functional and structural connectivity between the different regions of the occipital cortex and critical regions along the reading networks.

In conclusion, through this doctoral dissertation we have tried to further contribute to the understanding of the involvement of the two main pathways of the visual system in reading, examining their maturation, their functional correlates in the visual cortex and their functional and structural correlates along the reading networks. Our data revealed that the maturation of the magnocellular pathway over middle childhood seems to be more protracted than the parvocellular pathway maturation. Also, there is a functional gradient in the visual cortex as a function of pathway, with the more posterior regions being more engaged for processing parvocellular-biased stimuli and the more peripheral regions being more strongly involved for processing magnocellular-biased stimuli. Finally, we confirmed that the magnocellular and parvocellular pathways contribute to the reading networks, with the former being involved in the dorsal reading network and the parvocellular system being involved in the ventral reading network.

12. Bibliography

Aguirre, G. K., Zarahn, E., & D'Esposito, M. (1998). An area within human ventral cortex sensitive to "building" stimuli: evidence and implications. *Neuron*, *21*(2), 373-383.

Allison, T., Ginter, H., McCarthy, G., Nobre, A. C., Puce, A. I. N. A., Luby, M. A. R. I. E., & Spencer, D. D. (1994). Face recognition in human extrastriate cortex. *Journal of neurophysiology*, *71*(2), 821-825.

Allison, T., McCarthy, G., Nobre, A., Puce, A., & Belger, A. (1994). Human extrastriate visual cortex and the perception of faces, words, numbers, and colors. *Cerebral cortex*, *4*(5), 544-554.

Allman, J.M., and Kaas, J.H. (1971). A representation of the visual field in the caudal third of the middle temporal gyrus of the owl monkey. *Brain Res.* 31, 85–105.

Amano, K., Wandell, B. A., & Dumoulin, S. O. (2009). Visual field maps, population receptive field sizes, and visual field coverage in the human MT+ complex. *Journal of neurophysiology*, *102*(5), 2704-2718.

Amemiya, Kaoru, Eiichi Naito, and Hiromasa Takemura. (2021). Age Dependency and Lateralization in the Three Branches of the Human Superior Longitudinal Fasciculus. Cortex; a Journal Devoted to the Study of the Nervous System and Behavior 139 (June): 116–33.

American Psychiatric Association, 2013 Diagnostic and Statistical Manual of Mental Disorders, 5th ed. American Psychiatric Association, Washington, DC.

Angelucci, A., Levitt, J. B., & Lund, J. S. (2002). Anatomical origins of the classical receptive field and modulatory surround field of single neurons in macaque visual cortical area V1. *Progress in brain research*, *136*, 373-388.

Angelucci, A., Levitt, J. B., Walton, E. J., Hupe, J. M., Bullier, J., & Lund, J. S. (2002). Circuits for local and global signal integration in primary visual cortex. *Journal of Neuroscience*, *22*(19), 8633-8646.

Andersson, J. L., & Sotiropoulos, S. N. (2016). An integrated approach to correction for off-resonance effects and subject movement in diffusion MR imaging. *Neuroimage*, *125*, 1063-1078.

Arcaro, M. J., McMains, S. A., Singer, B. D., & Kastner, S. (2009). Retinotopic organization of human ventral visual cortex. *Journal of neuroscience*, *29*(34), 10638-10652.

Avants, B. B., Epstein, C. L., Grossman, M., & Gee, J. C. (2008). Symmetric diffeomorphic image registration with cross-correlation: evaluating automated labeling of elderly and neurodegenerative brain. *Medical image analysis*, *12*(1), 26-41.

Bar, M., Tootell, R. B., Schacter, D. L., Greve, D. N., Fischl, B., Mendola, J. D., ... & Dale, A. M. (2001). Cortical mechanisms specific to explicit visual object recognition. *Neuron*, *29*(2), 529-535.

Bar, M., Kassam, K. S., Ghuman, A. S., Boshyan, J., Schmid, A. M., Dale, A. M., ... & Halgren, E. (2006). Top-down facilitation of visual recognition. *Proceedings of the national academy of sciences*, *103*(2), 449-454.

Bar, M., & Neta, M. (2006). Humans prefer curved visual objects. *Psychological science*, *17*(8), 645-648.

Barcelo, F., Suwazono, S., & Knight, R. T. (2000). Prefrontal modulation of visual processing in humans. *Nature neuroscience*, *3*(4), 399-403.

Barbeau, E. B., Descoteaux, M., & Petrides, M. (2020). Dissociating the white matter tracts connecting the temporo-parietal cortical region with frontal cortex using diffusion tractography. *Scientific reports*, *10*(1), 1-13.

Barnard, N., Crewther, S. G., & Crewther, D. P. (1998). Development of a magnocellular function in good and poor primary school-age readers. *Optometry and vision science: official publication of the American Academy of Optometry*, *75*(1), 62-68.

Bartels, A., & Zeki, S. (2000). The architecture of the colour centre in the human visual brain: new results and a review. *European Journal of Neuroscience*, *12*(1), 172-193.

Beaulieu, C., Plewes, C., Paulson, L. A., Roy, D., Snook, L., Concha, L., & Phillips, L. (2005). Imaging brain connectivity in children with diverse reading ability. *Neuroimage*, *25*(4), 1266-1271.

Benardete, E.A., Kaplan, E. and Knight, B.W. (1992). Contrast gain control in the primate retina: P cells are not X-like, some M cells are. *Visual Neurosci.* 8:483-486.

Benardete, E. & Kaplan, E. (1997a) The receptive field of the primate P retinal ganglion cell, I: Linear dynamics. *Visual Neurosci.* 14:169-185.

Benardete, E. & Kaplan, E. (1997b) The receptive field of the primate P retinal ganglion cell, II: Nonlinear dynamics. *Visual Neurosci.* 14:187-205.

Benardete, E. and Kaplan, E. (1999) The Dynamics of Primate M Retinal Ganglion Cells. *Visual Neuroscience.* 16: 355-368.

Ben-Shachar, M., Dougherty, R. F., & Wandell, B. A. (2007). White matter pathways in reading. *Current opinion in neurobiology*, *17*(2), 258-270.

Binder, J. R., & Desai, R. H. (2011). The neurobiology of semantic memory. *Trends in cognitive sciences*, *15*(11), 527-536.

Blakemore, C. and Vital-Durand, F. (1986). Organization and post-natal development of the monkey's lateral geniculate nucleus. *J.Physiol.(Lond)* 380:453-491.

Brainard, D. H. (1997). The Psychophysics Toolbox. *Spatial Vision*, *10*, 433–436.

Brederoo, S. G., Nieuwenstein, M. R., Lorist, M. M., & Cornelissen, F. W. (2017). Hemispheric specialization for global and local processing: A direct comparison of linguistic and non-linguistic stimuli. *Brain and cognition*, *119*, 10-16.

Brewer, A.A., Liu, J., Wade, A.R., and Wandell, B.A. (2005). Visual field maps and stimulus selectivity in human ventral occipital cortex. *Nat. Neurosci*. 8, 1102–1109.

Brewer, A.A., Press, W.A., Logothetis, N.K., and Wandell, B.A. (2002). Visual areas in macaque cortex measured using functional magnetic resonance imaging. *J. Neurosci.* 22, 10416–10426.

Bucher, K., Dietrich, T., Marcar, V.L., Brem, S., Halder, P., Boujraf, S., Summers, P., Brandeis, D., Martin, E., Loenneker, T. (2006). Maturation of luminance- and motion-defined form perception beyond adolescence: a combined ERP and fMRI study. *NeuroImage* 31, 1625–1636.

BuFriston, K.J., Holmes, A.P., Poline, J.-B., Grasby, P.J., Williams, S.C.R., Frackowiak, R.S.J., Turner, R., (1995). Analysis of fMRI Time-Series Revisited. Neuroimage 2, 45–53.

Bukckner, R.L., Bandettini, P.A., O'Craven, K.M., Savoy, R.L., Petersen, S.E., Raichle, M.E., Rosen, B.R., (1996). Detection of cortical activation during averaged single trials of a cognitive task using functional magnetic resonance imaging. Proc. Natl. Acad. Sci. U. S. A. 93, 14878–83.

Bullier, J. (2001). Integrated model of visual processing. *Brain research reviews*, *36*(2-3), 96-107.

Burkhalter, A., Felleman, D.J., Newsome, W.T., and Essen, D.C.V. (1986). Anatomical and physiological asymmetries related to visual areas {V3} and {VP} in macaque extrastriate cortex. *Vision Res*. 26, 63–80.

Callaway, E. M. (2005). Structure and function of parallel pathways in the primate early visual system. *The Journal of physiology*, *566*(1), 13-19.

Castelo-Branco M, Formisano E, Backes W, Zanella F, Neuenschwander S, et al. (2002). Activity patterns in human motionsensitive areas depend on the interpretation of global motion. *Proc. Natl. Acad. Sci.USA* 99:13914–19

Catani, M., Jones, D.K., Donato, R., Ffytche, D.H., (2003). Occipito-temporal connections in the human brain. *Brain* 126, 2093–107.

Chase, C., Ashourzadeh, A., Kelly, C., Monfette, S., & Kinsey, K. (2003). Can the magnocellular pathway read? Evidence from studies of color. *Vision Research*, *43*(10), 1211-1222.

Chenevert, T. L., Brunberg, J. A., & Pipe, J. G. (1990). Anisotropic diffusion in human white matter: demonstration with MR techniques in vivo. *Radiology*, *177*(2), 401-405.

Cheng A, Eysel UT, Vidyasagar TR (2004) The role of the magnocellular pathway in serial deployment of visual attention. Eur J Neurosci 20:2188 –2192.

Chouake, T., Levy, T., Javitt, D. C., & Lavidor, M. (2012). Magnocellular training improves visual word recognition. *Frontiers in human neuroscience*, *6*, 14.

Clapp, W. C., Rubens, M. T., Sabharwal, J., & Gazzaley, A. (2011). Deficit in switching between functional brain networks underlies the impact of multitasking on working memory in older adults. *Proceedings of the National Academy of Sciences*, *108*(17), 7212-7217.

Cocosco, C. A., Kollokian, V., Kwan, R. K. S., Pike, G. B., & Evans, A. C. (1997). Brainweb: Online interface to a 3D MRI simulated brain database. In *NeuroImage*.

Cohen, L., Dehaene, S., Naccache, L., Lehéricy, S., Dehaene-Lambertz, G., Hénaff, M. a, Michel, F., (2000). The visual word form area: spatial and temporal characterization

of an initial stage of reading in normal subjects and posterior split-brain patients. *Brain* 123, 291–307.

Cohen, L., Lehéricy, S., Chochon, F., Lemer, C., Rivaud, S., Dehaene, S., (2002). Language-specific tuning of visual cortex? Functional properties of the Visual Word Form Area. *Brain* 125, 1054–69.

Catani, M., & De Schotten, M. T. (2008). A diffusion tensor imaging tractography atlas for virtual in vivo dissections. *cortex*, *44*(8), 1105-1132.

Cohen, M. X., & Van Gaal, S. (2013). Dynamic interactions between large-scale brain networks predict behavioral adaptation after perceptual errors. *Cerebral Cortex*, *23*(5), 1061-1072.

Conlon, E., Sanders, M., & Zapart, S. (2004). Temporal processing in poor adult readers. *Neuropsychologia*, *42*(2), 142-157.

Crewther, S. G., Crewther, D. P., Klistorner, A., & Kiely, P. M. (1999). Development of the magnocellular VEP in children: implications for reading disability. *Electroencephalography and clinical neurophysiology. Supplement*, *49*, 123-128.

Croner, L.J. and Kaplan, E. (1995). Receptive fields of P and M ganglion cells across the primate retina. *Vision Res.* 35:7-24.

Crook, J.M., Lange-Malecki, B., Lee, B.B. and Valberg, A. (1988). Visual resolution of macaque retinal ganglion cells. *J.Physiol.(Lond)* 396:205-224.

Damasio A, Yamada T, Damasio H, Corbett J, McKee J. (1980). Central achromatopsia: behavioral, anatomic, and physiologic aspects. *Neurology* 30:1064–71

Dehaene, S., Cohen, L., Sigman, M., & Vinckier, F. (2005). The neural code for written words: a proposal. *Trends in cognitive sciences*, *9*(7), 335-341.

Dehaene, S., & Cohen, L. (2011). The unique role of the visual word form area in reading. *Trends in cognitive sciences*, *15*(6), 254-262.

Dale, A.M., Buckner, R.L., (1997). Selective averaging of rapidly presented individual trials using fMRI. Hum. *Brain Mapp.* 5, 329–340.

Davis, M. H., & Johnsrude, I. S. (2007). Hearing speech sounds: top-down influences on the interface between audition and speech perception. *Hearing research*, *229*(1-2), 132-147.

Dawson, D. A., Lam, J., Lewis, L. B., Carbonell, F., Mendola, J. D., & Shmuel, A. (2016). Partial correlation-based retinotopically organized resting-state functional connectivity within and between areas of the visual cortex reflects more than cortical distance. *Brain connectivity*, *6*(1), 57-75.

Deutsch, G. K., Dougherty, R. F., Bammer, R., Siok, W. T., Gabrieli, J. D., & Wandell, B. (2005). Children's reading performance is correlated with white matter structure measured by diffusion tensor imaging. *Cortex*, *41*(3), 354-363.

DeYoe, E.A., Carman, G.J., Bandettini, P., Glickman, S., Wieser, J., Cox, R., Miller, D., and Neitz, J. (1996). Mapping striate and extrastriate visual areas in human cerebral cortex. Proc. Natl. Acad. Sci. USA 93, 2382–2386

Díaz, B., Hintz, F., Kiebel, S. J., & von Kriegstein, K. (2012). Dysfunction of the auditory thalamus in developmental dyslexia. *Proceedings of the National Academy of Sciences*, *109*(34), 13841-13846.

Dobkins, K. R., Anderson, C. M., & Lia, B. (1999). Infant temporal contrast sensitivity functions (tCSFs) mature earlier for luminance than for chromatic stimuli: evidence for precocious magnocellular development?. *Vision Research*, *39*(19), 3223-3239.

Donald, M. (1991*).* Origins of the modern mind: Three stages in the evolution of culture and cognition. New York, NY: Harvard University Press.

Donaldson DI, Buckner RL (2001): Effective paradigm design. In: Smith SM, editor. Functional MRI: an introduction to methods. Oxford: Oxford University Press; p 177–196.

Dougherty, R.F., Koch, V.M., Brewer, A.A., Fischer, B., Modersitzki, J., and Wandell, B.A. (2003). Visual field representations and locations of visual areas V1/2/3 in human visual cortex. *J. Vis.* 3, 586–598.

Duffau, H., Gatignol, P., Mandonnet, E., Capelle, L., & Taillandier, L. (2008). Intraoperative subcortical stimulation mapping of language pathways in a consecutive series of 115 patients with Grade II glioma in the left dominant hemisphere. *Journal of neurosurgery*, *109*(3), 461-471.

Dupont P, De Bruyn B, Vandenberghe R, Rosier AM, Michiels J, Marchal G, Mortelmans L, OrbanGA (1997) The kinetic occipital region in human visual cortex. *Cereb Cortex* 7:283–292.

Dronkers, N. F. (2011). The neural architecture of the language comprehension network: converging evidence from lesion and connectivity analyses. *Frontiers in systems neuroscience*, 5, 1.

Eden, G.F., Stein, J.F., Wood, H.M., & Wood, F.B. (1995). Temporal and spatial processing in reading disabled and normal children. *Cortex, 31*, 451-468.

Eklund, A., Nichols, T.E., Knutsson, H., (2016). Cluster failure: Why fMRI inferences for spatial extent have inflated false-positive rates. Proc. Natl. Acad. Sci. U. S. A. 113, 7900–5.

Engel, S.A., Rumelhart, D.E., Wandell, B.A., Lee, A.T., Glover, G.H., Chichilnisky, E.J., and Shadlen, M.N. (1994). fMRI of human visual cortex. *Nature* 369, 525.

Engel, S.A., Glover, G.H., and Wandell, B.A. (1997). Retinotopic organization in human visual cortex and the spatial precision of functional MRI. *Cereb. Cortex* 7, 181–192.

Enroth-Cugell, C. and Robson, J.G. (1966). The contrast sensitivity of retinal ganglion cells of the cat. *J.Physiol.(Lond)* 187:517-552.

Enroth-Cugell, C., & Shapley, R. M. (1973a). Adaptation and dynamics of cat retinal ganglion cells. *The Journal of physiology*, *233*(2), 271-309.

Enroth-Cugell, C. and Shapley, R.M. (1973b). Flux, not retinal illumination, is what cat retinal ganglion cells really care about. *J.Physiol.(Lond)* 233:311-326.

Epstein, R., & Kanwisher, N. (1998). A cortical representation of the local visual environment. *Nature*, *392*(6676), 598-601.

Facoetti, A., Paganoni, P., Turatto, M., Marzola, V., & Mascetti, G.G. (2000). Visual–spatial attention in developmental dyslexia. *Cortex*, *36*, 109-123.

Farrag, A. F., Khedr, E. M., & Abel-Naser, W. (2002). Impaired parvocellular pathway in dyslexic children. *European Journal of Neurology*, *9*(4), 359-363.

Felleman, D. J., & Van Essen, D. C. (1991). Distributed hierarchical processing in the primate cerebral cortex. *Cerebral cortex (New York, NY: 1991)*, *1*(1), 1-47.

Fernández-Miranda, J. C., Wang, Y., Pathak, S., Stefaneau, L., Verstynen, T., & Yeh, F.-C. (2014). Asymmetry, connectivity, and segmentation of the arcuate fascicle in the human brain. *Brain Structure and Function*, 220(3), 1665–1680.

Fields, R.D., (2009). The Other Brain: From Dementia to Schizophrenia, How New Discoveries about the Brain Are Revolutionizing Medicine and Science. Simon & Schuster, New York.

Finkelstein, D., McCleery, A.,(2013). An introduction to book history. Routledge.

Fischl, B., Van Der Kouwe, A., Destrieux, C., Halgren, E., Ségonne, F., Salat, D. H., ... & Dale, A. M. (2004). Automatically parcellating the human cerebral cortex. *Cerebral cortex*, *14*(1), 11-22.

Fisher, R.A., 1921. On the probable error of a coefficient of correlation deduced from a small sample. *Metron* 1, 3–32.

Fishman, R.S. (1997). Gordon Holmes, the cortical retina, and the wounds of war. The seventh Charles B. Snyder Lecture. Doc. Ophthalmol. 93, 9–28.

Franceschini, S., Gori, S., Ruffino, M., Pedrolli, K., & Facoetti, A. (2012). A causal link between visual spatial attention and reading acquisition. *Current biology*, *22*(9), 814-819.

Franceschini, S., Gori, S., Ruffino, M., Viola, S., Molteni, M., & Facoetti, A. (2013). Action video games make dyslexic children read better. *Current biology*, *23*(6), 462-466.

Frey, S., Campbell, J. S., Pike, G. B., & Petrides, M. (2008). Dissociating the human language pathways with high angular resolution diffusion fiber tractography. *Journal of Neuroscience*, *28*(45), 11435-11444.

Friederici, A. D. (2002). Towards a neural basis of auditory sentence processing. *Trends in cognitive sciences*, *6*(2), 78-84.

Friederici, A. D. (2011). The brain basis of language processing: from structure to function. *Physiological reviews*, *91*(4), 1357-1392.

Friederici, A. D. (2015). White-matter pathways for speech and language processing. Handbook of clinical neurology, 129, 177-186.

Friston, K.J., Holmes, A.P., Poline, J.-B., Grasby, P.J., Williams, S.C.R., Frackowiak, R.S.J., Turner, R., (1995). Analysis of fMRI Time-Series Revisited. *Neuroimage* 2, 45–53.

Friston, K.J., Zarahn, E., Josephs, O., Henson, R.N., Dale, a M., (1999). Stochastic designs in event-related fMRI. *Neuroimage* 10, 607–619.

Gabrieli, J. D., & Norton, E. S. (2012). Reading abilities: importance of visual-spatial attention. *Current biology*, *22*(9), R298-R299.

Gallant, J. L., Connor, C. E., Rakshit, S., Lewis, J. W., & Van Essen, D. C. (1996). Neural responses to polar, hyperbolic, and Cartesian gratings in area V4 of the macaque monkey. *Journal of neurophysiology*, *76*(4), 2718-2739.

Genç, E., Schölvinck, M. L., Bergmann, J., Singer, W., & Kohler, A. (2016). Functional connectivity patterns of visual cortex reflect its anatomical organization. *Cerebral cortex*, *26*(9), 3719-3731.

Giraldo-Chica, M., Hegarty II, J. P., & Schneider, K. A. (2015). Morphological differences in the lateral geniculate nucleus associated with dyslexia. *NeuroImage: Clinical*, *7*, 830-836.

Glasser, M. F., & Rilling, J. K. (2008). DTI Tractography of the Human Brain's Language Pathways. *Cerebral Cortex*, 18(11), 2471–2482.

Goodale, M.A., Milner, A.D. (1992). Separate visual pathways for perception and action. *Trends Neurosci*. 15, 20–25.

Gori, S., Mascheretti, S., Giora, E., Ronconi, L., Ruffino, M., Quadrelli, E. & Marino, C. (2015). The DCDC2 intron 2 deletion impairs illusory motion perception unveiling the selective role of magnocellular-dorsal stream in reading (dis) ability. *Cerebral Cortex*, *25*(6), 1685-1695.

Goswami, U. (2011). A temporal sampling framework for developmental dyslexia. *Trends in cognitive sciences*, *15*(1), 3-10.

Grill-Spector K, Kushnir T, Hendler T, Edelman S, Itzchak Y, Malach R (1998) A sequence of object-processing stages revealed by fMRI in the human occipital lobe. *Hum Brain Mapp* 6:316 –328.

Grill-Spector, K., Kourtzi, Z., & Kanwisher, N. (2001). The lateral occipital complex and its role in object recognition. *Vision research*, *41*(10-11), 1409-1422.

Grossberg, S. (1982). How does a brain build a cognitive code?. *Studies of mind and brain*, 1-52.

Grossberg, S. (1999). The link between brain learning, attention, and consciousness. *Consciousness and cognition*, *8*(1), 1-44.

Gudbjartsson, H., & Patz, S. (1995). The Rician distribution of noisy MRI data. *Magnetic resonance in medicine*, *34*(6), 910-914.

Hammarrenger, B., Leporé, F., Lippé, S., Labrosse, M., Guillemot, J. P., & Roy, M. S. (2003). Magnocellular and parvocellular developmental course in infants during the first year of life. *Documenta Ophthalmologica*, *107*(3), 225-233.

Harm, M. W., & Seidenberg, M. S. (1999). Phonology, reading acquisition, and dyslexia: insights from connectionist models. *Psychological Review*, *106*(3), 491-528.

Hendry, S. H., & Yoshioka, T. (1994). A neurochemically distinct third channel in the macaque dorsal lateral geniculate nucleus. *Science*, *264*(5158), 575-577.

Hendry, S. H., & Reid, R. C. (2000). The koniocellular pathway in primate vision. *Annual review of neuroscience*, *23*(1), 127-153.

Hickok, G., & Poeppel, D. (2000). Towards a functional neuroanatomy of speech perception. *Trends in cognitive sciences*, *4*(4), 131-138.

Hickok, G., & Poeppel, D. (2004). Dorsal and ventral streams: a framework for understanding aspects of the functional anatomy of language. *Cognition*, *92*(1-2), 67-99.

Hickok, G., & Poeppel, D. (2007). The cortical organization of speech processing. *Nature reviews neuroscience*, *8*(5), 393-402.

Hickok, G., Houde, J., & Rong, F. (2011). Sensorimotor integration in speech processing: computational basis and neural organization. *Neuron*, *69*(3), 407-422.

Holmes, G. (1918). Distrubances of vision by cerebral lesions. Bre. J. Opthal. 2, 353–384.

Hubel, D. H., & Wiesel, T. N. (1962). Receptive fields, binocular interaction and functional architecture in the cat's visual cortex. *The Journal of physiology*, *160*(1), 106-154.

Huk AC, Ress D, Heeger DJ. (2001). Neuronal basis of the motion aftereffect reconsidered. *Neuron* 32:161–72

Iglesias, J.E., Insausti, R., Lerma-Usabiaga, G., Bocchetta, M., Van Leemput, K., Greve, D.N., van der Kouwe, A., Fischl, B., Caballero-Gaudes, C., & Paz-Alonso, P.M. (2018). A probabilistic atlas of the human thalamic nuclei combining ex vivo MRI and histology. *NeuroImage*, 183, 314-326.

Inouye, T. (1909). *Die Sehstörungen bei Schussverletzungen der kortikalen Sehsphäre: nach Beobachtungen an Verwundeten der letzten japanischen Kriege*. Engelmann.

Ishai, A., Ungerleider, L. G., Martin, A., & Haxby, J. V. (2000). The representation of objects in the human occipital and temporal cortex. *Journal of Cognitive Neuroscience*, *12*(Supplement 2), 35-51.

Ishibashi, T., Dakin, K.A., Stevens, B., Lee, P.R., Kozlov, S. V., Stewart, C.L., Fields, R.D., (2006). Astrocytes promote myelination in response to electrical impulses. *Neuron* 49, 823–832.

Jeurissen, B., Leemans, A., Tournier, J.-D., Jones, D.K., Sijbers, J., (2013). Investigating the prevalence of complex fiber configurations in white matter tissue with diffusion magnetic resonance imaging. *Hum. Brain Mapp*. 34, 2747–2766.

Jeurissen, B., Tournier, J.D., Dhollander, T., Connelly, A., Sijbers, J., (2014). Multitissue shell diffusion MRI data. *Neuroimage* 103, 411–426.

Jednorog, K., Marchewka, A., Altarelli, I., Monzalvo Lopez, A. K., van Ermingen-Marbach, M., Grande, M., ... & Ramus, F. (2015). How reliable are gray matter disruptions in specific reading disability across multiple countries and languages? Insights from a large-scale voxel-based morphometry study. *Human brain mapping*, *36*(5), 1741-1754.

Jobard, G., Crivello, F., Tzourio-Mazoyer, N., (2003). Evaluation of the dual route theory of reading: a metanalysis of 35 neuroimaging studies. *Neuroimage* 20, 693–712.

Joo, S. J., Donnelly, P. M., & Yeatman, J. D. (2017). The causal relationship between dyslexia and motion perception reconsidered. *Scientific reports*, *7*(1), 1-7.

Kanwisher, N., Woods, R. P., Iacoboni, M., & Mazziotta, J. C. (1997). A locus in human extrastriate cortex for visual shape analysis. *Journal of Cognitive Neuroscience*, *9*(1), 133-142.

Kanwisher, N. (1996). Functional imaging of human visual recognition Nancy Kanwisher"", Marvin M. Chun", Josh McDermott", Patrick J. Ledden. *Cognitive Brain Research*, *5*, 55-67.

Kaplan, E. and Shapley, R.M. (1986) The primate retina contains two types of ganglion cells, with high and low contrast sensitivity *Proc.Natl.Acad.Sci.USA* 83:2755-2757.

Kaplan, E. (2004). The M, P, and K pathways of the primate visual system. *The visual neurosciences*, *1*, 481-493.

Kellner, E., Dhital, B., Kiselev, V. G., & Reisert, M. (2016). Gibbs-ringing artifact removal based on local subvoxel-shifts. *Magnetic resonance in medicine*, *76*(5), 1574-1581.

Klaver, P., Lichtensteiger, J., Bucher, K., Dietrich, T., Loenneker, T., & Martin, E. (2008). Dorsal stream development in motion and structure-from-motion perception. *Neuroimage*, *39*(4), 1815-1823.

Klingberg, T., Hedehus, M., Temple, E., Salz, T., Gabrieli, J.D.., Moseley, M.E., Poldrack, R.A., (2000). Microstructure of Temporo-Parietal White Matter as a Basis for Reading Ability. *Neuron* 25, 493–500.

Kosslyn, S. M., & Shin, L. M. (1994). Visual mental images in the brain: Current issues.

Kronbichler, M., Hutzler, F., Wimmer, H., Mair, A., Staffen, W., Ladurner, G., (2004). The visual word form area and the frequency with which words are encountered: evidence from a parametric fMRI study. *Neuroimage* 21, 946– 53.

Kveraga, K., Ghuman, A. S., & Bar, M. (2007). Top-down predictions in the cognitive brain. *Brain and cognition*, *65*(2), 145-168.

Lamme, V. A., & Roelfsema, P. R. (2000). The distinct modes of vision offered by feedforward and recurrent processing. *Trends in neurosciences*, *23*(11), 571-579.

Larsson, J., & Heeger, D. J. (2006). Two retinotopic visual areas in human lateral occipital cortex. *Journal of Neuroscience*, *26*(51), 13128-13142.

Larsson J, Landy MS, Heeger DJ (2006) Orientation-selective adaptation to first- and second-order patterns in human visual cortex. *J Neurophysiol* 95:862– 881.

Lau, E. F., Phillips, C., & Poeppel, D. (2008). A cortical network for semantics:(de) constructing the N400. *Nature Reviews Neuroscience*, *9*(12), 920-933.

Laycock, R., Crewther, S. G., & Crewther, D. P. (2007). A role for the 'magnocellular advantage'in visual impairments in neurodevelopmental and psychiatric disorders. *Neuroscience & Biobehavioral Reviews*, *31*(3), 363-376.

Lee, B.B., Martin, P.R. and Valberg, A. (1989). Nonlinear summation of M- and L-cone inputs to phasic retinal ganglion cells of the macaque. *J.Neurosci.* 9:1433-1442.

Lehongre, K., Ramus, F., Villiermet, N., Schwartz, D., & Giraud, A. L. (2011). Altered low-gamma sampling in auditory cortex accounts for the three main facets of dyslexia. *Neuron*, *72*(6), 1080-1090.

Lerma-Usabiaga, G., Carreiras, M., & Paz-Alonso, P. M. (2018). Converging evidence for functional and structural segregation within the left ventral occipitotemporal cortex in reading. *Proceedings of the National Academy of Sciences*, *115*(42), E9981-E9990.

Lerma-Usabiaga, G., Mukherjee, P., Perry, M. L., & Wandell, B. A. (2020). Data-science ready, multisite, human diffusion MRI white-matter-tract statistics. *Scientific data*, *7*(1), 1-9.

Leventhal, A.G, Rodieck, R.W. and Dreher, B. (1981). Retinal ganglion cell classes in the Old World monkey: morphology and central projections. *Science* 213:1139-1142.

Levy, T., Walsh, V., & Lavidor, M. (2010). Dorsal stream modulation of visual word recognition in skilled readers. *Vision research*, *50*(9), 883-888.

Livingstone, M. S., & Hubel, D. H. (1987). Psychophysical evidence for separate channels for the perception of form, color, movement, and depth. *Journal of Neuroscience*, *7*(11), 3416-3468.

Livingstone, M., & Hubel, D. (1988). Segregation of form, color, movement, and depth: anatomy, physiology, and perception. *Science*, *240*(4853), 740-749.

Livingstone, M.S., Rosen, G.D., Drislane, F.W., & Galaburda, A.M. (1991). Physiological and anatomical evidence for a magnocellular defect in developmental dyslexia. *PNAS*, *88*, 7943-7947.

Logothetis, N. K., & Sheinberg, D. L. (1996). Visual object recognition. *Annual review of neuroscience*, *19*(1), 577-621.

Lovegrove, W., Martin, F., Bowling, A., Blackwood, M., Badcock, D., & Paxton, S. (1982). Contrast sensitivity functions and specific reading disability. *Neuropsychologia*, *20*(3), 309-315.

Lovegrove, W., Martin, F., & Slaghuis, W. (1986). A theoretical and experimental case for a visual deficit in specific reading disability. *Cognitive neuropsychology*, *3*(2), 225-267.

Lueck, C. J., Zeki, S., Friston, K. J., Deiber, M. P., Cope, P., Cunningham, V. J., ... & Frackowiak, R. S. J. (1989). The colour centre in the cerebral cortex of man. *Nature*, *340*(6232), 386-389.

Lyon, D.C., and Kaas, J.H. (2002). Evidence for a modified V3 with dorsal and ventral halves in macaque monkeys. *Neuron* 33, 453–461.

M. Jenkinson, C.F. Beckmann, T.E. Behrens, M.W. Woolrich, S.M. Smith. (2012). FSL. *NeuroImage*, *62:*782-90, 2012

Makris, N., Kennedy, D. N., McInerney, S., Sorensen, A. G., Wang, R., Caviness Jr, V. S., & Pandya, D. N. (2005). Segmentation of subcomponents within the superior longitudinal fascicle in humans: a quantitative, in vivo, DT-MRI study. *Cerebral cortex*, *15*(6), 854-869.

Malach, R., Reppas, J. B., Benson, R. R., Kwong, K. K., Jiang, H., Kennedy, W. A., ... & Tootell, R. B. (1995). Object-related activity revealed by functional magnetic resonance imaging in human occipital cortex. *Proceedings of the National Academy of Sciences*, *92*(18), 8135-8139.

Maldonado, I. L., Mandonnet, E., & Duffau, H. (2012). Dorsal fronto-parietal connections of the human brain: A fiber dissection study of their composition and anatomical relationships. *The Anatomical Record: Advances in Integrative Anatomy and Evolutionary Biology*, *295*(2), 187-195.

Martensson, J., Eriksson, J., Bodammer, N. C., Lindgren, M., Johansson, M., Nyberg, L., & Lovden, M. (2012). Growth of language-related brain areas after foreign language learning. *NeuroImage*, *63*(1), 240-244.

Mason, A., Cornelissen, P., Fowler, S., & Stein, J. (1993). Contrast sensitivity, ocular dominance and specific reading disability. *Clinical Vision Sciences*, *8*(4), 345-353.

McKeefry, D. J., & Zeki, S. E. M. I. R. (1997). The position and topography of the human colour centre as revealed by functional magnetic resonance imaging. *Brain: a journal of neurology*, *120*(12), 2229-2242.

McLean, G. M., Stuart, G. W., Coltheart, V., & Castles, A. (2011). Visual temporal processing in dyslexia and the magnocellular deficit theory: the need for speed?. *Journal of Experimental Psychology: Human Perception and Performance*, *37*(6), 1957.

Mendola JD, Dale AM, Fischl B, Liu AK, Tootell RB (1999) The representation of illusory and real contours in human cortical visual areas revealed by functional magnetic resonance imaging. *J Neurosci* 19:8560–8572.

Merigan, W. H., Katz, L. M., & Maunsell, J. H. (1991). The effects of parvocellular lateral geniculate lesions on the acuity and contrast sensitivity of macaque monkeys. *Journal of Neuroscience*, *11*(4), 994-1001.

Merigan, W. H., & Maunsell, J. H. (1993). How parallel are the primate visual pathways?. *Annual review of neuroscience*, *16*(1), 369-402.

Mishkin, M., Ungerleider, L. G., & Macko, K. A. (1983). Object vision and spatial vision: two cortical pathways. *Trends in neurosciences*, *6*, 414-417.

Moseley, M. E., & Glover, G. H. (1995). Functional MR imaging. Capabilities and limitations. *Neuroimaging Clinics of North America*, *5*(2), 161-191.

Müller-Axt, C., Anwander, A., & von Kriegstein, K. (2017). Altered structural connectivity of the left visual thalamus in developmental dyslexia. *Current Biology*, *27*(23), 3692-3698.

Mumford, D. (1992). On the computational architecture of the neocortex. *Biological cybernetics*, *66*(3), 241-251.

Musel, B., Bordier, C., Dojat, M., Pichat, C., Chokron, S., Le Bas, J. F., & Peyrin, C. (2013). Retinotopic and lateralized processing of spatial frequencies in human visual cortex during scene categorization. *Journal of Cognitive Neuroscience*, *25*(8), 1315-1331.

Nagy, Z., Westerberg, H., & Klingberg, T. (2004). Maturation of white matter is associated with the development of cognitive functions during childhood. *Journal of Cognitive Neuroscience*, *16*(7), 1227-1233.

Navon, D. (1977). Forest before trees: The precedence of global features in visual perception. *Cognitive psychology*, *9*(3), 353-383.

Niogi, S. N., & McCandliss, B. D. (2006). Left lateralized white matter microstructure accounts for individual differences in reading ability and disability. *Neuropsychologia*, *44*(11), 2178-2188.

Norton, T. T., & Casagrande, V. A. (1982). Laminar organization of receptive-field properties in lateral geniculate nucleus of bush baby (Galago crassicaudatus). *Journal of Neurophysiology*, *47*(4), 715-741.

Ogawa, S., Lee, T.M., Kay, A.R., Tank, D.W., (1990). Brain magnetic resonance imaging with contrast dependent on blood oxygenation. *Proc. Natl. Acad. Sci. U. S. A.* 87, 9868–72.

Ogawa, S., and Lee, T.M. (1990). Magnetic resonance imaging of blood vessels at high fields: In vivo and in vitro measurements and image simulation. Magn. Reson. Med. 16, 9–18.

Ogawa, S., Lee, T.M., Nayak, A.S., and Glynn, P. (1990). Oxygenation sensitive contrast in magnetic resonance image of rodent brain at high magnetic fields. *Magn. Reson. Med.* 14, 68–78.

Ogawa, S., Tank, D., Menon, R., Ellermann, J., Kim, S., Merkle, H., and Ugurbil, K. (1992). Intrinsic signal changes accompanying sensory stimulation: Functional brain mapping with magnetic resonance imaging. Proc. Natl. Acad. Sci. USA 89, 5951–5955.

Qiu, F. T., & Von Der Heydt, R. (2005). Figure and ground in the visual cortex: V2 combines stereoscopic cues with Gestalt rules. *Neuron*, *47*(1), 155-166.

Qiu, A., Rosenau, B.J., Greenberg, A.S., Hurdal, M.K., Barta, P., Yantis, S., and Miller, M.I. (2006). Estimating linear cortical magnification in human primary visual cortex via dynamic programming. *Neuroimage* 31, 125–138.

Olulade, O. A., Napoliello, E. M., & Eden, G. F. (2013). Abnormal visual motion processing is not a cause of dyslexia. *Neuron*, *79*(1), 180-190.

Parrish, E. E., Giaschi, D. E., Boden, C., & Dougherty, R. (2005). The maturation of form and motion perception in school age children. *Vision Research*, *45*(7), 827-837.

Pascual-Leone, A. *et al.* (1995) The role of reading activity on the modulation of motor cortical outputs to the reading hand in Braille readers *Ann. Neurol*. 38, 910–915

Paz-Alonso, P.M., Bunge, S.A., Anderson, M.C., Ghetti, S., (2013). Strength of coupling within a mnemonic control network differentiates those who can and cannot suppress memory retrieval. *J. Neurosci*. 33, 5017–5026.

Paz-Alonso, P. M., Oliver, M., Lerma-Usabiaga, G., Caballero-Gaudes, C., Quiñones, I., Suárez-Coalla, P., ... & Carreiras, M. (2018). Neural correlates of phonological, orthographic and semantic reading processing in dyslexia. *NeuroImage: Clinical*, *20*, 433-447.

Pearlman AL, Birch J, Meadows JC. (1979). Cerebral color blindness: an acquired defect in hue discrimination. *Ann. Neurol.* 5:253–61

Pelli, D. G. (1997). The VideoToolbox software for visual psychophysics: transforming numbers into movies. *Spatial Vision*

Perea, G., Sur, M., Araque, A., (2014). Neuron-glia networks: integral gear of brain function. *Front. Cell. Neurosci*. 8, 378.

Perry, V.H., Oehler, R. and Cowey, A. (1984). Retinal ganglion cells that project to the dorsal lateral geniculate nucleus in the macaque monkey. *Neuroscience* 12:1101-1123.

Pfefferbaum, A., Sullivan, E. V., Hedehus, M., Adalsteinsson, E., Lim, K. O., & Moseley, M. (2000). In vivo detection and functional correlates of white matter microstructural disruption in chronic alcoholism. *Alcoholism: Clinical and Experimental Research*, *24*(8), 1214-1221.

Pierpaoli, C., Barnett, A., Pajevic, S., Chen, R., Penix, L.R., Virta, A., Basser, P., (2001). Water diffusion changes in Wallerian degeneration and their dependence on white matter architecture. *Neuroimage* 13, 1174–85.

Plaut, D. C., McClelland, J. L., Seidenberg, M. S., & Patterson, K. (1996). Understanding normal and impaired word reading: computational principles in quasi-regular domains. *Psychological Review, 103*(1), 56-115.

Poldrack, R.A., (2007). Region of interest analysis for fMRI. Soc. Cogn. Affect. Neurosci. 2, 67–70. Saxe, R., Brett, M., Kanwisher, N., (2006). Divide and conquer: A defense of functional localizers. *Neuroimage* 30, 1088–1096.

Poldrack, R. A. (2012). The future of fMRI in cognitive neuroscience. *Neuroimage*, *62*(2), 1216-1220.

Preston, J.L., Felsenfeld, S., Frost, S.J., Mencl, W.E., Fulbright, R.K., Grigorenko, E.L., Landi, N, Seki, A., Pugh, K.R. (2012). Functional brain activation differences in school-age children with speech sound errors: Speech and print processing. *Journal of Speech, Language & Hearing Research*, 55(4), 1068-1082.

Price, C.J., Devlin, J.T., (2011). The interactive account of ventral occipitotemporal contributions to reading. *Trends Cogn. Sci*. 15, 246–53.

Puce, A., Allison, T., Gore, J. C., & McCarthy, G. (1995). Face-sensitive regions in human extrastriate cortex studied by functional MRI. *Journal of neurophysiology*, *74*(3), 1192-1199.

Pugh, K.R., Mencl, W.E., Jenner, A.R., Katz, L., Frost, S.J., Lee, J.R., Shaywitz, S.E., Shaywitz, B.A., (2001). Neurobiological studies of reading and reading disability. *J. Commun. Disord*. 34, 479–492.

Raichle, M.E., (2009). A brief history of human brain

Rauschecker, J. P., & Scott, S. K. (2009). Maps and streams in the auditory cortex: nonhuman primates illuminate human speech processing. *Nature neuroscience*, *12*(6), 718-724.

Rees G, Friston K,Koch C. (2000).Adirect quantitative relationship between the functional properties of human and macaque V5. *Nat. Neurosci.* 3:716–23

Reppas, J.B. *et al.* (1997) Motion boundaries are represented in retinotopic human visual cortical area *Nature* 388, 175–179

Rissman, J., Gazzaley, A., D'Esposito, M., (2004). Measuring functional connectivity during distinct stages of a cognitive task. *Neuroimage* 23, 752– 763.

Rizzolatti, G., & Matelli, M. (2003). Two different streams form the dorsal visual system: anatomy and functions. *Experimental brain research*, *153*(2), 146-157.

Robinson, A., 2009. Writing and script: a very short introduction. OUP, Oxford.

Ruffino, M., Gori, S., Boccardi, D., Molteni, M., & Facoetti, A. (2014). Spatial and temporal attention in developmental dyslexia. *Frontiers in human neuroscience*, *8*, 331.

Sandak, R., Mencl, W.E., Frost, S.J., Pugh, K.R., (2004). The Neurobiological Basis of Skilled and Impaired Reading: Recent Findings and New Directions. *Sci .Stud. Read.* 8, 273–292.

Sarubbo S, De Benedictis A, Maldonado IL et al. (2013). Frontal terminations for the inferior fronto-occipital fascicle: anatomical dissection, DTI study and functional considerations on a multi-component bundle. *Brain Struct Funct* 218: 21–37.

Saur, D., Kreher, B.W., Schnell, S., Kümmerer, D., Kellmeyer, P., Vry, M.-S., Umarova, R., Musso, M., Glauche, V., Abel, S., Huber, W., Rijntjes, M., Hennig, J., Weiller, C.. (2008). Ventral and dorsal pathways for language. Proc. Natl. Acad. Sci. U. S. A. 105, 18035–40.

Saur D, Schelter B, Schnell S et al. (2010). Combining functional and anatomical connectivity reveals brain networks for auditor language comprehension. *Neuroimage* 49: 3187–3197.

Sayres, R., & Grill-Spector, K. (2008). Relating retinotopic and object-selective responses in human lateral occipital cortex. *Journal of Neurophysiology*, *100*(1), 249-267.

Schlaggar, B.L., McCandliss, B.D.,(2007). Development of neural systems for reading. *Annu. Rev. Neurosci*. 30, 475–503.

Schuster, S., Hawelka, S., Hutzler, F., Kronbichler, M., Richlan, F., (2016). Words in Context: The Effects of Length, Frequency, and Predictability on Brain Responses during Natural Reading. *Cereb. Cortex* 26, 3889–3904.

Seidenberg, M. S., & McClelland, J. L. (1989). A distributed, developmental model of word recognition and naming. *Psychological Review*, *96*(4), 523-568.

Seidenberg, M.S., (2012). Connectionist models of reading. Oxford Handb. Psycholinguist. 235–250.

Sereno, M.I., Dale, A.M., Reppas, J.B., Kwong, K.K., Belliveau, J.W., Brady, T.J., Rosen, B.R., and Tootell, R.B. (1995). Borders of multiple human visual areas in humans revealed by functional mri. *Science* 268, 889–893.

Shapley, R.M. & Victor, J.D. (1978). The effect of contrast on the transfer properties of cat retinal ganglion cells. *J.Physiol.(Lond)* 285:275-298.

Shapley, R., Kaplan, E. and Soodak, R. (1981). Spatial summation and contrast sensitivity of X and Y cells in the lateral geniculate nucleus of the macaque. *Nature* 292:543-545.

de Schotten, M. T., Dell'Acqua, F., Valabregue, R., & Catani, M. (2012). Monkey to human comparative anatomy of the frontal lobe association tracts. *Cortex*, *48*(1), 82-96.

Skottun, B. C. (2013). On using very high temporal frequencies to isolate magnocellular contributions to psychophysical tasks. *Neuropsychologia*, *51*(8), 1556-1560.

Skottun, B. C. (2015). On the use of spatial frequency to isolate contributions from the magnocellular and parvocellular systems and the dorsal and ventral cortical streams. *Neuroscience & Biobehavioral Reviews*, *56*, 266-275.

Smith, Robert E; Tournier, Jacques Donald; Calamante, Fernando; Connelly, Alan. (2013) SIFT: Spherical-deconvolution informed filtering of tractograms. *Neuroimage* 67, 298-312.

Solan, H. A., Shelley-Tremblay, J., Hansen, P. C., Silverman, M. E., Larsone, S., & Ficarra, A. (2004). M-cell deficit and reading disability: a preliminary study of the effects of temporal vision-processing therapy. *Optometry-Journal of the American Optometric Association*, *75*(10), 640-650

Stein, J., & Walsh, V. (1997). To see but not to read; the magnocellular theory of dyslexia. *Trends in neurosciences*, *20*(4), 147-152.

Stein, J. (2001). The magnocellular theory of developmental dyslexia. *Dyslexia*, *7*(1), 12-36.

Stein, J. (2014). Dyslexia: the role of vision and visual attention. *Current developmental disorders reports*, *1*(4), 267-280.

Stigliani, A., Jeska, B., & Grill-Spector, K. (2017). Encoding model of temporal processing in human visual cortex. *Proceedings of the National Academy of Sciences*, *114*(51), E11047-E11056.

Stikov, N., Perry, L.M., Mezer, A., Rykhlevskaia, E., Wandell, B.A., Pauly, J.M., Dougherty, R.F., (2011). Bound pool fractions complement diffusion measures to describe white matter micro and macrostructure. *Neuroimage* 54, 1112– 1121.

Strother, L., Coros, A. M., & Vilis, T. (2015). Visual cortical representation of whole words and hemifield-split word parts. *Journal of cognitive neuroscience*, *28*(2), 252-260.

Strother, L., Zhou, Z., Coros, A. K., & Vilis, T. (2017). An fMRI study of visual hemifield integration and cerebral lateralization. *Neuropsychologia*, *100*, 35-43.

Talairach, J., Tournoux, P., (1988). Co-planar stereotaxic atlas of the human brain: 3-dimensional proportional system: an approach to cerebral imaging, Neuropsychologia.

Talbot, S.A. (1940). Arrangement of visual field on cat's cortex. *Am. J. Physiol*. 129, 477–478.

Talbot, S., and Marshall, W. (1941). Physiological studies on neural mechanisms of visual localization and discrimination. *Am. J. Ophthalmol*. 24, 1255–1263.

Talbot, S.A. (1942). A lateral localization in the cat's visual cortex. Fed. Proc. 1, 84.

Thompson, J.M., Woolsey, C.N., and Talbot, S.A. (1950). Visual areas I and II of cerebral cortex of rabbit. *J. Neurophysio*. 12, 277–288.

Takemura, H., Caiafa, C. F., Wandell, B. A., & Pestilli, F. (2016). Ensemble tractography. *PLoS computational biology*, *12*(2), e1004692.

Tanaka, K. (1996). Inferotemporal cortex and object vision. *Annual review of neuroscience*, *19*(1), 109-139.

Tanaka, K. (1997). Mechanisms of visual object recognition: monkey and human studies. *Current opinion in neurobiology*, *7*(4), 523-529.

Teuber, H.L., Battersby, W.S., and Bender, M.B. (1960). Visual Field Defects After Penetrating Missile Wounds of the Brain (Cambridge, MA: Harvard University Press).

Tootell RB, Reppas JB, Kwong KK, Malach R, Born RT, et al.(1995). Functional analysis of human MT and related visual cortical areas using magnetic resonance imaging. *J. Neurosci.* 15:3215–30

Tootell RB, Taylor JB. (1995). Anatomical evidence for MT and additional cortical visual areas in humans. *Cereb. Cortex* 5:39– 55

Tootell, R.B.H. *et al.* (1996) New images from human visual cortex *Trends Neurosci.* 19, 481–489.

Tootell, R.B.H. *et al.* (1997) Functional analysis of V3A and related areas in human visual cortex *J. Neurosci.* 17, 7076–7078.

Tournier, J.-D., Calamante, F., Connelly, A., (2010). Improved probabilistic streamlines tractography by 2 nd order integration over fibre orientation distributions, in: ISMRM. p. 1670.

Tournier, J. D., Smith, R., Raffelt, D., Tabbara, R., Dhollander, T., Pietsch, M., ... & Connelly, A. (2019). MRtrix3: A fast, flexible and open software framework for medical image processing and visualisation. *Neuroimage*, *202*, 116137.

Tusa, R.J., Palmer, L.A., and Rosenquist, A.C. (1978). The retinotopic organization of area 17 (striate cortex) in the cat. J. Comp. Neurol. 177, 213–235.

Tustison, N. J., Avants, B. B., Cook, P. A., Zheng, Y., Egan, A., Yushkevich, P. A., & Gee, J. C. (2010). N4ITK: improved N3 bias correction. IEEE transactions on medical imaging, 29(6), 1310-1320.

Tyler CW, Baseler HA, Kontsevich LL, Likova LT, Wade AR, Wandell BA (2005) Predominantly extra-retinotopic cortical response to pattern symmetry. *NeuroImage* 24:306 –314.

Tyler, C.W., Likova, L.T., Chen, C.-C., Kontsevich, L.L., Schira, M.M., and Wade, A.R. (2005). Extended Concepts of Occipital Retinotopy. *Current Medical Imaging Reviews* 1, 319–329.

Tyler CW, Likova LT, Kontsevich LL, Wade AR (2006) The specificity of cortical region KO to depth structure. *NeuroImage* 30:228 –238.

Ullman, S., Vidal-Naquet, M., & Sali, E. (2002). Visual features of intermediate complexity and their use in classification. *Nature neuroscience*, 5(7), 682-687.

Ungerleider, L. G., Courtney, S. M., & Haxby, J. V. (1998). A neural system for human visual working memory. *Proceedings of the National Academy of Sciences*, *95*(3), 883-890.

Van Essen, D. C., Newsome, W. T., & Maunsell, J. H. (1984). The visual field representation in striate cortex of the macaque monkey: asymmetries, anisotropies, and individual variability. *Vision research*, *24*(5), 429-448.

Van Essen, D. C., Felleman, D. J., DeYoe, E. A., Olavarria, J., & Knierim, J. (1990, January). Modular and hierarchical organization of extrastriate visual cortex in the macaque

monkey. In *Cold Spring Harbor symposia on quantitative biology* (Vol. 55, pp. 679-696). Cold Spring Harbor Laboratory Press.

Van Essen, D. C., Lewis, J. W., Drury, H. A., Hadjikhani, N., Tootell, R. B., Bakircioglu, M., & Miller, M. I. (2001). Mapping visual cortex in monkeys and humans using surface-based atlases. *Vision research*, *41*(10-11), 1359-1378.

Van Essen, D. C. (2003). Organization of visual areas in macaque and human cerebral cortex. *The visual neurosciences*, *1*, 507-521.

Van Oostende S, Sunaert S, Van Hecke P, Marchal G, Orban GA (1997) The kinetic occipital (KO) region in man: an fMRI study. *Cereb Cortex* 7:690 –701.

Veraart, J., Novikov, D. S., Christiaens, D., Ades-Aron, B., Sijbers, J., & Fieremans, E. (2016). Denoising of diffusion MRI using random matrix theory. *Neuroimage*, *142*, 394-406.

Vidyasagar, T. R. (2004). Neural underpinnings of dyslexia as a disorder of visuo-spatial attention. *Clinical and Experimental Optometry*, *87*(1), 4-10.

Vidyasagar, T.R., & Pammer, K. (2010). Dyslexia: a deficit in visuo-spatial attention, not in phonological processing. *Trends in Cognitive Science, 14* (2), 57–63.

Vogels, R., Biederman, I., Bar, M., & Lorincz, A. (2001). Inferior temporal neurons show greater sensitivity to nonaccidental than to metric shape differences. *Journal of Cognitive Neuroscience*, *13*(4), 444-453.

Wakana, Setsu, Arvind Caprihan, Martina M. Panzenboeck, James H. Fallon, Michele Perry, Randy L. Gollub, Kegang Hua, et al. (2007). Reproducibility of Quantitative Tractography Methods Applied to Cerebral White Matter. NeuroImage 36: 630–44.

Wang, L., Mruczek, R. E., Arcaro, M. J., & Kastner, S. (2015). Probabilistic maps of visual

topography in human cortex. *Cerebral cortex*, *25*(10), 3911-3931.

Wilmer, J. B., Richardson, A. J., Chen, Y., & Stein, J. F. (2004). Two visual motion processing deficits in developmental dyslexia associated with different reading skills deficits. *Journal of Cognitive Neuroscience*, *16*(4), 528-540.

Wandell, B. A., Baseler, H., Poirson, A. B., Boynton, G. M., & Engel, S. (2000). Computational neuroimaging: color tuning in two human cortical areas measured using fMRI. *Colour vision: From genes to perception*, 269-282.

Wandell, B.A., Brewer, A.A., and Dougherty, R.F. (2005). Visual field map clusters in human cortex. *Philos. Trans. R. Soc. Lond. B Biol. Sci*. 360, 693–707.

Wandell, B. A., Dumoulin, S. O., & Brewer, A. A. (2007). Visual field maps in human cortex. *Neuron*, *56*(2), 366-383.

Wandell, B.A., Yeatman, J.D., (2013). Biological development of reading circuits. *Curr. Opin. Neurobiol*. 23, 261–8.

Watson JD, Myers R, Frackowiak RS, Hajnal JV,Woods RP, et al. (1993). Area V5 of the human brain: evidence from a combined study using positron emission tomography and magnetic resonance imaging. *Cereb. Cortex* 3:79–94

World Health Organization, 2008. International Statistical Classification of Diseases and Related Health Problems—Tenth Revision, 2nd ed. World Health Organization, Geneva, Switzerland.

Yagmurlu, K., Middlebrooks, E. H., Tanriover, N., & Rhoton, A. L. (2016). Fiber tracts of the dorsal language stream in the human brain. *Journal of neurosurgery*, *124*(5), 1396-1405.

Yarkoni, T., Balota, D., Yap, M., (2008). Moving beyond Coltheart's N: a new measure of orthographic similarity. *Psychon*. Bull. Rev. 15, 971–979. 1

Yeatman, J.D., Dougherty, R.F., Ben-Shachar, M., Wandell, B.A., (2012a). Development of white matter and reading skills. Proc. Natl. Acad. Sci. U. S. A. 109, E3045-53.

Yeatman, J.D., Dougherty, R.F., Myall, N.J., Wandell, B.A., Feldman, H.M., (2012b). Tract profiles of white matter properties: automating fiber-tract quantification. *PLoS One* 7, e49790.

Yu, D., Jiang, Y., Legge, G. E., & He, S. (2015). Locating the cortical bottleneck for slow reading in peripheral vision. *Journal of vision*, *15*(11), 3-3.

Zeki, S., & Shipp, S. (1988). The functional logic of cortical connections. *Nature*, *335*(6188), 311-317.

Zeki S. (1990). A century of cerebral achromatopsia. *Brain* 113(Pt. 6):1721–77

Zeki S, Watson JD, Lueck CJ, Friston KJ, Kennard C, Frackowiak RS. (1991). A direct demonstration of functional specialization in human visual cortex. *J. Neurosci.* 11:641–49

Zeki, S. (2003). Improbable areas in the visual brain. *Trends Neurosci*. 26, 23–26.

Annexes

Annex I

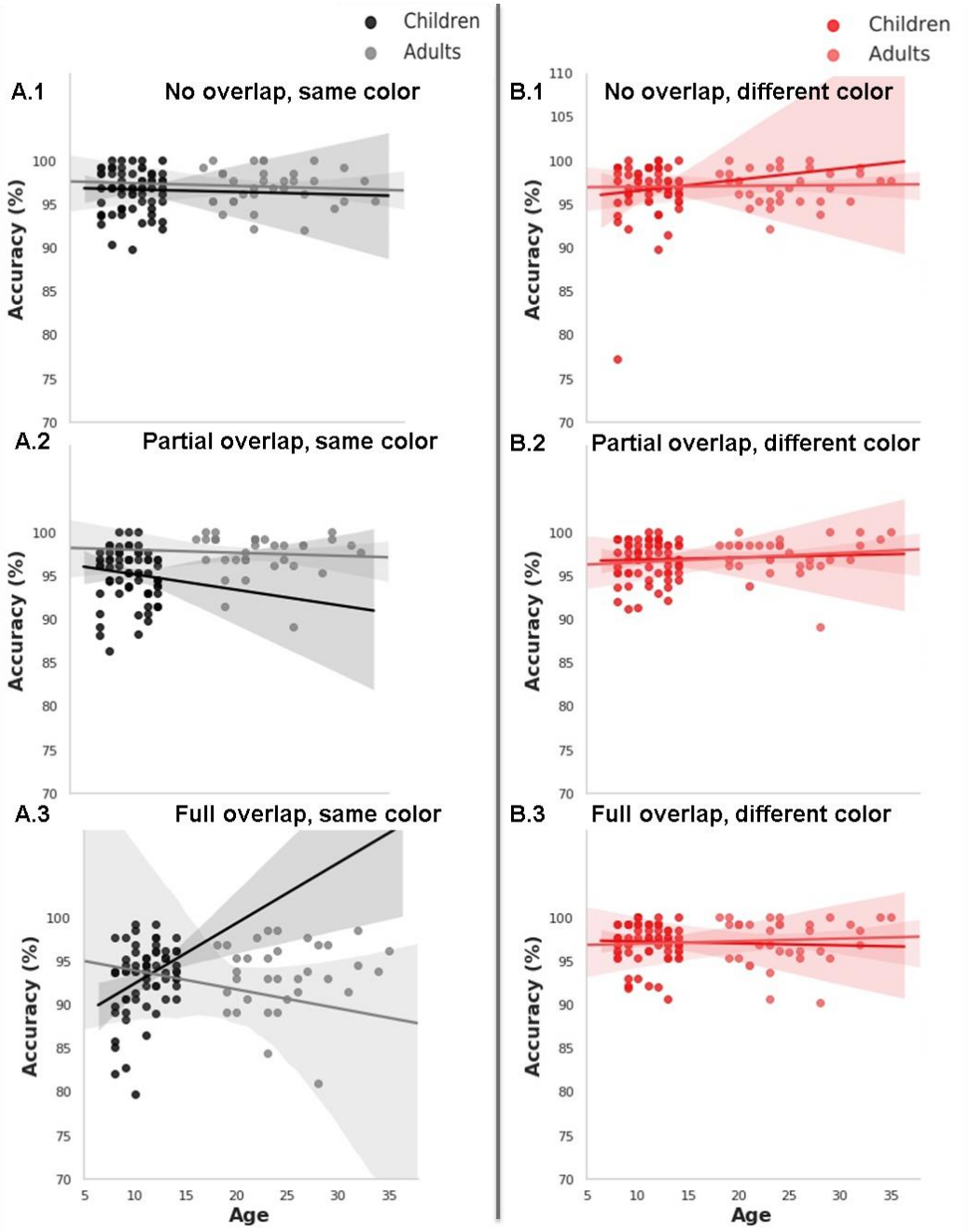

Figure 12 Annex I: Associations between age and accuracies in the visual discrimination task for children and adults: A.1) No overlap, same color (black) stimuli; A.2) Partial overlap, same color (black) stimuli; A.3) Full overlap, same color (black) stimuli; B.1) No overlap, different color stimuli; B.2) Partial overlap, different color stimuli; and, B.3) Full overlap, different color stimuli. Darker lines correspond to the associations between visual discrimination stimuli reaction times and children, while the lighter lines correspond to the associations between visual discrimination stimuli accuracies and adults.

Annex II

1. ROI analysis

The same ROI analyses reported for the left hemisphere visual cortex were also conducted for right visual cortex. Again, we conducted analyses at the individual-subject level to characterize the activation profile across hemisphere specific visual regions. To avoid potential biases in the observed effects due to stronger signal strength in more posterior than anterior regions, parameter estimates (i.e., scaled % signal change and signal t-values) for the specific contrasts (Magnocellular > Parvocellular Words and Magnocellular > Parvocellular Images) were extracted and submitted to a 6 (ROI: V1, V2, V3, hV4, LO1, TO1) X 2 (Stimuli: words, images) repeated measures ANOVA. Right hemisphere ROI analysis of the % signal change values revealed a main effect of ROI ($F_{5,150} = 40.94$; $p \leq 0.001$, $\eta_p^2 = 0.58$, BF10 = 1.84 e^{26}). We found no significant main effect of Stimuli ($F_{1,30} = 0.29$; $p = 0.593$, $\eta_p^2 = 0.01$, BF10 = 0.16). Simple-effect analysis for the ROI main effect revealed an anterior to posterior functional gradient with stronger engagement of the more anterior relative to the most posterior visual cortex regions (see Figure 1*A*, upper panel). All comparisons were statistically significant ($qs \leq 0.001$, $d' \geq 0.45$, BF10 ≥ 34.22), with the exception of V2-hV4, V3-hV4, and LO1-TO1, which did not differ statistically ($qs \geq 0.05$, $d' \leq 0.15$, BF10 ≤ 0.26).

Second, the same analysis was carried out with t-values instead of % signal change values and the same pattern of results emerged (main effect of ROI: $F_{5,130} = 40.82$; $p \leq 0.001$, $\eta_p^2 = 0.61$, BF10 = 4.96 e^{30}) (Figure. 1A, bottom panel). As for the % signal change analysis, there was no significant effect of Stimuli ($F_{1,26} = 1.64$; $p = 0.059$, $\eta_p^2 = 0.06$, BF10 = 0.60). Simple-effect analysis for the ROI main effect confirmed the anterior to posterior functional gradient that was observed for the % signal change values (all comparisons were statistically

significant, qs ≤ 0.001, d' ≥ 0.49, B10 ≥ 64.53), with the exception of V3-hV4 and LO1-TO1, which did not differ statistically (qs ≥ 0.05, d' ≤ 0.13, BF10 ≤ 0.22).

Third, the same 6 X 2 repeated measures ANOVAs using % signal change and t-values as dependent measures was conducted for the specific contrast Parvocellular > Magnocellular Words and Parvocellular > Magnocellular Images for each right visual cortex ROIs. Again, the exact same pattern of results emerged in the ANOVAs and post-hoc analysis for % signal change (Figure 1B, upper panel): the main effect of ROI ($F_{5,130}$ = 36.82; p ≤ 0.001, η_p^2 = 0.57, BF10 = 1.38 e^{26}); and for t-values (Figure 1B, bottom panel): main effect of ROI ($F_{5,130}$ = 40.82; p ≤ 0.001, η_p^2 = 0.61, BF10 = 4.88 e^{30}).

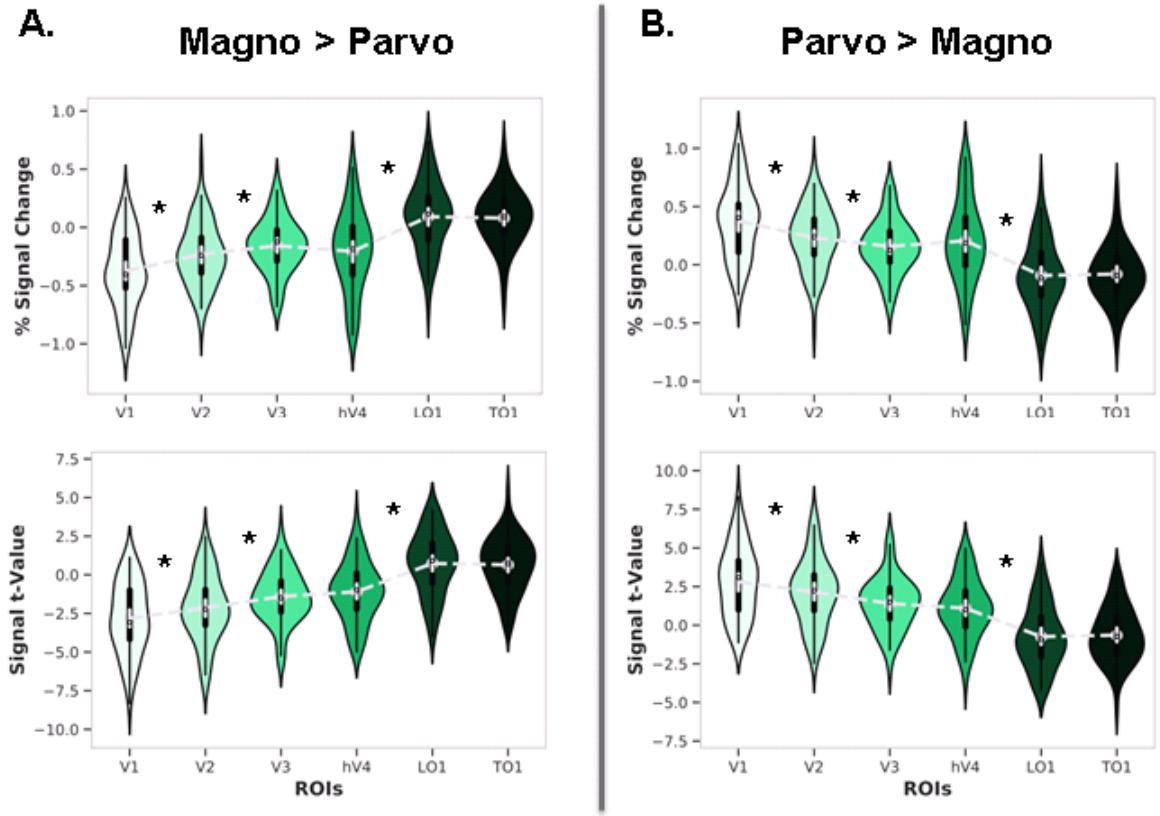

Figure 1 Annex II: ROI analyses. A) Percent signal change (top panel) and regional t-values (bottom panel) of right hemisphere visual cortex ROIs for the Magnocellular > Parvocellular contrast. B) Percent signal change (top panel) and regional t-values (bottom panel) of right hemisphere visual cortex ROIs for the Parvocellular > Magnocellular contrast. The black bar in the center of the violins represents the interquartile range, while the gray dash lines reflect the median. * asterisks denote statistically significant effects between contiguous regions (FDR corrected). Magno = magnocellular; Parvo = parvocellular.

2. Probabilistic maps

As for the left hemisphere, we conducted an additional fMRI analysis using right visual cortex surface-based probabilistic maps, which allowed us to examine the probability that a given voxel was significantly engaged in a functional contrast of interest. Since in the ROI Analysis we did not observe any significant interaction involving the factor Stimuli, we performed probabilistic maps for Magnocellular > Parvocellular and Parvocellular > Magnocellular contrasts across stimuli conditions. Figure 2 shows the probabilistic maps that correspond to the contrasts Magnocellular Words > Parvocellular Words, Parvocellular Words > Magnocellular Words, Magnocellular Images > Parvocellular Images and Parvocellular Images > Magnocellular Images in the left hemisphere. These maps revealed that in the Magnocellular > Parvocellular contrast, higher probabilities were located in more anterior regions within the visual cortex (i.e., LO1, TO1; see Figure 3*A*). In contrast, the probabilistic map for the Parvocellular > Magnocellular contrast showed higher probabilities in more posterior regions, including primary visual cortex (V1, V2, V3 and hV4; Figure. 3*B*). The color-coded voxels denote the likelihood of that voxel being assigned to one or the other pathway in the probabilistic map. Maps are not fully complementary since their probability is assigned based on each specific contrast. Figure 4 shows right visual cortex probabilistic maps for words and images separately.

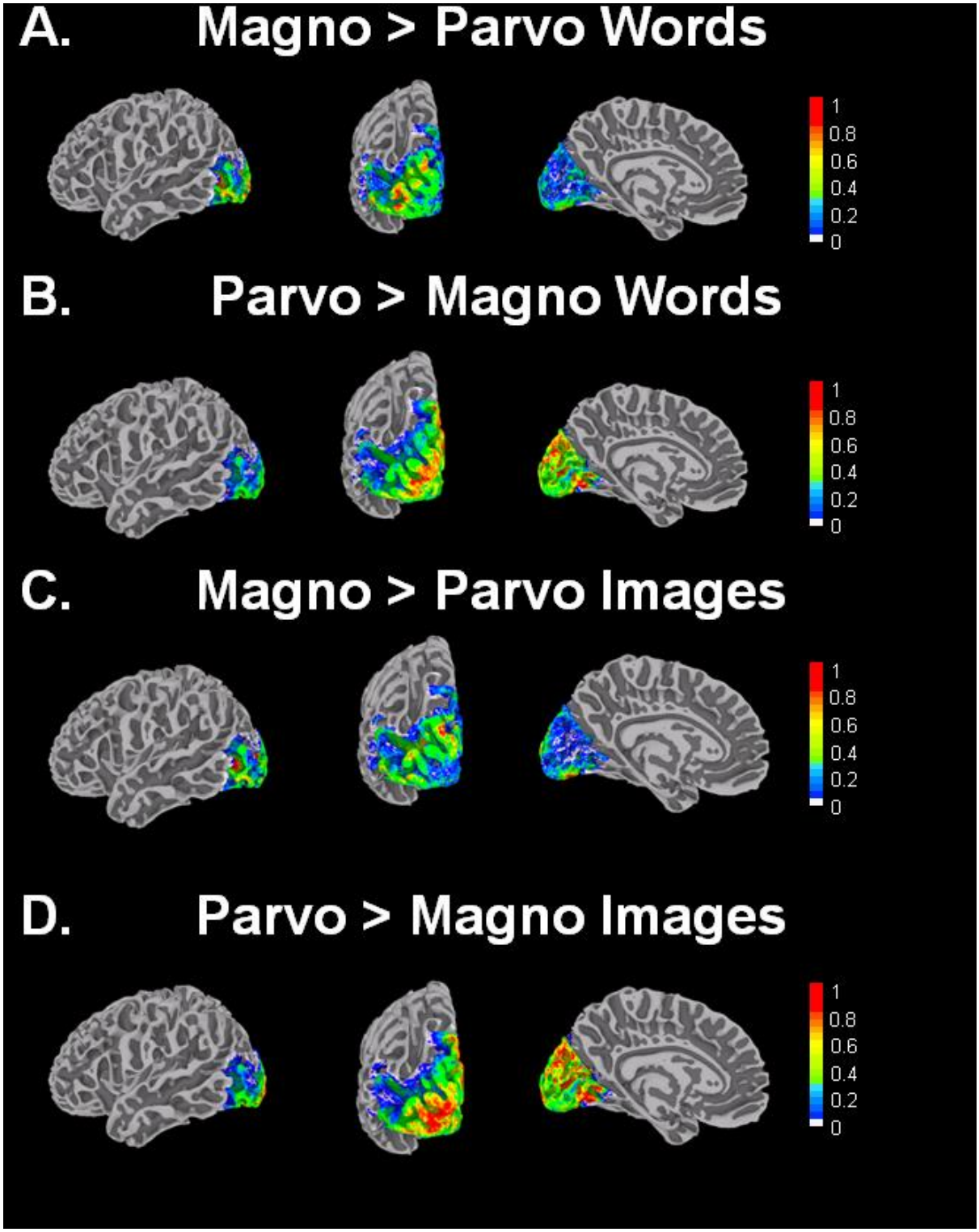

Figure 2 Annex II: Probabilistic maps showing the percentage of involvement of left visual cortex voxels on surface renderings for the contrasts A) Magno > Parvo Words, B) Parvo > Magno Words, C) Magno > Parvo Images and D) Parvo > Magno Images. The probabilistic maps A and B and C and D are not fully complementary in terms of voxel correspondence; while they represent opposite contrasts, they were generated by separate analyses. Magno = magnocellular; Parvo = parvocellular.

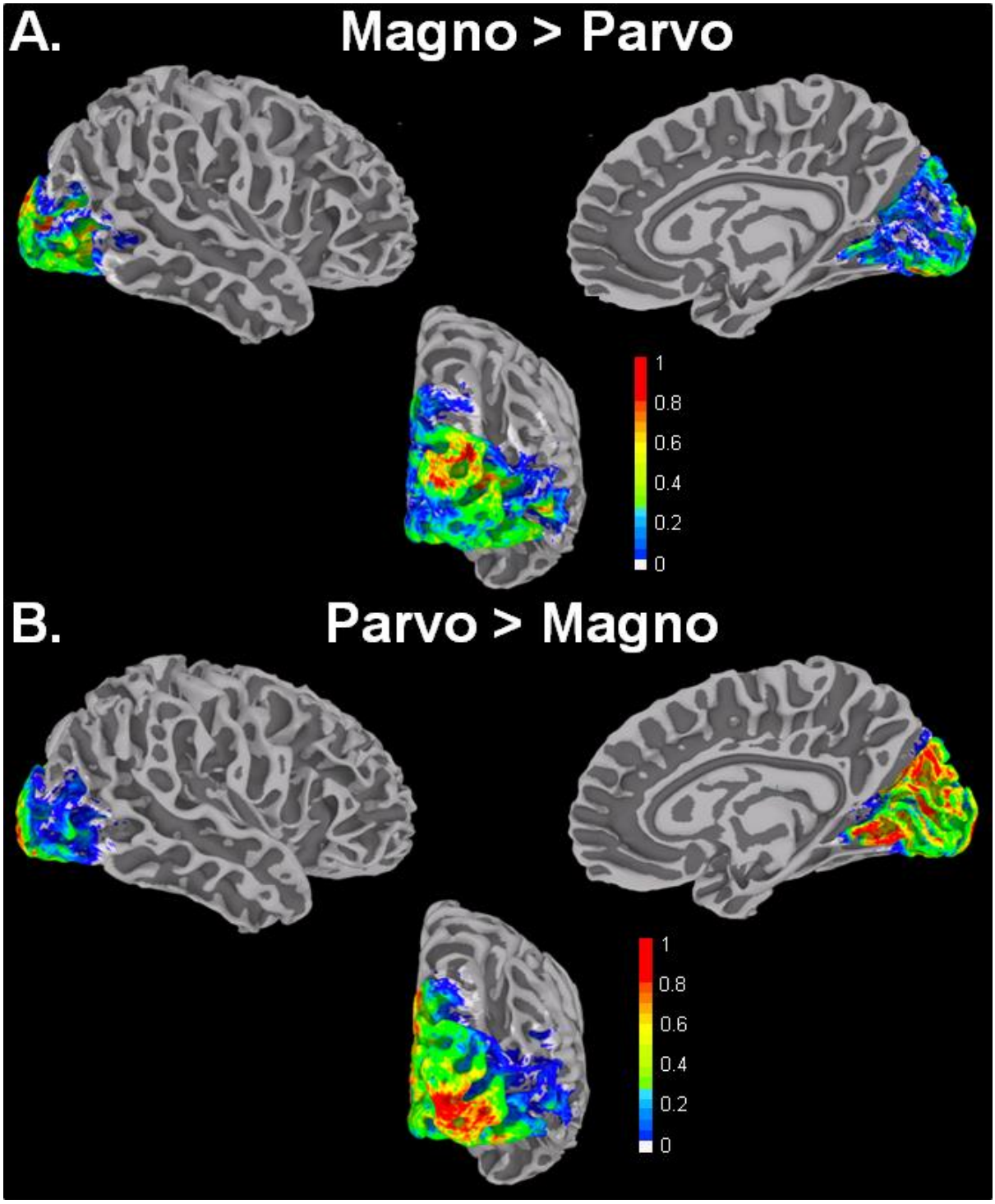

Figure 3 Annex II: Probabilistic maps showing the percentage of involvement of right visual cortex voxels on surface renderings for the contrasts A) Magno > Parvo and B) Parvo > Magno. The two probabilistic maps are not fully complementary in terms of voxel correspondence; while they represent opposite contrasts, they were generated by separate analyses. Magno = magnocellular; Parvo = parvocellular.

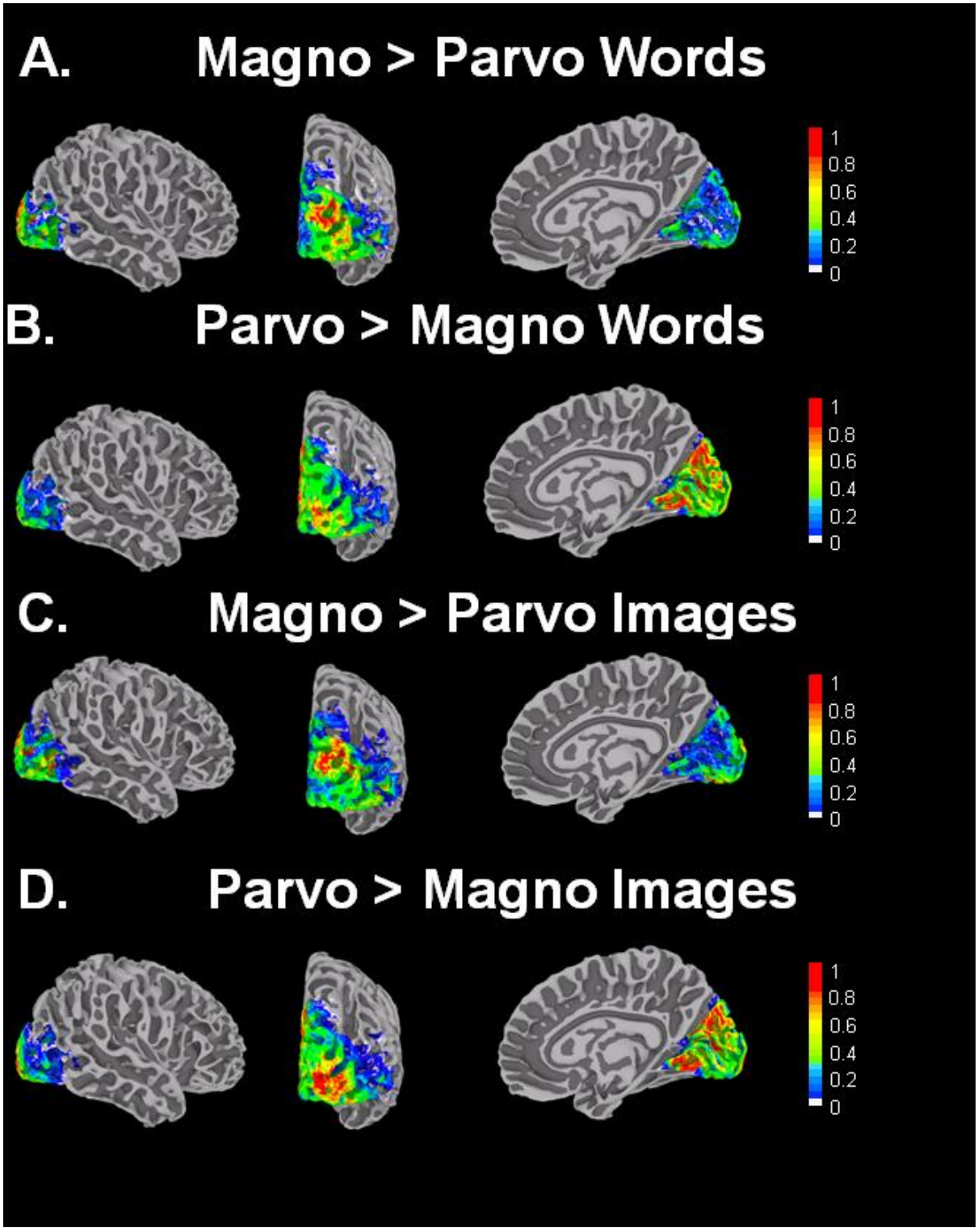

Figure 4 Annex II: Probabilistic maps showing the percentage of involvement of right visual cortex voxels on surface renderings for the contrasts A) Magno > Parvo Words, B) Parvo > Magno Words, C) Magno > Parvo Images and D) Parvo > Magno Images. The probabilistic maps A and B and C and D are not fully complementary in the correspondence of the voxels; while they represent opposite contrasts, they were generated by separate analyses. Magno = magnocellular; Parvo = parvocellular.

3. Pairwise functional connectivity analysis

We characterized the coupling strength across study conditions in the right hemisphere as done for the left hemisphere. Figure 5*A* shows the correlation matrix for Pearson's r values between pairs of ROIs (red colored circles indicate statically significant FC, $r \geq 0.57$, Bonferroni corrected) as well as a representation of the Euclidean distance against Pearson's r values between each pair of nodes (shadowed areas indicate statistically significant FC). Figure 5*B* is a surface rendering, with edges representing statistically significant correlations between visual cortex regions. Overall, posterior visual regions (i.e., V1, V2, V3) and anterior visual regions (i.e., hV4, LO1, TO1) tended to show local coactivations. In contrast, more distant anterior-posterior regions did not show statistically significant functional coupling.

Second, Fisher's Z transformed FC values of the right hemisphere were submitted to a series of 5 (ROI Pairs) X 2 (Pathway) X 2 (Stimuli) repeated measures ANOVAs, one for each of the examined visual cortex regions. All of the analysis revealed a main effect of ROI Pair ($F_{4,132} \geq 4.60$; $p \leq 0.002$, $\eta_p^2 \geq 0.20$, BF10 $\geq 2.54\ e^{-4}$) as was the case for the left hemisphere (Supplementary Fig. 5*C*). From more anterior to more posterior regions, simple-effect analyses revealed that *V1* was more strongly tied functionally to V2 than to V3, hV4, LO1 and TO1 (ps ≤ 0.030, d' ≥ 0.27, BF10 ≥ 7.44), but no differences in FC emerged between V1-hV4 and V1-TO1 or between V1-LO1 and V1-TO1 (ps ≥ 0.050, d' ≤ 0.18, BF10 ≤ 0.64). Second, there was stronger FC between *V2* and V3 and between V1 and V2 than between V2 and all the other visual regions (i.e., hV4, LO1 and TO1) with ps ≤ 0.020, d' ≥ 0.28, BF10 ≥ 9.09; again, with no significant differences emerging in FC between V2-V1 and V2-V3, V2-hV4 and V2-TO1, or between V2-LO1 and V2-TO1 (ps ≥ 0.050, d' ≤ 0.19, BF10 ≥ 0.94). Third, a similar pattern of results emerged for *V3*: stronger FC between V3-V2 than between V3 and the rest of the visual regions (i.e., V1, hV4, LO1, and TO1) with ps ≤ 0.020,

d' ≥ 0.29, BF10 ≥ 10.72; there was also no FC difference observed between V3-V2 and V3-hV4, V3-V1 and V3-LO1, or V3-LO1 and V3-TO1 (ps ≥ 0.050, d' ≤ 0.25, BF10 ≤ 0.02).

On the other hand, more anterior right visual cortex regions hV4, LO1 and TO1 presented a similar FC pattern. *hV4* showed stronger connectivity with V3 than to either V2 or V1 with ps ≤ 0.001, d' ≥ 0.36, BF10 ≥ 148.04; but there were no differences in coactivation between hV4-TO1 and hV4-LO1, hV4-V1 and hV4-LO1, hV4-V2 and hV4-LO1, hV4-V2 and hV4-TO1 or hV4-V3 and hV4-TO1 (ps ≥ 0.050, d' ≤ 0.20, BF10 ≤ 0.97). FC of the *LO1* was similar to visual regions V3, hV4 and TO1; and stronger to all of these regions than to visual cortex regions V1 and V2 with ps ≤ 0.020, d' ≥ 0.29, BF10 ≥ 13.52; but there was no differences in coactivation between LO1-V3 and LO1-hV4, LO1-V3 and LO1-TO1, or LO1-hV4 and LO1-TO1 (ps ≥ 0.050, d' ≤ 0.14, BF10 ≤ 0.30). Finally, FC of the *TO1* was similar to visual regions LO1 and hV4; and stronger to these two regions than to visual cortex regions V1, V2, and V3 with ps ≤ 0.001, d' ≥ 0.32, BF10 ≥ 42.11. There were no differences in the coactivation between TO1-V2 and TO1-V3, TO1-V2 and TO1-LO1, TO1-V3 and TO1-LO1 or TO1-hV4 and TO1-LO1 (ps ≥ 0.050, d' ≤ 0.23, BF10 ≤ 2.86).

In sum, right hemisphere V1, V2 and V3 were tightly coupled to each other as a function of their proximity, showing statistically significant lower FC with the more anterior visual cortex regions (LO1, TO1) (see Figure 5*C*). Right hemisphere hV4, LO1 and TO1 were also strongly coupled with statistically higher FC to each other than to V1 and V2 (see Figure. 5*C*). The results resemble the pattern of results observed for left visual cortex regions.

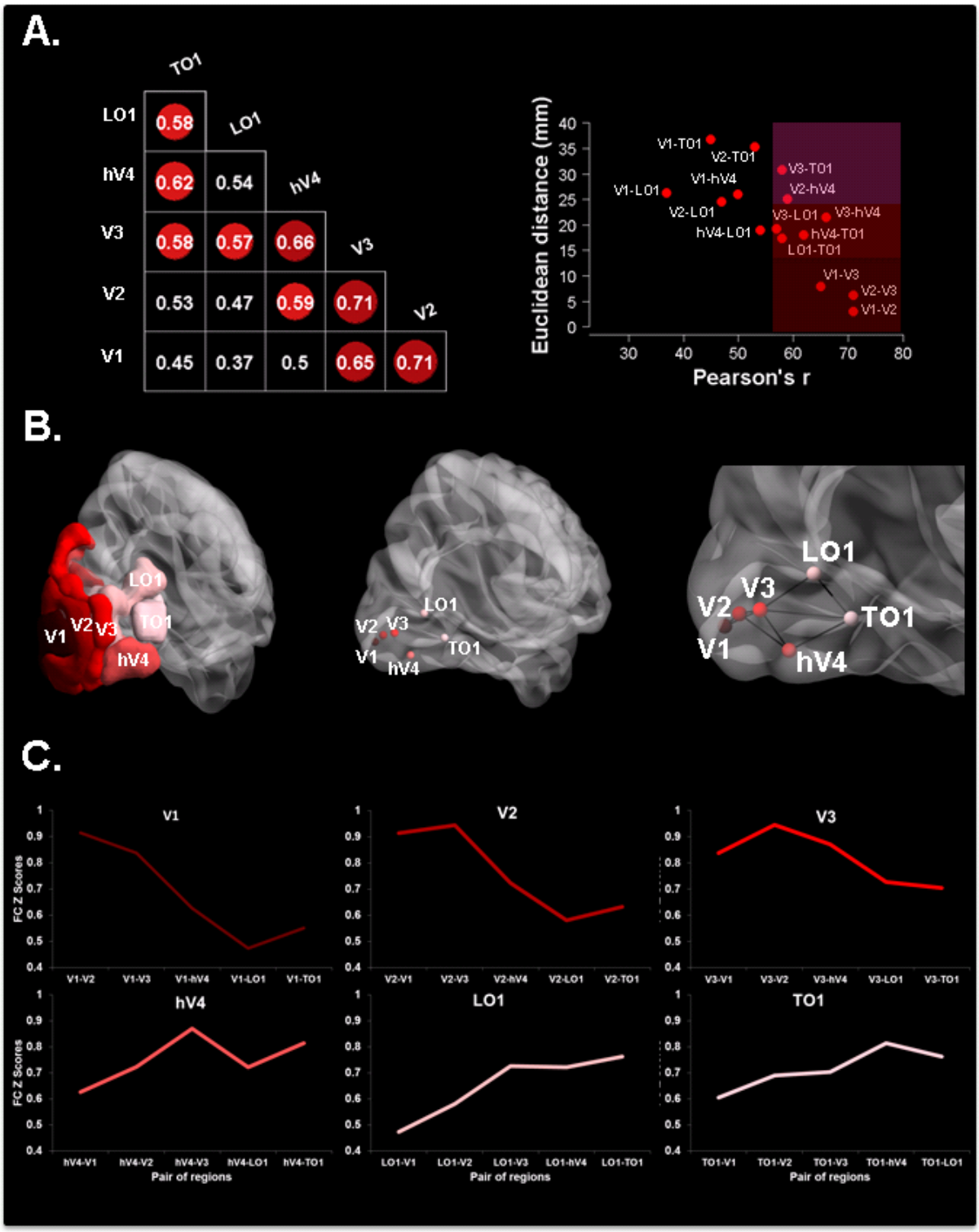

Figure 5 Annex II: Task-related pairwise functional connectivity between right visual cortex ROIs across experimental conditions (i.e., magnocellular-biased words, parvocellular-biased words, magnocellular-biased images, parvocellular-biased images. A) Left panel shows correlation matrix with significant Pearson's r correlations (r ≥. 57) colored in red tones. Right panel shows Euclidean distances from posterior (V1, 0-value) to anterior (TO1) left visual cortex regions plotted against Pearson's r values for each ROI pair, with shaded areas indicating pairs showing significant coupling. B) Left panel shows the sagittal rendering of the right visual cortex ROIs. Central panel shows the sagittal rendering of right

visual cortex nodes centered at the ROIs center of mass. Right panel shows statistically significant pairwise correlations (i.e., edges) between right visual cortex nodes in a rendering of the posterior sagittal section. C) Task-related pairwise functional connectivity (Z scores) between right visual cortex ROI pairs across experimental conditions. The upper left panel shows Z scores between V1 and the rest of the ROIs, upper middle panel shows Z scores between V2 and the rest of the ROIs, and upper right panel shows Z scores between V3 and the rest of the ROIs. The lower left panel shows Z scores between hV4 and the rest of the ROIs, lower middle panel shows Z scores between LO1 and the rest of the ROIs, and lower right panel shows Z scores of TO1 and the rest of the ROIs.